Modelling and Analysis of traction control systems in automobiles

P.R. Crossley

A Thesis submitted to the University of Warwick for the degree of Doctor of Philosophy

Department of Engineering
University of Warwick

February 1992

Summary

This thesis begins with a brief overview of vehicle control. The thesis places powertrain control, which is discussed in more detail, within the wider context of vehicle control. Traction control is one aspect of powertrain control. The available methods of traction control are reviewed together with a discussion on the systems in current production. The traditional method adopted by the automotive industry for traction control is analysed. The powertrain system is analysed from a control stand-point and a control oriented approach to traction control design identified.

The emphasis in this thesis is on the analysis of traction control systems. The analysis is performed on simulation models and is supported by implementations on the real vehicle. The level of modelling appropriate for the analysis is justified and models developed in a modular manner. The individual modules are developed on the basis of published material and previous work within Ford Motor Company.

Based on the analysis, two traction control strategies are developed which are subsequently developed and implemented on real vehicles. The results of this vehicle work is discussed.

Acknowledgements

I would like to acknowledge the support of my supervisor, Dr R.P. Jones for his encouragement and guidance with the work. I would like to acknowledge Mr R.M. Windett, Powertrain Systems Engineering, Ford of Britain, for obtaining company support of the work.

The detail help from Dr D.D. Hrovat, Research Staff, Ford U.S.A, who in the early days of the work was particularly valuable. For the engine understanding I would like to acknowledge Mr J Cook, Research Staff, Ford U.S.A.

For help in implementation of the Engine strategy I would like to acknowledge the contributions of Messrs L. Roller, R Stuntz & C. Swick formerly of Electronics Division, Ford U.S.A.

Finally I would like to acknowledge Mr J.P. Schwab, Bendix Division Technique, Paris, for support in the Brake Control Development. I would also like to thank the Directors of Ford Motor Company Ltd for permission to perform & publish this work.

Table of Contents

Nomenclature

T_e	Engine torque (Nm)
T_{imp}	Torque converter impellor torque (Nm)
T_{tur}	Torque converter turbine torque (Nm)
T_c	Clutch torque (Nm)
T_s	Axle shaft torque (Nm)
T_{wr}	Tyre/road interface torque (Nm)
T_{wl}	Tyre/road interface torque (Nm)
T_r	Torque ratio across the torque converter (T_{tur}/T_{imp})
ω_e	Engine flywheel speed (s^{-1})
θ_e	Clutch deflection (rad)
ω_i	Gearbox input shaft speed (s^{-1})
s_r	speed ratio across the torque converter (ω_i/ω_e)
θ_s	Axle deflection (rad)
ω_{wl}	Left wheel speed (s^{-1})
ω_{wr}	Right wheel speed (s^{-1})
s	tyre slip ratio
v	vehicle sprung mass velocity (m/s)
r	effective rolling radius of tyre (m)
ω	angular velocity of driven wheel (rad/s)
J_e	Engine Flywheel Inertia (kgm^2)
J_t	Transmission inertia (kgm^2)
J_{wr}	Right wheel inertia (kgm^2)
J_{wl}	Left wheel inertia (kgm^2)
K_{eq}	Equivalent axle shaft stiffness (Nm/rad)
K	Torque converter K factor

m_s	vehicle sprung and unsprung mass (kg)
r_o	Overall gear ratio ($1/(r_{gb}r_{fd})$)
b	Clutch damping (Nms/rad)
k	Clutch stiffness (Nm/rad)
F_t	Tractive force (N)
F_n	Normal force on tyre (N)
μ_0	Peak coefficient of friction (F_t/F_n)
μ	Slip dependent coefficient of friction (F_t/F_n)
C_s	Tyre slip stiffness ($N/slip$) ($C_s \in 25000, 100000, 200000$)
A_s	Friction reduction factor (0.00353)
F_{load}	Road load (N)
v	vehicle speed (m/s)
a_{rl}	Road load equation constant term (N)
b_{rl}	Road load equation velocity term (Ns/m)
c_{rl}	Road load equation aerodynamic term (Ns^2/m)
K_p	Proportionality constant $f\left(\frac{pRT}{V}\right)$
K_θ	Throttle flow sensitivity ($\frac{\partial \dot{m}_{ai}}{\partial \theta}$)
K_N	Pumping feedback ($\frac{\partial \dot{M}}{\partial \omega}$)
G_p	Torque/Manifold pressure gain
F_N	Engine friction ($\frac{\partial T_f}{\partial \omega}$)
P	Manifold pressure (bar)
$\dot{M}$	Mass flow rate pumped by the engine (g/s)
$\dot{m}_{ai}$	Mass flow rate through the throttle (g/s)
τ_p	Manifold time constant (s)
A_a	Flow cross sectional area of MAF sensor m^2
θ	Throttle angle (degrees from closed)

T_a	Temperature upstream of the throttle (^oK)
p_m	Manifold pressure (bar)
p_{atm}	Atmospheric pressure (bar)
p_a	Pressure upstream of throttle (bar)
p_a	Partial pressure in manifold due to air (bar)
p_{egr}	Partial pressure in manifold due to egr (bar)
τ_{egr}	Time constant of EGR valve (s)
K_{fe}	Experimentally determined constant for exhaust flow relationship
R	Universal gas constant (J/kg/k)
T	Temperature of manifold gas (^oK)
V	Volume of intake manifold (m^3)
γ	Ratio of specific heats
$\dot{m}_a$	Mass-air flow into manifold (g/s)
$\dot{m}_{ai}$	Mass-egr flow into manifold (g/s)
$\dot{m}_{ao}$	Mass-air flow out of manifold (g/s)
$\dot{m}_{ao}$	Mass-egr flow out of manifold (g/s)
$\dot{m}_e$	Total mass flow out of manifold (g/s)
$\dot{m}_{exh}$	Mass flow in to exhaust (g/s)
$\dot{m}_{exo}$	Mass flow out of exhaust (g/s)
ω	Engine angular speed (rad/s)
T_b	Engine brake torque (Nm)
AF	Air fuel ratio
σ	Spark advance (deg)
m_a	Mass-air charge (g)
m_e	Mass-egr charge (g)
d_c	PWM to EVR (0 to 1)

x_{egr} EGR valve position

y_{opt} ideal slip response (%)

y_m actual slip response (%)

e error function between ideal and actual response (%)

b parameters which give the ideal response

B parameters which give the actual response

γ_n adjustment factor for parameter update

p_{egr} Pressure to EGR valve (bar)

p_{exh} Exhaust manifold pressure (bar)

K_{pe} Exhaust back pressure constant

T_{exh} Temperature of exhaust manifold gas

V_{exh} Volume of exhaust manifold (m^3)

Q_p Volumetric flow rate of pump (cm^3/s)

Q_{rw} By pass valve flow rate (cm^3/s)

V_{pipe} Volume of pipe work after pump

Q_i Flow to brake caliper (cm^3/s)

Q_o Return flow from brake caliper (cm^3/s)

V_b Volume of oil in right hand brake caliper (cm^3)

p_{pipe} Pressure upstream of brake control valve (bar)

V_{oil} Volume of oil in pipework upstream of brake valves (cm^3)

p_b Brake pressure ($10^5 N/m^2$)

T_b Torque on wheel (Nm)

dc PWM to solenoid valve. 1 = increase open 0 = decrease open.

N.B. subscript l and subscript r refer to left and right hand wheels.

1 Introduction

The increasing use of control systems on vehicles has been driven by three developments in the 1970's. These were the advent of the low cost micro-processor (and digital computer), emission control legislation and the fuel crisis. The digital computer changed the whole approach to design and manufacture of the automobile. The low-cost micro-processor has enabled the implementation of sophisticated control algorithms to control the vehicle to deliver good fuel economy together with low emissions. More recently, advances have seen the development of control systems which give the driver safety features. This thesis is concerned with the latter.

Automotive systems represent an extremely wide and diverse area in terms of system dynamics (1). The application of modern control techniques to these systems is widely recognised (2), (3), (4), (5). In order to place this thesis within this wide area of automotive control, the systematic approach presented by Costa et al (45) will be briefly considered. In this approach, vehicle control sub-systems are considered to ultimately act through the wheels of the vehicle. These sub-systems are concerned with:-

(a) propulsion control;

(b) steering control;

(c) suspension control.

Suspension Control

Suspension control is associated with the control of the vertical forces between the wheel and the vehicle body, thereby influencing the roll and pitch motions.

Steering Control

Steering control concerns the control of side forces at the tyres and hence is concerned with lateral motion of the vehicle and yaw of the vehicle.

Propulsion Control

Propulsion control is concerned with all elements within the vehicle powertrain from the throttle angle through to the driven wheels. Propulsion control concerns the longitudinal force applied to the vehicle. The propulsion control system can be considered to consist of 3 major sub-systems:

(a) engine management and idle speed control

(b) transmission control

(c) traction control, anti-lock braking and four-wheel drive control

Engine Management Systems

The use of micro-processor control systems in automotive control was first applied to engine management. A typical engine management system is shown in Figure 1.1. This system is typical of production systems in the late 1980s, however such a system has gradually evolved over time. Initial developments were on electronic spark timing which was introduced in 1976 by both G.M. and Chrysler (7). This was done in order to overcome the many limitations of conventional flyweight/vacuum spark advance schedulers. This step was very significant. Following this the introduction of electronic fuel injection provided enhanced control capabilities to meet emission control regulations (8),(9). The next major shift occurred with the introduction of the three way catalyst, as an exhaust after-treatment necessary in order to meet increasingly stringent emission control standards. This required precise control of AFR (Air Fuel Ratio) at stoichiometry (approx 14.7:1). In order to maintain good conversion efficiency of the catalyst (> 80%) AFR needs to be controlled to within 0.05 AFR.

Returning to Figure 1.1 the basic idea in such systems is to sense air flow and meter the fuel to maintain stoichiometry. The other variables (i.e Spark Advance and Exhaust Gas Recirculation) tend to be statically programmed into the engine strategy, based upon engine mapping procedures. The intention of these calibrated strategies is

to optimise the fuel economy, subject to emission constraints (10), (11). Such an approach does not cater for engine-to-engine variability or ageing effects. Whilst some attention to adaptive control schemes has occurred (12), it is anticipated that this area will expand over the forthcoming decade with the wide availability of very powerful microprocessor control systems. The driving force here is the introduction in 1994 in the U.S.A. of the Clean Air Act which requires yet more stringent emission control standards and, most importantly, the certification by automakers that the vehicle will maintain these standards for 10 years or 100,000 miles. Such controllers will include the use of adaptive control schemes to optimise engine performance 'on-line'.

An additional control variable speculated upon by Bowler in 1980 (8) is the management of both the fuel and air requirements for the engine. This requires the use of an electronically controlled throttle system and should lead to improved AFR control during transients in addition to improved driveability.

Engine Idle Speed

The purpose of an engine idle speed control system is to regulate idle speed in the presence of load disturbances and varying ambient conditions. The regulated idle speed is generally set at a minimum value determined by Noise, Vibration and Harshness (NVH) considerations. This speed is usually so low that, without some form of compensation, the engine would stall as loads are applied. The reduced idle speed improves the fuel economy of the vehicle. A reduction in idle speed of 100 r/min yields a fuel economy improvement of approximately 0.5 mpg on the U.S. metro-highway drive cycle (13).

Engine Idle speed control has received considerable attention over the past two decades (14), (15), (16), (17). During this period, engines have been typically down-sized in capacity and number of cylinders (14). This has effectively made the

problem more difficult and partially explains the continuing interest in its solution. In addition, lower idle speed set-points - motivated by improved fuel economy over the federal drive cycle - have made the problem even more difficult. These problems have prompted the use of feedforward control (14) and a growing interest in smart accessory drives.

The problem in principle is very simple - to regulate Engine Idle Speed in the presence of load disturbances. Typical load disturbances are shown in Table 1.1.

Table 1.1 Typical idle speed loads

Load	Approximate Power required (kW)
Torque convertor stall torque	2
Power Assisted Steering pump	1.5 to 2
Air conditioning compressor	2
Alternator load (saturated)	0.5

The loads in general are step-like in application and any combination may be engaged. In addition, the effect of the loads is to cause the engine to run at significantly different operating (i.e. load) points. Furthermore, the engine can operate at widely varying ambient conditions (pressure and temperature). This may be from a fully warmed-up condition to coolant temperature as low as -30 deg C. The engine has a mix of discrete, possibly multi-rate (15), and continuous processes, hence control system design is usually addressed using discrete control design techniques (14), (15), (17). Powell et al (15) considered the multi-rate nature of a banked fuel injection system and derived an analytical technique which reduces the stability

analysis to that of a single rate system. Morris et al (14) approached the problem with a reduced order (5 state) physically based model and since the problem is a regulator problem (14) looked at an LQG 'optimal' feedback control law.

Four-Wheel Drive, Traction Control and Anti-Lock brakes

The need for devices and systems to limit wheel-spin has arisen with the increased power-to-weight ratio of modern vehicles (43). This need has led to the development of both four-wheel drive (4WD) vehicles for on-road use and traction control. These systems are concerned with the propulsive forces generated at the tyre-road interface. Three key forces are involved. These are the longitudinal, lateral and normal forces at the tyre contact patch. The lateral force is concerned with the steering and handling qualities of the vehicle. The longitudinal force is concerned with traction, or braking. The normal force is directly related to the magnitude of the vector sum of the lateral and longitudinal forces.

Four-wheel drive actually improves vehicle traction, compared with two wheel drive, by effectively taking advantage of the normal force provided by the total weight of the vehicle. However, 4WD has the disadvantage of added weight and cost, and results in the deterioration in the NVH characteristic (40).

Traction control systems, and anti-lock braking systems, 'optimise' the available tractive effort at the two driven wheels. Whilst traction control systems should improve traction, the intention of traction control is primarily to maintain control (i.e. steerability) when accelerating (43),(40),(39). For ABS operation, wheel-spin is controlled by brake modulation only, whilst for traction control engine power may also be reduced.

Four-Wheel Drive Control

Four-wheel drive vehicles have traditionally been used for off-road driving with the four-wheel drive being manually engaged. Although such systems still exist, four-wheel drive for on-road use can be split into (a) permanently engaged systems and (b) automatic systems (41).

With permanent systems, the four-wheel drive is always engaged and the differentials are either free and then locked, using visco-clutches, or limited slip differentials are used.

With automatic systems (32), (71), two wheel drive is normally engaged and either viscous clutches or hydraulically controlled clutches are engaged at the onset of wheel-spin, thereby engaging the four-wheel drive.

Despite the enhanced levels of traction available with four-wheel drive systems, significant control problems are posed if ABS or anti wheel-spin systems are added. This is due to the difficulty of measuring the vehicle's absolute speed. Two wheel drive systems do not suffer such difficulties, because the non-driven wheel speeds provide the vehicle speed and, although it is possible to measure vehicle speed using a Doppler effect radar, no such systems currently exist due to the expense of such a sensor. With automatic four-wheel drive systems, the problem can be overcome by disengaging the four-wheel drive during ABS intervention.

Anti-Lock Brakes

Anti-lock brakes (ABS) represent the first control system fitted to vehicles which under normal vehicle use is never used. The function of ABS is to intervene between the driver and the vehicle brake and take over control. Such a control system is unique within the automotive industry. Other systems which intervene in an analogous way have been the subject of recent controversy. Two examples are (i) the safety of commercial aircraft 'fly-by-wire' systems and (ii) the unintended acceleration associated with 'suspect' idle speed control systems. Anti lock brakes have been in

series production since 1978 (43) and have not, very impressively, suffered similar problems. Indeed, studies in Germany (20) suggest that 7% of accidents have been avoided due to ABS.

It is important to understand that ABS systems do not under all circumstances shorten stopping distances (33). The primary intention is to allow the driver to maintain control during panic braking.

ABS systems can be categorised in a number of ways. This is usually on the basis of:-

(i) whether the system is integrated or add-on

(ii) number of speed sensors and control valves and

(iii) control technique

With a fully integrated system the standard master cylinder and vacuum booster are replaced with a hydraulic booster (31), (37) and accumulator. Integrated systems are more compact with simpler external hydraulic circuitry and have a very short, hysteresis free , response time (20). In addition since the hydraulic booster necessitates the use of an accumulator , fully integrated systems are more readily extended to a fast response traction control system. Further advantages occur when the hydraulics are further extended to a hydraulic network supplying hydraulic energy to power assisted steering and suspension. This system is fitted to the BMW 850i (37). The main disadvantage is associated with cost.

Add-on systems form the majority of ABS production systems. The system has a conventional master cylinder and vacuum booster. Downstream of this is the hydraulic pump and valve assembly which takes over control of the brakes during ABS operation.

The number of control channels (i.e. pressure modulators) and speed sensors is clearly a cost versus complexity issue. The most complex system is a four channel system with four speed sensors. In this system it is clearly possible to control each wheel speed independently and thereby achieve optimum control. In practice however, during braking, the rear axle provides a small contribution to the overall braking effort (33). For this reason the rear wheels are often controlled together to yield a three channel system. Whilst the rear wheels contribute a small proportion of the braking effort, it is important to control the rear wheels since if they become locked the vehicle becomes unstable.

The first ABS systems tended to be three and four channel systems, notably the Bosch S2 system (20) - the first production system. The systems can be simplified to two control channels and even single channel systems. The motivation for this is reduced cost.

The control techniques are generally characterised as either:-

(i) independent control

(ii) select low and

(iii) select high.

With independent control the left and right wheels are controlled independently. When braking on split μ surfaces the high μ wheel is clearly braked more, resulting in a yawing action of the vehicle in which the driver needs to apply a steering correction. With select low, the low μ wheel determines the control pressure. The vehicle will not yaw on split μ surfaces however, the total braking force will be sub-optimal. Only Honda (33),(20) use a select high principle. In this system when braking on split μ surfaces the high μ wheel is not allowed to lock but the low μ wheel (at the same pressure) may lock.

The above discussion represents an overview of ABS systems. A more comprehensive classification of systems is presented by Klein (20). This takes account of brake circuit layout (e.g. diagonal split), signal processing and brake force modulation.

Traction Control

Traction control can be seen as a logical extension to anti-lock braking (ABS) systems. It was not until the availability of relatively inexpensive microprocessors that ABS, and hence traction control, developed significantly.

High speed traction control systems are generally defined as engine intervention systems where it is safe to use the system at high vehicle speeds. It is possible to use brake intervention at high speeds if both wheels spin and the brake pressure to both wheels controlled to be exactly the same, and is determined by the wheel on the low μ surface (37).

Low speed systems are generally brake intervention systems and are really just a traction aid for low speed manoeuvres at speeds below about 30 km/h. Above these speeds, it is unwise to apply differential braking as vehicle stability can be impaired (37),(42),(39).

The development-led approach of traction control is clear from a review of the published literature in this area (28),(42). The majority of papers give a detailed description of the components, system diagrams and the benefits of such systems (42). Only a broad general description of traction algorithm is usually given.

Toyota (28), (40) use a combination of a rule-based approach to brake control and a classical PI controller for the throttle which has been modified to prevent interaction with the brake control. Initially, to prevent engine brake fight, Toyota

used a lower target slip for the throttle (28) in order to ensure that the brakes were only used during transients. A later development (40) involves the addition to the PI controller of an integral term acting on brake pressure.

Teves (42) use a rule-based approach for brake control, and allow high levels of slip to avoid driveline oscillations and engine stall. Volkswagen calculate the excess torque in the driveline and reduce this through a combination of engine and brake intervention, again allowing high slip levels to avoid engine stall (39).

The majority of activity in investigating traction control schemes has occurred relatively recently. The following list (Table 1.2) outlines the systems which are currently in production to date (22 Jan 1992):

Table 1.2 Current status of Traction Control Systems

MANUFACTURER	MODEL	SYSTEM	YEAR	SOURCE
Volvo		Fuel		
BMW	735,750,850	Throttle, Spark, Fuel & Gear shift	1987	(37)
Mercedes	S type	Throttle and brake	1987	(38)
Toyota	Crown, Lexus	Throttle and brake	1987 ?	(28), (40)
Mitsubishi	Galant	Fuel and spark	1988 ?	
Saab	900	Throttle and brake	1990	
Volkswagen	Golf	High speed ?	1991	
Nissan	Cima	?	1991	
Opel (GM)	Astra	Low speed ?	1991	

Patent activity focuses on i) the brake hydraulic hardware necessary to provide brake control and ii) different approaches to modulating engine power. Since this thesis does not address hardware design, only a brief outline of the brake hydraulic hardware currently being used is given in section 2.2, from a control stand-point. Patent activity in this area will not be discussed.

In the area of engine power modulation, a number of patents exist. These cover the use of spark, fuel and throttle to regulate engine power. The patents tend to give little information on the control algorithms employed, although reference to the use of simple 'proportional' controllers is a common feature (88),(89) and (90).

Thesis Content

This thesis concerns the modelling and analysis of a traction control system. The work is essentially an application of Computer Aided Engineering and analysis to an automotive control system. The control system study follows the following particular routes:

a) the familiar route of dynamic modelling of the system, linearisation of the model, control system development and test on the non-linear simulation.

b) optimisation of parameters on a non-linear simulation model.

Each of these routes has been followed with implementation on a vehicle and subsequent refinement using the model. The aim of the work is to investigate techniques capable of use for the design of an algorithm which, in addition to giving good dynamic performance, is simple to implement and follows a logical structure. This latter point is particularly important in a safety critical system which involves modulation of both brakes and engine power.

Although the major systems defined earlier may interact, the interactions are not obvious. An area where interactions do occur is in the area of chassis control (i.e. suspension, steering and traction) via the tyres. Interactions in the currently used

passive systems exist, but when the addition of feedback control-loops occurs in these safety critical areas great care needs to be taken in their development. If we consider the action of driving a vehicle, it is necessary to steer, accelerate and brake the vehicle and negotiate uneven road surfaces. The design of the car thus needs to consider the vehicle system response in the three translational degrees of freedom and the three rotational degrees of freedom. The active control systems which are currently being investigated include (i) Active or adaptive suspension, (ii) anti-lock braking (ABS) and (iii) traction control. It is essential that a systematic approach is taken to their design. Costa & Jones (44) refer to this as 'motion management'. Whilst a systematic approach has been important for the design of passive systems, the control of these interacting systems makes a systematic approach essential.

This thesis will focus in particular on traction control algorithm development. The algorithm development for ABS and traction control has, in general, been on the basis of in-vehicle development with little recourse to dynamic simulation. The use of dynamic simulation to develop control algorithms opens up the possibility of all year round development rather than the brief periods of winter test. In addition, and more importantly, the validated model can be used as a basis for classical and modern control theory design techniques which should lead to algorithms which are nearer to the optimum in performance terms, and are simpler to code than the commonly used rule-based algorithms.

Traction control algorithm structure of the major automotive manufacturers tends to be a closely guarded secret and hence is not seen in the published literature. However, much of the work (particularly for the European automotive companies) is carried out by independent suppliers and, based upon information supplied to Ford Motor Co, it is known that the majority of the control algorithms used are rule-based. Of more relevance to this study is the work being carried out on behalf of GM by Tan

(27) who reports on the application of a sliding-mode controller. Toyota (28) use a combination of a rule-based algorithm for the brake intervention and a Proportional, Integral and Derivative (PID) controller on throttle control. This approach is similar to the one adopted in chapter 3 of this thesis.

Thesis organisation

This thesis is organised in the order in which the work has been performed. The work was supported by experiments conducted on two vehicles - a Rear Wheel Drive vehicle (RWD) and a Front Wheel Drive Vehicle (FWD) - with different drive-lines as shown in Table 1.3. The RWD vehicle is current production and the FWD vehicle is a prototype.

Table 1.3 Test Vehicle Platforms

Transmission	Engine	Drive-line	Brake system
Automatic	2.9 l V6	Rear Wheel Drive (RWD)	Teves Mk IV
Manual	1.6 l I4	Front Wheel Drive (FWD)	Bendix

Chapter 2 covers the initial modelling and analysis of a powertrain performed in order to understand phenomena associated with traction control. Parameters specific to the RWD vehicle have been used. This chapter introduces the traction control problem in detail and justifies the modelling approach taken. A full non-linear simulation model of the powertrain was built which was based largely upon the work of Hrovat et al (48) (49). The engine model used was treated as a 'black box', which was produced by Hrovat, along similar lines to the models described by Powell et al (52). The model has been used to examine the effects of the main non-linearities on

the open-loop dynamics of the vehicle powertrain. This analysis brings together in a formal setting a thorough examination of the open-loop dynamics of the traction control problem and as such is original work.

Chapter 3 covers the traction control investigation of the throttle enhancement to the rule-based brake control of the RWD vehicle. In this phase of the work the throttle and brake controllers were designed separately. The specific intention of the work was to develop a throttle controller with a brake controller having already been designed.

The simulation model, based on RWD vehicle data, was subjected to parameter sensitivity studies of the known non-linearities, delays and variable sample intervals in order to examine the feasibility of a particular control scheme. Having established feasibility of the approach, the model was used to develop a PID controller for the throttle control involving optimisation theory. The approach adopted in Chapter 3 represents original analysis and simulation studies carried out by the author. The work described identified major weaknesses in the rule-based brake controller, and as soon as a prototype vehicle became available the second phase of the work commenced.

The second phase of the work involved a new vehicle platform and hence a need to re-model the powertrain especially the engine model. Although the work covered in Chapter 5 was carried out on a different vehicle, it can be viewed as a logical extension to the work in chapter 3. Since only the torsional dynamics are being represented, the model structure for the FWD configuration remains similar to that of the RWD configuration. A simple representation of the fully engaged clutch replaced the torque converter model. In order to gain a better understanding of the engine dynamics, and to include spark and fuelling effects, the engine modelling in Chapter 4 was undertaken with Cook (72). This is described in Chapter 4 and forms a significant amount of the work for this phase of the study. This work was published by Crossley and Cook (72) and represents joint research by Jeff Cook and the author. A significant

amount of validation of the engine model has been performed. The full non-linear simulation is necessary because the traction control algorithm is required to operate over the entire operating envelope of the vehicle.

Chapter 5 is all original work by the author. The work was motivated by discussions and a brief study carried out jointly with Hrovat and was subsequently undertaken because of dissatisfaction with rule-based control. The results of the brief joint study are however not reported here. The work was carried out on the FWD model. The model reduction, control analysis and control system development represents original work which has been implemented on a prototype vehicle. The specific implementation was performed by Bendix, France as a supplier to Ford. The vehicle was transported to Arjeplog, Sweden where the system was tested on a polished frozen lake. The system was developed further on artificial low μ surfaces on test tracks in France and Belgium.

1.1 Figures

Figure 1.1 Typical Engine Management System

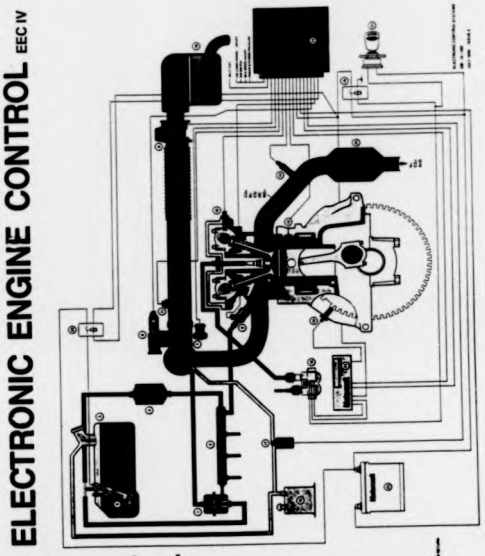

2 Powertrain model for Traction Control Studies

In this chapter, the necessary modelling requirements for the traction control study will be considered. The objective of the traction controller in terms of wheel slip will be discussed and the available solutions will be outlined. The model development for each of the individual sub-systems comprising the powertrain will also be considered. Having assembled a powertrain model, the model is analysed and the requirements for the throttle algorithm will be elaborated.

2.1 Powertrain Systems and Phenomena

A knowledge of the system dynamics, and phenomena associated with the powertrain, is an important requisite for appreciation of the difficulties associated with powertrain control. In understanding the system performance, a dynamic model of the system is helpful. Figure 2.1 shows two outline analytical models for a vehicle powertrain. The first model, Figure 2.1a, includes the dominant inertias and compliances necessary to describe phenomena up to approximately 80 Hz . This model describes two important phenomena, shuffle and gear rattle. The shuffle mode is the first vibration mode, normally associated with the 'kangaroo' start, with engine and vehicle inertias vibrating in anti-phase. The gear rattle mode is the second mode associated with the gear inertia in anti-phase with the vehicle and engine inertias. Typical frequencies for these phenomena are shuffle (2 to 7 Hz) and gear rattle (40 to 80 Hz) (73). The first model, Figure 2.1a, is a considerable simplification and does not show any damping. The second model, Figure 2.1b, introduces damping and, because the most significant amount of 'damping' exists at the tyre/road interface, the wheel inertia has to be included. It should be stressed that although the tyre characteristic is represented in Figure 2.1b as a variable viscous damper, no viscous pumping of fluid - as in the classic viscous damper - occurs; we are merely representing a force which varies. The arrow through the 'damper' is intended to show that the 'damping' varies. The second

major source of damping is from the clutch or torque converter. Damping is an important feature in vehicle drive-lines for it generally improves the driveability of the vehicle (51).

Figure 2.2 shows a schematic of the variation of longitudinal and lateral force with tyre slip ratio where the tyre slip ratio is defined as,

$$s = \left(\frac{r\omega}{v} - 1\right) \qquad (2.1)$$

During ordinary driving on good dry road surfaces, the tyres operate on the region of positive slip of the longitudinal force curve. From the perspective of the automotive designer , the slope of this region is fixed with a small variation around a nominal value. Its effect is analogous to the damping provided by the torque converter - i.e. a damper in series with the torsional elements of the drive-line (51). The level of damping achieved by a torque converter (see page 29 for a full description) is seen in Figure 2.12 which shows the relationship between input and output torque as functions of speed ratio across the converter where,

$$T_{imp} = \frac{1}{g^2}\omega_e^2 \qquad (2.2)$$

ω_e Engine flywheel/Torque converter impellor speed (s^{-1})

ω_t Gearbox input shaft/Torque converter turbine speed (s^{-1})

T_{in}/T_{imp} Torque ratio

ω_t/ω_e Speed ratio across the converter

If we assume that engine speed is fixed during a driveline oscillation, then the torque converter effectively applies to the drive-line a linear 'viscous' damping force above speed ratios of about 0.86. It is this factor which makes vehicles with automatic transmissions extremely smooth to drive.

Whilst the vehicle is being driven on ice, high levels of slip can occur at which the slope of the longitudinal force curve for the tyre (see Figure 2.2) can be positive, zero or negative. Under these conditions both the magnitude and the slope of the

longitudinal force curve influence the vehicle. The change in the slope leads to a very lightly damped system which can even become unstable. The reduction in magnitude of the curve clearly reduces the acceleration of the vehicle. Also shown in Figure 2.2 is the lateral force. This is also severely reduced at high slip levels, which tends to result in the loss of steerability in the case of FWD vehicles or lateral instability in the case of RWD vehicles.

The clutch damper is a damper in parallel with a stiffness over each of which the automotive designer has a degree of control. The damping provided by the clutch has the task of damping out gear rattle and shuffle. The two phenomena require different levels of stiffness and damping which leads to clutches having multiple stages as shown in Figure 2.3. The low stiffness region, with damping in parallel, is extremely effective for damping gear rattle and could be useful for damping out shuffle. The limitation is that such low levels of stiffness would require excessive clutch defections during drive, hence a two stage stiffness is necessary as shown in Figure 2.3. The use of a 'twin mass flywheel' overcomes this compromise by permitting a low stiffness and permitting large deflections. Typically a stiffness of 2.5 Nm per degree is possible over deflections of up to 120 degrees (73). Returning to Figure 2.1 and increasing the inertia of the clutch/transmission, it is possible to reduce the natural frequency of the second vibration mode (i.e. gear rattle) which together with increased damping now serves to reduce gear rattle. The increased damping levels also dampen the first vibration mode and thereby improve the shuffle response.

It is this core system which describes many drive-line difficulties and control problems, and although the drive-line could be further sub-divided into smaller distinct stiffnesses, inertias and dampers representing higher frequency phenomena, these would be beyond the frequency range of interest. Additionally, the drive-line models described in the previous paragraphs do not represent the individual drive wheels but

aggregate these into a single drive wheel. It will be seen that it is necessary to consider the dynamics of each wheel for the traction control schemes addressed in this study, hence the next logical extension to the model is to represent the differential and individual drive wheels as shown in Figure 2.4. This model will represent the higher frequency modes associated with the axle which are important for individual wheel speed control on slippery surfaces.

2.2 Traction Control

2.2.1 Introduction

Traction control can be considered to be analogous to anti-lock braking (ABS) but operating in the opposite sense i.e. the ideal system will provide maximum traction regardless of conditions and always maintain vehicle stability and driver control.

Figure 2.5 shows two typical longitudinal force versus slip relationships for a modern road tyre at two speeds (55). The force generated increases rapidly with tyre slip until a maximum is reached, typically between 8% - 20% slip. The force then decreases with percentage slip , the final point yielding a reduced force. In practice - without electronic control - the latter part of the curve is not usable because, as the slip relating to the maximum force is exceeded, the wheel rapidly over-spins (or locks in the case of braking) due to the negative slope.

Figure 2.6 shows a schematic representation of the relationship between lateral and longitudinal force for a modern road tyre. This indicates that at maximum longitudinal force the lateral force available for steering and vehicle stability is already severely reduced. By the point of over-spin (or lock up) shown by the extreme ends of the curve, the lateral force is so low that loss of steering and vehicle stability can occur.

Traction Control, like ABS, is aimed at maintaining near-to-peak longitudinal force while ensuring the lateral force available is not reduced to critical levels.

2.2.2 Traction Physics

When a vehicle is driven along a road, the driven wheels revolve faster than the non-driven wheels. The ensuing slip generates a longitudinal force to provide the vehicle acceleration. A longitudinal force-slip curve is shown in Figure 2.5. This figure shows the force/slip ratio relationship at two speeds and for two coefficients of friction. Each curve can be broadly divided into two regions:

i) the positive slope region for low slip values and

ii) the negative slope region for high slip values.

Insight into why the tyre characteristic follows its typical shape can be attained through consideration of a simple tyre model. A number of models have been proposed which give insight into the physics associated with tyre force-slip dynamics. The brush model explains the characteristic well (61). The tyre is considered to consist of radially oriented brush elements, see Figure 2.7, which bend as the driving torque increases. As the elements pass through the contact patch they bend more. The elements towards the end of the contact zone actually slide. This is due to the bending force exceeding the friction force between the element and the road. There are thus two regions in the contact patch:

i) Region a where the brush elements bend and

ii) Region b where the brush elements slide.

The positive slope region is explained by the bending of the brush elements. The tractive effort reaches a maximum as all the elements begin to slide. Maximum tractive effort is achieved when the tyre force is at a maximum. For good road surfaces, this is usually well in excess of the engine's capability. However, on less good surfaces such as wet roads or ice, this is not the case. The aim of the traction controller is to maintain the tyre slip at a level close to the optimum force point. The slip level at which the optimum force is achieved varies with surface (26). This

suggests that a traction controller should aim for a value of target slip which depends upon surface (22). In addition to maximising tractive effort, a traction controller also maintains vehicle stability. This is because the lateral force available also varies with longitudinal slip as shown in Figure 2.6. The lateral force is at a peak value for a rolling tyre and reduces as slip increases. If the tyre is allowed to operate at high levels of slip, then due to the low lateral force available, vehicle instability is likely. In the case of a RWD vehicle, the result of this destabilising effect is to cause severe oversteer and, in the case of a FWD vehicle, severe understeer.

2.2.3 Candidate solutions

The intention of a traction controller is to maintain wheel slip on the stable side of the peak of the mu-slip curve. This can be achieved using a variety of methods. These are outlined below (21). The reduction of drive torque can be achieved by the following techniques:-

i) throttle valve control for SI (Spark Ignition) engines

ii) fuel flow control

iii) spark advance control for SI engines

iv) transmission control

v) brake control or

vi) a combination of the above.

In addition, the distribution of drive torque to the driven wheels can be achieved by either:-

i) brake actuation to individual wheels or

ii) the use of a limited slip differential.

i) Throttle valve control

This is the primary method by which the driver controls power delivery to the wheels in a vehicle equipped with an SI engine. It has a full range of control between idle and maximum power. However, both its steady state and dynamic characteristics are highly non-linear. Figure 2.8 shows the non-linear steady state throttle-torque characteristic. These will be described more fully in Section 2.4. In addition the manifold filling effect, coupled with the induction-to-combustion stroke delay, limit the speed with which torque can be reduced at low speed/low load conditions, whereas at high speed/high load the throttle response is extremely fast. Thus it is likely that at high speeds throttle control will be fast enough to contain excessive wheel slip. This is extremely fortunate since it is undesirable to apply the brakes at high vehicle speeds. A further benefit of throttle intervention systems is that excessive engine overrun torque during gear shifts or deceleration can be controlled (43), (37).

ii) Fuel-flow Control

For a diesel engine, fuel-flow control is the primary method by which power output from the engine is controlled. This is in contrast to throttle valve control for SI engines. Fuelling control is very fast in comparison to throttle control since there is no manifold dynamic lag. In addition, the torque-fuel characteristic is approximately linear. These two factors would suggest that traction control of a diesel powered vehicle should be easier.

Similarly for an SI engine, fuel flow control does not have the manifold dynamic lag. Although there may be some dynamics associated with wall-wetting, it is well known that fuel control improves the transient response of SI engines. In contrast with the diesel case there is a limited range of authority since knock can occur. In addition, engine emissions will deteriorate as the engine is operated further from stoichiometry.

iii) Spark Advance Control

Clearly this is only an option for SI engines. The effect of spark advance on engine torque is immediate but, as with fuel control, is of limited range. In the case of the 2.9V6 Ford engine the torque can be reduced by approximately 35% before misfires occur. The reason for the torque reduction is that fuel is burnt less efficiently. This results in partially burnt hydrocarbons being exhausted which subsequently burn in the catalyst. This causes overheating of the exhaust catalyst and will ultimately lead to early catalyst failure. Hence spark control can only be used for brief periods early in the transient. BMW (37) retard the ignition by a scheduled amount during the throttle closing phase of a traction control cycle but, as the throttle opens, the ignition timing is restored.

iv) Transmission Control

Most drivers are aware of the fact that if, under slippery conditions, it proves difficult to take-off from rest (due to wheel-spin), it can be beneficial to repeat the attempt in a higher gear. The driver is effectively reducing the gain of the system by doing this. Thus if the vehicle is fitted with automatic transmission, by selecting a higher gear under low μ conditions, it is easier to drive the car. This type of solution is not a control solution but merely exploits a system characteristic and has been used by General Motors as a 'traction aid'. BMW (37) also modify the gear-shift schedule towards early up-shifting in order to 'control' wheel-spin.

Clutch Control and Torque Converter control are feasible methods of transmission torque control and may be practicable (43). However, engine speed flare coupled with the possibility of high clutch wear are severe disadvantages. Continuously Variable Transmissions (CVTs) could also be used and this idea has been introduced into the Ford concept vehicle ELTEC (18).

v) Brake Control

It is generally agreed by most of the major manufacturers that brakes cannot be used for a sustained period due to problems with overheating and wear. Teves (42) have a temperature model in the traction control algorithm which can predict brake temperature and shut the system down if the predicted temperature is excessive.

On uniform low μ surfaces, there seems to be some disagreement as to how brakes can be used in traction control systems. Toyota (28) use a combined throttle and brake system on the Toyota Crown, with only a single driven wheel-speed sensor and state that the brake control is to 'compensate for the disadvantage of [the throttle] response'. There appears to be disagreement within BMW as to the speed of response of brake controllers. Wallenowitz et al (41) state that 'pressure in the wheel brakes cannot build up very quickly for reasons of comfort' whereas Kraft et al (37) use brakes to improve the response of the system.

It is the author's view that brake control can be used for fast response if an accumulator is fitted. Without an accumulator, there will be a delay in response due to the hydraulic pump starting. This delay can be of the same order as the engine dynamics.

For a split-μ capability, brake control offers an inexpensive option (in contrast to a limited slip or locking differential) if ABS is already fitted. Traction control development using brake intervention has followed anti-lock braking as a logical extension. This is because there is much common hardware for the two systems and the control problem is essentially the same. The hardware used varies with manufacturer. They each comprise of a power source (a hydraulic pump), a system of electro-hydraulic valves to control the brake actuation pressure and hence braking torque. A hydraulic accumulator is often also included which is kept primed for rapid response. If an accumulator is used, the system can be used to increase the speed of

response of engine intervention systems (28). However this item has been deleted in a number of recent systems to reduce cost. In such cases, the vacuum booster (24) can be used for initial pressure build whilst the pump is started.

There are two major divisions in the way in which brake pressure is controlled. The first type (adopted by Bosch, Bendix, Kelsey Hayes and Lucas Automotive) uses a single valve to modulate the pressure at the wheels shown in Figure 2.11 (54). The second type (adopted by Teves (42) and Toyota (28)) uses two valves to control pressure, also shown in Figure 2.11.

From a control stand-point, the first type is preferable since the brake pressure is a function of the pulse-width-modulated (PWM) signal applied to the valve. This means that virtually no restriction exists in the control algorithm which can be applied. In the second type, the PWM needs to be directed to either of the two valves depending on what control action is sought. If the PWM is applied to the pressure increase valve, the first derivative of pressure changes and the restricted volume of the actuator acts as an integrator. This effectively adds an integrator into the brake control loop which has a destabilising effect. A further complication is that extra software needs to direct the control action to the appropriate valve.

2.3 Simulation Model Structure

There is a trade-off between simulation model complexity and development time for the model and eventual simulation time. Thus it is important to closely define the frequency range of interest in simulation study in order that the model constructed adequately represents the appropriate phenomena in that frequency range and does not include superfluous phenomena. For low frequency phenomena, such as vehicle fuel consumption over a driving cycle or prediction of vehicle acceleration, a relatively low order model (<5Hz) is all that is required.

For traction control, the torsional dynamics of the powertrain are of interest. The inclusion of a differential is essential to the study of μ-split phenomena and so a torsional model with the following characteristics was selected:-

i) complexity as shown in Figure 2.1b

ii) differential to be included

iii) non-linear tyre characteristic applied to each wheel

iv) non-linear engine dynamics

The intention of the powertrain model is to represent the dominant dynamics of the driveline between the throttle and driven wheels, including the brake actuation dynamics. In addition, a force/slip tyre-road interface characteristic is included for each driven wheel. The whole powertrain model was developed in an incremental modular manner. Distinct sub-models, such as the engine or tyre/road interface, were developed as separate modules whose function could be tested independently prior to assembly into the entire model. This process was facilitated by use of the modelling and control analysis package Matrix$_x$ (60). A further benefit of the graphically oriented modular structure of Matrix$_x$ is that it permits the incorporation of sub-models developed for other studies to be used. These distinct powertrain models are described more fully in (21),(52),(86),(55).

2.3.1 Engine Model

A representation of the 2.9 V6 engine was developed by Hrovat (49) for other research work within the company. A detailed description is not included since the model was treated as a black box and does not represent the work of the author. The model includes a representation of the non-linear manifold gas dynamics, torque generation dynamics assuming stoichiometric fuelling and spark timing determined by the Engine Management System (EEC IV). The model accounts for the speed-dependent

induction-to-combustion stroke delay. It has two state variables representing crankshaft position and manifold pressure. The model does not include exhaust gas recirculation (EGR) or the effect of spark advance on torque.

2.3.2 Torsional Dynamics

A schematic overview of the torsional model is given in Figure 2.4. The equations of motion for this model, moving from the flywheel to the road wheels, are readily obtained through the application of Newton's Second Law and are as follows:-

Flywheel

$$\dot{\omega}_e = \frac{1}{J_e}(T_e - T_{imp}) \tag{2.3}$$

Gearbox input shaft

$$\dot{\omega}_i = \frac{1}{J_i}(T_{tur} - 2r_e T_s) \tag{2.4}$$

Axle shafts and Differential Gear

$$\dot{\theta}_d = 2r_e\omega_i - \omega_{tur} - \omega_{wl} \tag{2.5}$$

$$T_s = K_{eq}\theta_d \tag{2.6}$$

where

T_e Engine torque (Nm)

T_{imp} Torque converter impellor torque (Nm)

T_{tur} Torque converter turbine torque (Nm)

T_s Axle shaft torque (Nm)

ω_e Engine flywheel speed (s^{-1})

ω_i Gearbox input shaft speed (s^{-1})

θ_d Axle deflection (rad)

J_e Engine Flywheel Inertia θ_e kgm^2

J_i Transmission inertia kgm^2

K_{eq} Equivalent axle shaft stiffness Nm/rad

r_e Overall gear ratio

The axle equations cannot be deduced by Newton's Second Law directly and hence are not immediately apparent. They can be derived using Bond Graph techniques (48). Alternatively, the application of Newton's Second Law followed by elimination of the higher order states using 'static condensation' (66) will yield the same result. Bond Graphs consider the energy flows through ports and therefore a detailed picture of the differential is unnecessary. The technique can be considered to be more appropriate since it is energy flow in which we are interested. However, if a detailed model of all the individual components is produced, then the same result can be obtained by setting the inertias of the small intermediate components to zero and 'condensing' out that state variable. This is identical to how model order reduction algorithms operate.

Wheels

$$\dot{\omega}_{wr} = \frac{1}{J_{wr}}(T_r - T_{wr}) \tag{2.7}$$

$$\dot{\omega}_{wl} = \frac{1}{J_{wl}}(T_r - T_{wl}) \tag{2.8}$$

where

J_{wr} Right wheel inertia kgm^2

J_{wl} Left wheel inertia kgm^2

T_{wr} Tyre/road interface torque (Nm)

T_{wl} Tyre/road interface torque (Nm)

ω_{wl} Left wheel speed (s^{-1})

ω_{wr} Right wheel speed (s^{-1})

2.3.3 Torque Converter

The torque converter is represented here by its static characteristic. This relates the input and output torques to the speed ratio across the torque converter. These static characteristics are based on data obtained from a test rig. The test data is represented

as a table of values of measured torques and speeds and is generally referred to as a 'torque absorption characteristic'. This method is satisfactory for the low frequency approach adopted in this study.

There are two approaches to modelling the torque converter statically:-

i) represent the static data Figure 2.12 by multiple linear regression equations or

ii) represent the static data by non-linear equations physically derived by consideration of the fluid flow and power loss.

The procedure adopted in this particular study is as (i) above. An area of improvement to the model would be to adopt the method (as in (ii) above) as shown in Lucas (63) and Kotwicki (64) and used in a previous study by Crossley et al (65). However, what is required is a black box model of the torque converter rather than a detailed understanding of the effects of parameter changes (e.g. fluid viscosity) on the vehicle powertrain.

The two key characteristics, which are both functions of speed ratio ($\omega_{out}/\omega_{imp}$)), are:-

(i) the K-factor which defines the relationship between the impellor torque and angular velocity where $K = \omega_{imp}/\sqrt{T_{imp}}$ and

(ii) the torque ratio which defines the relationship between impellor torque and turbine torque.

The static characteristic is given in Figure 2.12. This shows:-

i) the parameter $1/K^2$. The data is presented in this way since $1/K^2$ is directly proportional to the torque capacity of the converter (see equation 2.2).

ii) the torque ratio cross the torque converter (T_{out}/T_{imp}).

Each curve shows the measured data points together with the 'least squares fit' to the data.

As can be seen in Figure 2.12 each of these curves has a discontinuous derivative at a speed ratio of approximately 0.86. This is due to the transition which occurs when the static reactor blades begin to turn and the torque converter behaves as a fluid coupling with a torque ratio of unity.

In fitting equations to the data this discontinuity needs to be accounted for by fitting a pair of simple equations rather than a high order equation to attempt to describe the non-linearity. The equations are as follows:

If $s_r < 0.863$

$$T_r = 2.239 - 1.4439 s_r \quad (2.9)$$

$$\frac{1}{k^2} = 3.168 * 10^{-5} - 1.838 * 10^{-5} s_r^2 \quad (2.10)$$

If $s_r > 0.863$

$$T_r = 0.99 \quad (2.11)$$

$$\frac{1}{k^2} = 1.357 * 10^{-4} - 1.362 * 10^{-4} s_r^2 \quad (2.12)$$

2.3.4 Tyre Road Interface

This area of the modelling represents one of the most non-linear effects of the whole powertrain model. This sub-section addresses specifically the tyre contact patch. It should be noted that the stiffness of the tyre side walls, which is lumped with the axle shaft stiffness, is not part of this sub-model.

The tyre contact patch is central to the traction control problem and has been briefly referred to in section 2.2 when articulating the traction control problem. The general characteristic of longitudinal force generated by the tyre contact patch as a function of tyre slip is shown in Figure 2.2. The underlying physics behind the shape of the curve is only qualitatively understood, and it is for this reason that a phenomenological model is not available and a 'black box' static approach has been adopted. All that remains therefore is to obtain data and employ any standard curve fitting technique to provide a model of Forces versus slip. This presents significant practical problems because measurement of tyre slip and force requires the construction of special

bespoke rigs in order to obtain high quality data. In this particular study the equations justified, based on limited data and significant analysis, by Dugoff et al has been used (55). Dugoff's equations describe the more complex relationships between side force and longitudinal force with slip angle and longitudinal force. Qualitative agreement between these variables is shown. The complex relationships are shown to result in equations 2.13 to 2.16 for a tyre in which the slip angle and side force are each zero.

A normalised slip ($\bar{s}$) is derived for a braked wheel which for traction (50) becomes:-

$$\bar{s} = C_s \frac{s}{\mu F_z (1+s)} \qquad (2.13)$$

Two regimes are then defined which depend on whether or not there is sliding in the contact patch. These are:-

If $|\bar{s}| > 0.5$

$$F_t = \mu F_z \left(sign(\bar{s}) - \frac{1}{4\bar{s}} \right) \qquad (2.14)$$

If $|\bar{s}| \leq 0.5$

$$F_t = \mu F_z \bar{s} \qquad (2.15)$$

The tyre road friction coefficient varies with many variables. Of these speed is the most significant (55) which can be represented as follows:-

$$\mu = (1 - A_s v s)\mu_0 C_s \qquad (2.16)$$

where:-

F_t Tractive force (N)

F_z Normal force on tyre (N)

μ_0 Peak coefficient of friction (F_t/F_z)

μ Speed dependent coefficient of friction (F_t/F_z)

C_s Tyre slip stiffness ($N/slip$) ($C_s \in 25000, 100000, 200000$)

A_s Friction reduction factor 0.00353

The values chosen for A_s and C_s are the same as those used by Dugoff based on 'limited experimental data'.

2.3.5 Vehicle Linear Acceleration Dynamics

$$\dot{v} = \frac{1}{m_v}(F_d + F_w - F_{load}) \quad (2.17)$$

$$F_{load} = a_{rl} + b_{rl}v + c_{rl}v^2 \quad (2.18)$$

where:-

F_{load} Road load (N)

v vehicle speed (m/s)

a_{rl} Road load equation constant term (N)

b_{rl} Road load equation velocity term (Ns/m)

c_{rl} Road load equation aerodynamic term (Ns^2/m^2)

2.3.6 Model Parameterisation

This was based initially upon vehicle data obtained from drawings and data-sheets for the vehicle. This is given in the Table 2.1 below.

Table 2.1 RWD Model data

Parameter	Symbol	Value
Engine Flywheel Inertia	J_e	$0.14kgm^2$
Transmission inertia	J_t	$0.0594kgm^2$
Overall gear ratio	r_o	see Table 2.2 below
Wheel inertia	J_w	$1.1kgm^2$
Equivalent axle shaft stiffness	k_{eq}	$1700Nm/rad$
vehicle mass	m_v	$1750kg$
rolling radius of tyre	r	$0.303m$
Road load (constant term)	a_l	110.0
Road load (velocity term)	b_l	$0Ns/m$
Road load (aerodynamic term)	c_l	$0.381Ns^2/m$

Table 2.2 Gear Ratios

Gear	1st	2nd	3rd	4th
Ratio (r_{gb})	2.414	1.414	1.0	0.575
Overall ratio (r_o)	0.1138	0.1943	0.2747	0.4777

(N.B. Final Drive Ratio (r_{fd}) 3.64)

2.4 Open loop Analysis

The approach to the control system in this study has been to use the model to understand the stability issues with the traction control problem and with this knowledge develop a controller which is stable under all the conditions. This is to be achieved by using a PID algorithm and using gain scheduling to adapt the controller to changes in system dynamics. This should lead to a control system which is robust to known non-linearities. In this section, the powertrain model developed will be used to explore the control and stability issues of the system.

In this section, the four key non-linear effects will be explored. These are:-

i) The tyre force/slip relationship.

ii) Torque converter

iii) The engine torque production characteristic.

iv) Gear Ratio

Tyre Force-slip effects

Figure 2.13 shows a root locus of the open loop poles of the system for the powertrain, excluding the torque converter characteristic as the slip to the driven wheels increases from pure rolling to approximately 20% slip. The μ-slip characteristic of the tyre is shown also in Figure 2.13. The root-locus shows:

i) The natural modes for the wheels

ii) An oscillatory mode associated with the axle compliance/wheel & engine inertias

iii) The pole due to the vehicle inertia/vehicle road load.

The wheel modes are initially in the far left half of the complex plane. This is not shown for scaling reasons, but the modes begin at the points $(-945, j0)$ & $(-954, j0)$. As the tyre characteristic is traversed, these poles move to the right and, as the peak of the μ-slip curve is approached, the poles accelerate very rapidly towards the imaginary axis.

The vehicle mode is situated slightly to the left of the origin (due to the damping provided by the road load) and this mode also moves to the right as the peak of the μ-slip curve is traversed.

The oscillatory pole pair begin at the points ($-1.55, \pm j21.8$) and initially move to the left. This mode is associated with the vehicle shuffle mode and clearly shows the damping increasing as the slope of the tyre characteristic decreases. This is consistent with work by Hrovat (51). At a critical tyre slope, the mode becomes very well damped at the ($-34.3, \pm j23.56$) point. As the slope progressively decreases from this critical value, a higher frequency mode emerges with the damping reducing eventually to zero as the peak is traversed. This higher frequency mode is due to the wheels beginning to oscillate independently of the vehicle body mass.

At the peak of the μ-slip curve, all of the poles are on the imaginary axis and, as the negative part of the slope is reached, the poles move to the right half plane and the system becomes unstable. It is worth noting that when a vehicle drives from a good road surface onto ice, the above transition into instability occurs extremely quickly (i.e. within several milliseconds) and therefore a control scheme requires high derivative action to catch the over-spin.

Torque converter effects

The effect of introducing the torque converter can be seen in Figure 2.14. This introduces one additional state. This is associated with the engine inertia now being split into (i) the transmission inertia (including the torque converter turbine) and (ii) a reduced engine inertia (i.e. flex plate, torque converter impellor and gears). The torque converter generates an input torque which is related by the k factor (Figure 2.12) to slip across the converter and an output torque multiplied by the torque ratio (Figure 2.12). This slip related torque is effectively a damper in series between the engine and gearbox inertias.

The addition of a torque converter does not significantly change the wheel modes and vehicle mode described above. The change introduces a further pole at the origin and increases the damping of the oscillatory mode. The oscillatory pole pair now start at $(-8.9, \pm j23.4)$. This represents the same shuffle mode described above, but with considerably more damping. This is due to the significant damping provided by the torque converter described above. This complex pole pair follow the same trend as described above for the situation without the torque converter, except that for the same level of slip, the high frequency oscillatory mode finishes at $(-3.14, \pm j61.42)$ rather than crossing the imaginary axis - i.e. more stable. This illustrates how the torque converter introduces more damping into the powertrain.

Engine torque production

As was stated in section 2.3.1, the engine model used was a black box description (coded in Fortran with a variable delay and non-linear manifold) incorporated within the code. This model represents both the non-linear steady-state and dynamic behaviour of the engine. With this structure, it was not possible to linearise the model and analyse the engine system dynamics. For this reason, the engine characteristics will be analysed directly.

The steady-state torque characteristic for the engine is shown in Figure 2.8. This clearly shows a non-linear dependence of torque on throttle angle. This is approximately logarithmic with low throttle angles giving a large change in torque compared with high throttle angles giving a relatively small change in torque (i.e. at 1000 r/min, 2% to 5% throttle gives a change in torque of approx 68Nm whereas 22% to 27% gives a change in torque of approx 8Nm).

Significant dynamics are associated with manifold filling. Powell et al (52) show that the manifold dynamics can be represented as a first order lag with a time constant given by:-

$$\tau_p = \frac{K_p}{\left(\frac{\partial \dot{m}}{\partial P} - \frac{\partial \dot{m}_a}{\partial P}\right)}$$

Hence the manifold time constant can be interpreted directly from the induction map (Figure 2.9) as being inversely proportional to the angle subtended between the constant speed lines and the constant throttle lines. At high loads and high speeds this angle is large, implying a small time constant; whereas at low speed and low load this angle is small, implying a large time constant. From the induction map for the engine (Figure 2.9) the partial derivatives, and hence the manifold time constant, have been calculated. This yields the characteristic shown in Figure 2.10.

The effect of engine operating point upon both the steady state and dynamic torque production characteristics is large.

Gear Ratio effects

In order to explore the effects of gear ratio, an analytically linearised model has been subjected to eigenvalue analysis at (i) fixed vehicle speed and varying gear ratio and (ii) fixed engine speed and varying gear ratio.

Figure 2.15 shows the eigenvalues of the system with varying gear ratio from 1st to 5th at a constant vehicle speed of 5m/s. There are 6 modes as follows:

i) Two high speed wheel modes at $(-1669.3, j0)$ and $(-1690.3, j0)$(not shown).

ii) A manifold mode fixed at $(-15.6, j0)$ (not shown).

iii) A vehicle mode which moves from $(-3.14*10^{-3}, j0)$ to $(-7.96*10^{-3}, j0)$ as gear ratio goes from 1st to 4th.

iv) An oscillatory pole pair associated with axle compliance which moves from $(-1, \pm j36.5)$ in first gear to $(-1, \pm j88.5)$ in fourth gear.

Clearly it is this latter mode which would be of most interest to a throttle controller, and any strategy which attempts to place a zero on these highly oscillatory poles would fail as the poles move.

The effect of increasing vehicle speed with gear ratio in order to maintain a constant engine speed is shown in Figure 2.16. Compared with the constant vehicle speed analysis above, the wheel modes move further left with increasing vehicle speed. The vehicle mode moves slightly less towards the right. These changes are relatively trivial in comparison with the increased damping now associated with the oscillatory pole pair.

As we move towards the peak of the μ-slip curve, the higher frequency mode seen previously in Figure 2.13 and Figure 2.14 is clearly seen to emerge at $(-0.61 \pm j66.2)$ for first gear moving to $(-.30 \pm j104.3)$ in fourth gear, and it is this oscillatory mode which moves most with gear ratio as shown in Figure 2.17. Also shown in Figure 2.17 are the wheel modes which are now much closer to the origin, but these shift less with ratio. The effect of increasing vehicle speed serves to provide increased damping to the oscillatory poles as shown in Figure 2.18.

2.5 Figures

Figure 2.1 Outline analytical models for a drive train

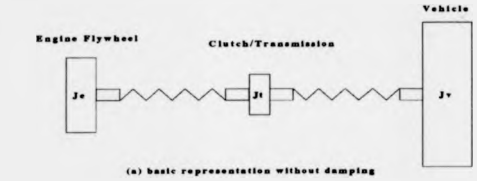

(a) basic representation without damping

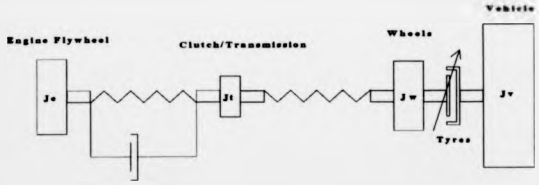

(b)Clutch damping and tyre/road interface shown

Figure 2.2 Typical tyre characteristic

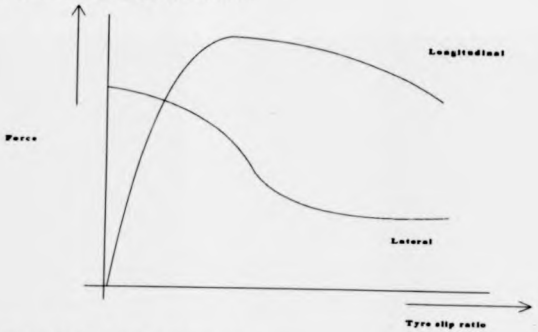

Figure 2.3 Typical clutch characteristic

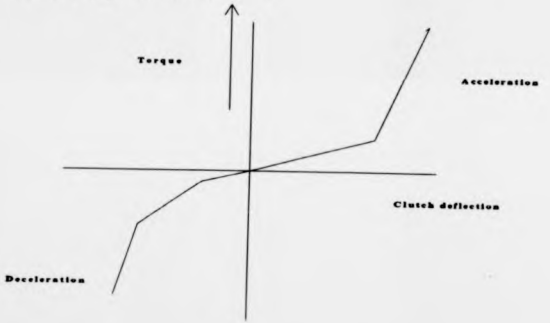

Figure 2.4 Torsional model of rear wheel drive vehicle

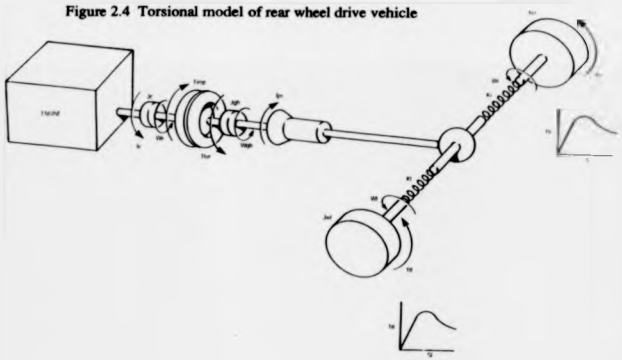

Figure 2.5 Longitudinal Force as a function of tyre slip

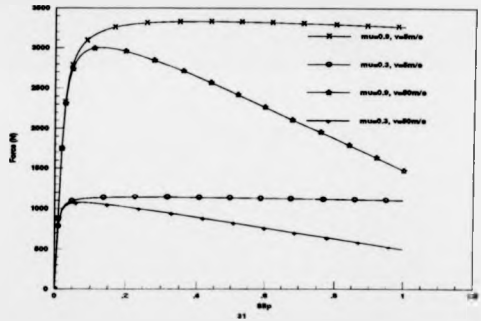

Figure 2.6 Schematic curve showing longitudinal Force vs lateral force for an automobile tyre.

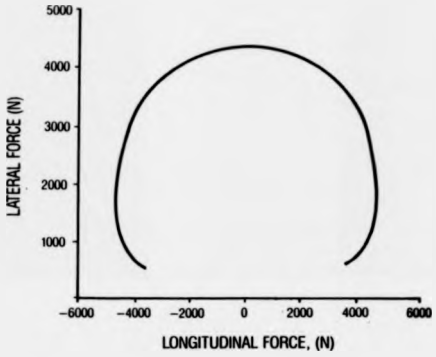

Figure 2.7 Brush Type Tyre Model

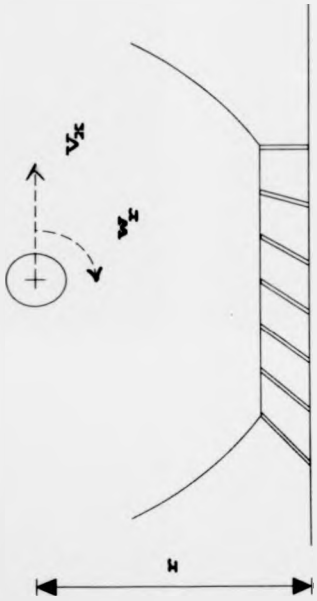

Figure 2.8 Steady state engine torque characteristic

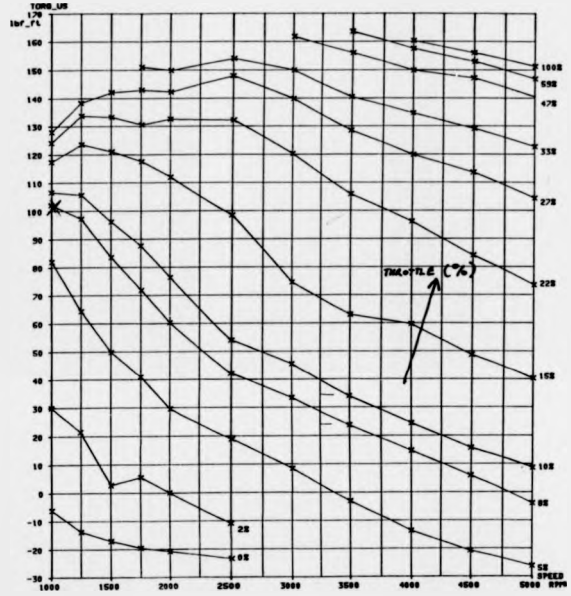

Figure 2.9 Induction map for the Ford 2.9V6 engine

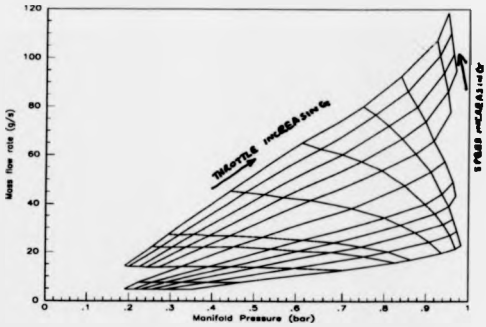

Figure 2.10 Manifold time constant variation with speed and throttle angle

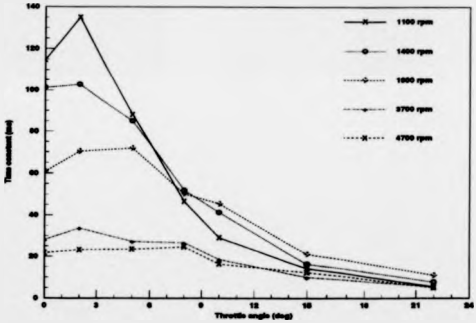

Figure 2.11 Schematic of ABS valve configurations

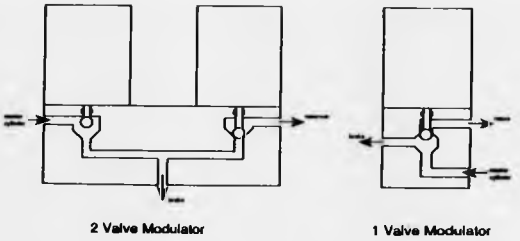

Figure 2.12 Static torque converter characteristic

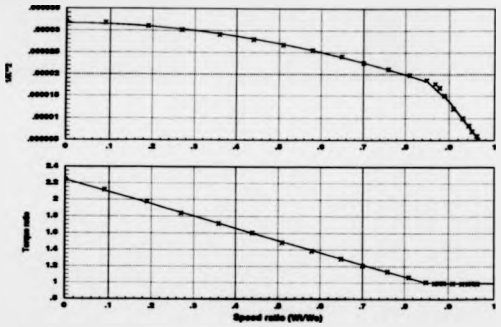

Figure 2.13 Root locus of the powertrain for an excursion on the tyre characteristic without the torque converter

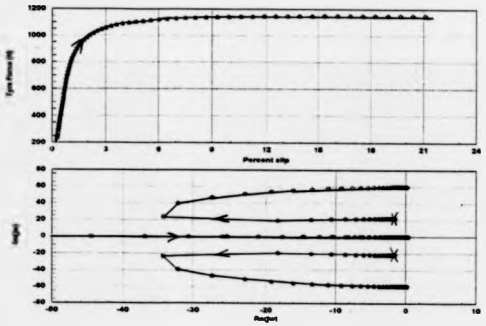

Figure 2.14 Root locus of the powertrain for an excursion of the tyre characteristic with the torque converter included.

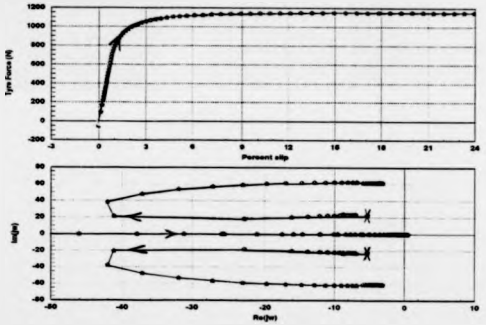

Figure 2.15 Root locus of the FWD powertrain with gear ratio, at constant vehicle speed, and to the left of the μ-slip curve peak

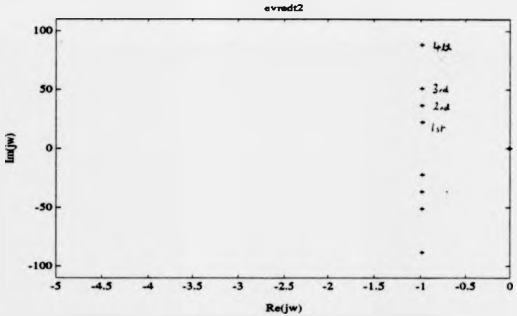

Figure 2.16 Root locus of the FWD powertrain with gear ratio, at constant engine speed, and to the left of the μ-slip curve peak

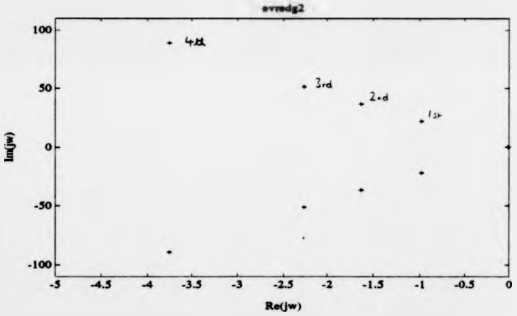

Figure 2.17 Root locus of the FWD powertrain with gear ratio, at constant vehicle speed, and close to the μ-slip curve peak

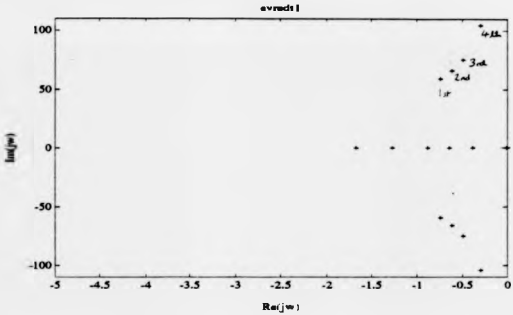

Figure 2.18 Root locus of the FWD powertrain with gear ratio, at constant engine speed, and close to the μ-slip curve peak

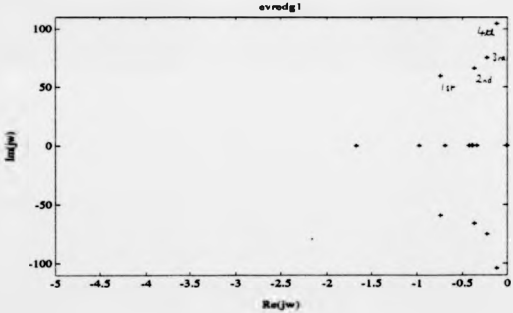

3 Throttle control enhancement to rule-based ASR

The scheme addressed in this particular study uses a combination of throttle and brake intervention on a rear wheel drive vehicle. An electronically controlled throttle valve is used for engine torque modulation. The brake intervention scheme uses a similar electro-hydraulic system to that currently used in ABS. The system is outlined in Figure 3.1. Figure 3.1 shows a system outline for the traction control system; the brake control module is used to perform the wheel speed signal processing, control the brakes and send wheel slip error information to the engine management system. This controls the throttle and its function is to attempt to maintain the wheel slip error at zero.

In principle, the brakes are required to provide slip control on a split μ surface and for a very rapid response to controlling wheel-spin on uniform low μ surfaces. The throttle control which is slower is used following the initial control of wheel-spin by the brakes. It should be stressed that the great advantage of using brakes is that a split μ capability is obtained, with a small on-cost, if ABS is fitted.

Under ideal circumstances, the development of a combined throttle and brake controller would be based upon a control theory approach in order to handle the interaction in the individual control loops. However, for the scheme addressed in this chapter (21) and outlined in Figure 3.1, the brake algorithm had been previously fixed and this used a rule-based ASR strategy.

The intention behind structuring the controller in this way was to see if a PID algorithm could be successfully implemented with a rule-based brake controller. The unfortunate effect is that it is not possible to linearise the system and thereby apply any control system design technique to the throttle system when brake intervention is active.

3.1 Rule-based ASR - how it works

The type of control laws implemented by the major ABS/TCS suppliers are rule-based algorithms. They operate on slip and acceleration thresholds being exceeded before control action is taken.

The intention of these algorithms is to allow the wheel slip to limit cycle around the peak of the mu-slip curve. The reason for this development is that, in general, the algorithms are inverted ABS algorithms whose original intent was to mimic cadence braking.

The number of decisions taken can be considerable. Detailed analysis of the strategy used for this system showed that approximately 20 slip and acceleration thresholds are used to establish whether to actuate the brakes to pressure build, hold or decay. The rate of build or decay is based upon a further series of decisions. These thresholds are derived experimentally relying largely upon trial and error. A typical rule is shown below:-

```
If wheel slip is low then
        If wheel acceleration is high then
                Actuate brakes {Brake actuation = f(vehicle acceleration)}
        Else
                Do nothing
Else
                Actuate brakes {Brake actuation = f(vehicle acceleration)}
Endif
```

This approach is evidently typical of rule-based traction control. Tan (27) describes another rule-based controller which also divides the wheel slip/acceleration

phase plane into sectors corresponding to a control action (Apply, Hold or Release). The intention of this algorithm is to produce an 'optimal' limit cycle in the phase plane.

Another way of looking at rule based ASR is that it seeks to establish realistic wheel slip and acceleration levels in determining what is happening. During vehicle acceleration, wheel acceleration should never exceed a value which would give vehicle acceleration of over 1g and if we know that the peak of the μ slip curve always occurs at slip values of less than, say, 20%, it is possible to define a slip/acceleration region in which we are sure that we require intervention. In contrast, as the wheel recovers from over-spin, either because of control action or a change in surface, a similar slip/acceleration region can be defined which can be used to remove the control action.

3.2 System configuration and Feasibility

Figure 3.2 shows the block diagram of the traction control scheme described above. The non-linear dynamics have been discussed previously in Chapter 2. Before constructing hardware, a simulation study of the scheme was embarked upon specifically to investigate the effects of the variable delays. These delays are associated with the EEC IV (i.e. the throttle controller) and the communication delay.

3.2.1 Overview of the control problems

The experimental traction control vehicle is rear wheel drive with an automatic transmission. The vehicle has a stand-alone brake control module based around the Intel 8052 microprocessor which drives an expanded electro-hydraulic system also used for ABS. This module communicates wheel slip and brake activity information using an 81C62 RAM/CART device, especially designed for use with the EEC IV

microprocessor. The brake control algorithm uses a rule-based algorithm, whilst the engine module uses a PID based algorithm to control the full authority electronic throttle.

The control system proposed above is multi-variable and non-linear. The system and control issues are fully described in reference (21). The system is outlined in Figure 3.1. A complication of this scheme is that it involves the interaction of two computers with the vehicle drivetrain. The communication process itself poses potential difficulties as this will introduce a delay into the control loops. This delay is made up of:-

i) signal processing within the brake control module. This runs at a constant loop time of 7ms.

ii) transmission of information from the brake control module to the EEC IV. The communication time is inversely proportional to the amount of data being transferred.

iii) calculation delays within the engine management system. This delay is also variable.

In view of the inherent complexity of the powertrain control system, there is a clear need for a systematic approach to the control algorithm development. In order to assist in the process of controller development, the mathematical model described in Chapter 2 together with a discrete black box model of the brake control strategy provided, communication delays and EECIV microprocessor loop time was used. A schematic overview of the model is given in Figure 3.2.

In particular, the intention of this study - in addition to establishing acceptability - was to develop a preliminary calibration of the PID throttle strategy.

3.2.2 Loop time variation study

Figure 3.7 illustrates the response of the throttle control system. In this simulation, the vehicle is accelerating on a good road surface when, after 1.2 seconds, it encounters a low μ surface representing packed snow. The target normalised wheel-spin is 0.3. The control action has not been optimised but does reduce wheel-spin within approximately 1.5 seconds with a small amount of undershoot between 3 and 4 seconds into the simulation.

Figure 3.8 & Figure 3.9 illustrate how the response varies when the loop time of the EEC IV system is increased and decreased by 50%. The response time of the controller is similar for each case. In the case of an increasing loop time, Figure 3.8, a small ripple in wheel-spin has been introduced. This illustrates a marginally stable situation being approached which the simulation indicates occurs when the loop time is doubled. In the case of a decreasing loop time, Figure 3.9, the response remains stable. The results illustrate the robustness of the control algorithm used and permit an examination of the bounds of variability in the loop time of the engine management system.

3.2.3 Asynchronous communication issues

A similar study has been performed in which the transmission delay was also varied in order to determine how large a delay is feasible. The transmission delay associated with transferring wheel slip to each wheel and brake status to each wheel and a checksum led to a 14ms delay. On the basis of the simulation model analysis before hardware was constructed this response was judged as being acceptable.

3.3 Development of Throttle loop Control Strategy

Since the brake algorithm is rule-based, it initially proved necessary to calibrate the controller by trial and error. An alternative method which relies on optimisation theory (62) was developed (22) which tunes the PID algorithm in the throttle controller

to minimise an integral error-squared based cost-function. The intention was to minimise the over-spin when a low μ surface is suddenly encountered. The PID controller was tuned for a number of different operating conditions using the optimisation routine. The rationale behind the choice of operating conditions has been discussed in chapter 2. This led to the implementation of gain scheduling for gear ratio and engine speed, both of which were measurable. The model was tuned using the optimiser, described below, for particular operating points defined in terms of gear ratio and engine speed in order to determine how to adjust the PID calibration.

3.3.1 Tuning of the PID controller

The PID gains for each operating point, specified in terms of initial engine speed and ratio, were derived using an optimisation routine. This was done because, as previously outlined, the brake control algorithm has already been fixed with a rule-based strategy. In addition, the model is multi-rate due to the sample intervals associated with the EEC IV, brake control module and engine firing frequency.

If an error is defined between the model output and an ideal response as equation 3.1:-

$$e = y_{opt}(t, b) - y_m(t, \beta) \qquad 3.1$$

where:-

t = time

y_{opt} = the best possible response see Figure 3.3

y_m = the actual model response see Figure 3.3

b = the parameter(s) (unknown) which give the optimum response.

β = the actual parameter(s) which yield the simulated response.

N.B. The best possible response, which is no over-spin occurring when the accelerating vehicle hits ice, is probably unachievable. Despite this, it is still a sensible target for the optimiser.

We need to minimise the error squared as in equation 3.2.

$$E = \int_0^T e^2 dt \tag{3.2}$$

This will in general be an even function where the sign of the error does NOT indicate in which direction it is necessary to adjust the parameter to reduce the error. Substituting equation 3.1 into equation 3.2 and differentiating with respect to the parameter β yields equation 3.3.

$$\frac{dE}{d\beta} = 2\int_0^T (y_{sp}(t,b) - y_m(t,\beta))\frac{de}{d\beta}dt \tag{3.3}$$

where

$\frac{de}{d\beta} = -\frac{dy_m}{d\beta}$ from equation 3.1

This is an odd function where the sign of the error does indicate in which direction it is necessary to adjust the parameter. The computed derivative $dE/d\beta$ is a parameter sensitivity coefficient which can be used to adjust the parameter β as shown in equation 3.4.

$$\beta_{(i+1)} = \beta_{(i)} + \gamma_n \frac{dE}{d\beta} \tag{3.4}$$

This adjustment scheme is called a 'steepest descent algorithm' and is very stable. It has been used in preference to the standard more sophisticated algorithms available within Matrix$_x$ since it is very robust.

For the PID controller, we need to alter each of the three P, I & D gains and so equation 3.4 is normalised for each gain as shown below:-

$$P_{(i+1)} = P_{(i)} + \left[\frac{\gamma_n}{E_{ms}}\right]\frac{\partial E}{\partial P} \tag{3.5}$$

$$I_{(i+1)} = I_{(i)} + \left[\frac{\gamma_n}{E_{ms}}\right]\frac{\partial E}{\partial I} \tag{3.6}$$

$$D_{(i+1)} = D_{(i)} + \left[\frac{\gamma_n}{E_{ms}}\right]\frac{\partial E}{\partial D} \tag{3.7}$$

where

$$E_{sc} = \sqrt{\left(\frac{\partial E}{\partial P}\right)^2 + \left(\frac{\partial E}{\partial I}\right)^2 + \left(\frac{\partial E}{\partial D}\right)^2} \qquad (3.8)$$

This theory has been incorporated into a command file within Matrix$_x$ which leads to a menu-driven user-friendly routine. It is necessary to select:-

i) an initial PID calibration which is preferably stable

ii) a perturbation for each of the P,I & D values (α%)

iii) a value for the magnitude of parameter adjustment (γ_c)

Having provided an initial PID calibration, the routine runs a simulation and then re-runs a further three simulations with each of the P,I & D parameters perturbed as in (ii) above. From these four simulations, the parameter sensitivity coefficients $\left(\frac{\partial E}{\partial P}, \frac{\partial E}{\partial I}, \frac{\partial E}{\partial D}\right)$ are computed. The new values for the PID controller are calculated as in equations 3.5 to 3.8 above and the process is repeated. At each new PID calibration, the simulation is plotted together with a value for the cost function (equation 3.2) so that the user can monitor the progress of the 'optimiser'.

Care needs to be taken in selection of values for γ and α. A perturbation of 10% in the parameters ($\partial P, \partial I \& \partial D$) was found to be a reasonable value. The value chosen for γ depends on the scaling of the problem and length of simulation and was found very quickly by trial and error. Too high values cause the 'optimiser' to oscillate around an optimum and too low values causes too slow a convergence on the optimum. Figure 3.4 shows a typical run with the upper plot showing the progress of the PID calibration as the parameters are adjusted. The model output being optimised is slip error. The parameter 'slip error' is defined as the difference between actual driven wheel speed and desired driven wheel speed. The desired driven wheel speed is a function of the non-driven wheel speed, hence zero slip error means that the controller is achieving the target slip. Clearly the optimum level of slip error is 0

km/h. The lower curve of Figure 3.4 shows the progress of the optimiser cost function (equation 3.2) for the starting point for the optimiser and four subsequent iterations. A good calibration is achieved within four iterations, however if the optimiser is left running for a further eight iterations, the cost function is further reduced very slightly whilst the quality of control degrades slightly. Figure 3.5 shows the result of the starting point of the optimisation routine and, for clarity, the cost function after the fourth, eighth and twelfth iteration. Clearly the optimum calibration in terms of cost function is more oscillatory than desired and in this respect, care is necessary in the use of this procedure. Figure 3.6 shows the PID calibration during the whole 12 iteration optimisation shown in Figure 3.5. If the optimiser is left to run for more iterations, then the PID gains shown actually oscillate between the last two shown in Figure 3.5.

3.3.2 Gain scheduling rationale

The open loop analysis in Chapter 2 has justified the inclusion of scheduling of gains as functions of engine speed and gear ratio. For this reason, the optimiser was run on the model for a number of speeds and ratios in order to calibrate the control algorithm.

In addition to the PID strategy defined above, it proved necessary to make a large scheduled cut in throttle as the wheels began to spin excessively. This is due to the rapid transition from a stable system to instability as shown in Chapter 2.

Figure 3.10 shows the response of the control system to a step change in μ whilst the vehicle is accelerating in third gear. This simulates the vehicle being driven from a good road surface onto packed snow. The parameter shown is slip error where zero slip error represents the optimum value for traction. The wheel-spin is contained within approximately 0.6 seconds. Figure 3.11 shows the response of the same controller, this time with first gear engaged. Engine speed remains the same as for Figure 3.10. The wheel-spin is now contained within approximately 0.7 seconds, but with significant 'overshoot' illustrating a deterioration in the controller performance.

If the controller is re-tuned for these new conditions, see Figure 3.11, the response of the controller now contains the wheel-spin, again within approximately 0.6 seconds and without any significant 'overshoot'. It is worth noting at this point the drive-line oscillation which is clear in Figure 3.11 and Figure 3.12. This is due to drive-line compliance and illustrates that drive-line oscillations tend to be more severe at lower vehicle speeds. Furthermore, the oscillation tended to upset the PID controller for high values of derivative gain. For this reason, PI control was used under most conditions. The justification for this is that the brake control will give the speed of response for the system.

3.4 Validation with vehicle tests

Having established a table of gains for varying conditions (gear ratio, engine speed and brake status), the algorithm was implemented on a vehicle. The preliminary gains derived through this simulation work were found to give good performance with only minor re-adjustment. The work has been taken further to account for variations in the tyre-road interface on the vehicle.

The following signals were logged during the testing:-

i) engine speed

ii) each wheel speed

iii) throttle position

iv) brake pressure and

v) gear ratio

The data was logged using the Ford Vehicle Data Acquisition System (VDAS) which uses a Data Translation data acquisition card in an IBM PC. This acquires data using Direct Memory Access. VDAS is based around a series of macros for the Asyst data acquisition package.

The work was carried as part of a larger project within Ford (19) looking at advanced control system design and for this reason the test work was carried out at Sault St Marie, Michigan, U.S.A. The climate here is ideally suited with temperatures consistently below freezing from November through to March. The test track is a disused U.S. air force base with the aircraft runway modified to yield the surfaces required for testing - polished ice (μ approx 0.1), packed snow (μ approx 0.3) and dry concrete.

The testing was carried out in a structured manner with initial trials being restricted to throttle only control with first gear only being engaged. The controller was tuned to be stable for the take-off from rest manoeuvre. Figure 3.13 shows the response of the controller to an aggressive take-off from rest.

Having established stable control, the brake intervention was restored and it was found that the controller remained stable without re-tuning. This can be seen in Figure 3.13 and Figure 3.14. The brake intervention persisted for only the initial wheel-spin flare up.

The feature to note in these two responses is that the control action remains stable irrespective of brake status. The reason for the improvement in acceleration for Figure 3.14 is most likely due to the variation in snow surface conditions.

It will be recalled that the throttle controller is working to the same slip level as the brake controller. Due to variability in the condition of the test surfaces with increased temperature, the controller response varied and proved to be incapable of being stabilised. Under these conditions a significant enhancement in control occurred through the modification of the target wheel slip so that the controller now limited the wheel-spin to a lower value (i.e. a manual adjustment of the controller set-point was made). This modification led to a considerable improvement in performance as can be seen by comparing the two responses in Figure 3.15. With this modified lower target

slip the response of the controller became more consistent irrespective of temperature. The disadvantage of using a lower value of target slip is that when the vehicle is accelerating hard on a good road surface, the traction controller becomes operative. This is consistent with tyre/slip data measured and presented by Schulze et al (39). It is therefore necessary for the controller not to work to a specific value of slip as this depends on surface conditions. For the two results shown in Figure 3.15, the acceleration times were within the bounds of experimental error thus indicating that both slip levels achieve approximately the same wheel force.

The data gathered during this study has been used to partially validate the Matrix$_x$ model of the vehicle powertrain. The degree to which the model and vehicle correlate is encouraging as can be seen in Figure 3.16. In Figure 3.16 the throttle value recorded during the experiment was used to drive the simulation model. The engine simulation model is too idealised in that it takes no account of the delay in torque production due to fuel transients, and subsequent partial misfires which occur with the real engine. In order to attain the correct response, a delay was introduced into the throttle perturbation applied to the simulation to mirror the expected engine torque response. The other responses shown in Figure 3.16 compare the model and vehicle response. This behaviour, i.e. the idealised torque production, was consistent across all the data considered. To ensure that this is the case, the engine model needs to be separately validated.

3.5 Concluding Remarks

The PID throttle controller proved to be very robust and the same set of gains worked well irrespective of brake status. The PID controller was tuned very rapidly on the vehicle. The pole/zero positions of the PID controller was as predicted by the

simulation, with only a simple adjustment of the loop gain being made on the vehicle. This should be compared with threshold controllers which take many weeks of intensive calibration.

Due to commercial pressures, the work on this vehicle platform had to be abandoned and for this reason no further development was carried out. However, the general lesson learned, i.e. that the approach using a classically based control algorithm - developed through the use of simulation - can be successful, was worthwhile and can be continued for the next phase. The work also revealed that the brake control could be improved. The second phase of the work involved a new vehicle platform and hence a need to re-model the powertrain, including the engine.

3.6 Figures

Figure 3.1 System outline of the traction control system

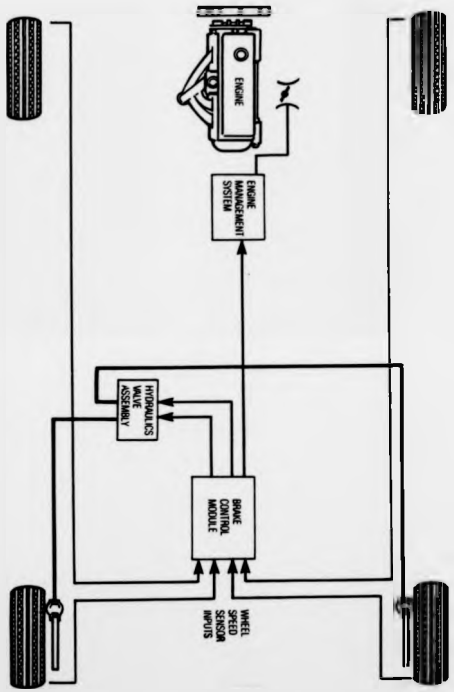

Figure 3.2 Block diagram for the traction control scheme.

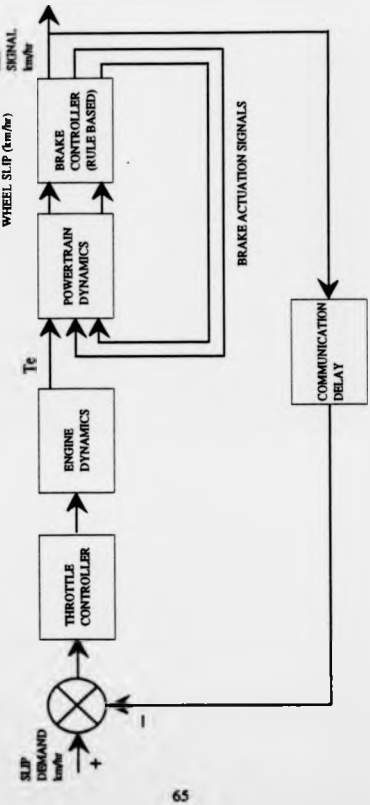

Figure 3.3 Basis for design technique used for choosing P,I & D gains for throttle controller

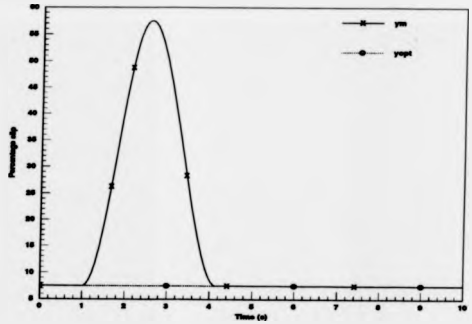

Figure 3.4 Optimiser output for the starting condition and four iterations (Simulation)

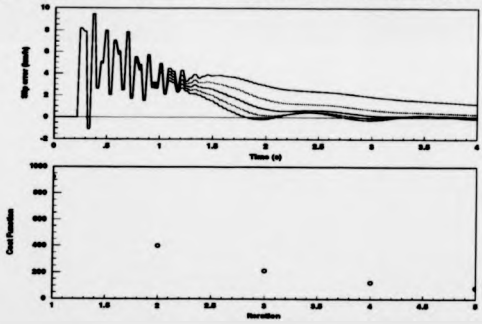

Figure 3.5 Optimiser output for the starting condition and after the fourth, eighth and twelfth iteration (Simulation)

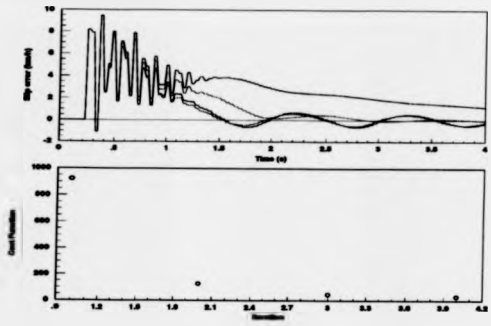

Figure 3.6 Progress of the PID calibration during the whole 12 iteration optimisation process

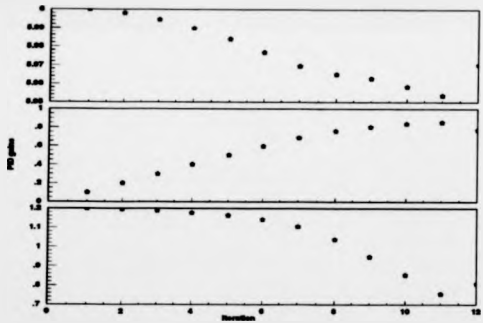

Figure 3.7 Response of throttle controller to step change in mu-value. Nominal loop time (Simulation)

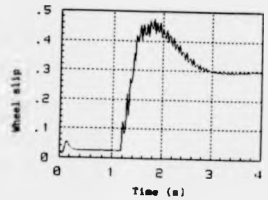

Figure 3.8 Response of throttle controller to a step change in mu-value. Increase loop time by 50% (Simulation)

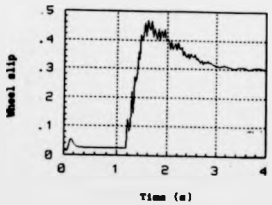

Figure 3.9 Response of throttle controller to a step change in mu-value. Decrease loop time by 50 % (Simulation).

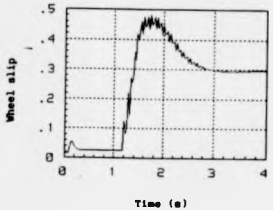

Figure 3.10 Response of throttle controller to a step change in mu-value. Third gear engaged (Simulation).

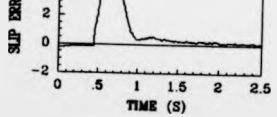

Figure 3.11 Response of throttle controller to a step change in mu-value. First gear engaged (Simulation).

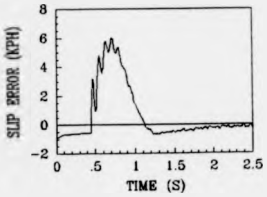

Figure 3.12 Response of throttle controller to a step change in mu-value. First gear engaged and controller re-tuned (Simulation).

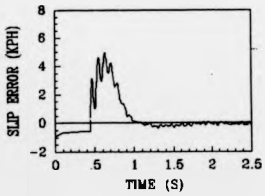

Figure 3.13 Throttle only control. Take off from rest in first gear on packed snow.

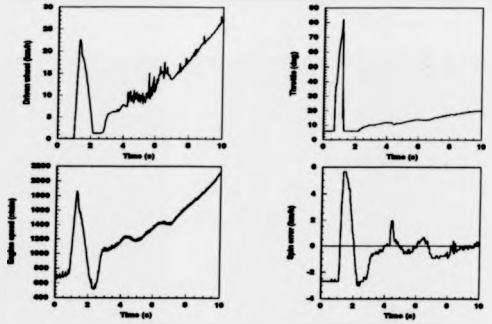

Figure 3.14 Throttle and brake control. Take off from rest in first gear on packed snow

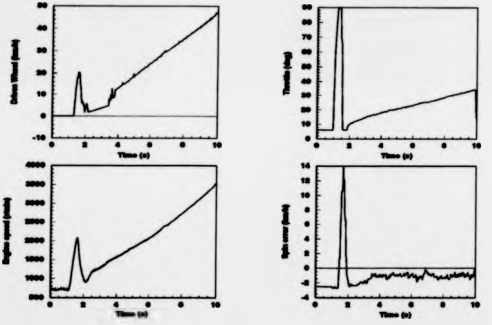

Figure 3.15 throttle and brake control. Pull step to accelerator pedal at steady cruise in first gear on packed snow

(a) Higher target slip used.

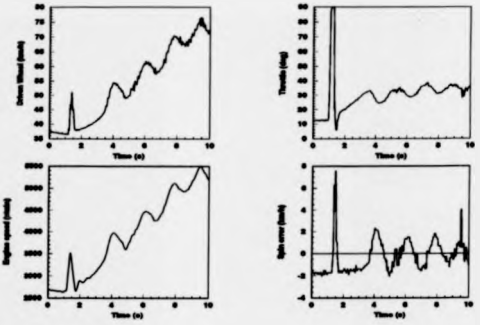

(b) Lower target slip used.

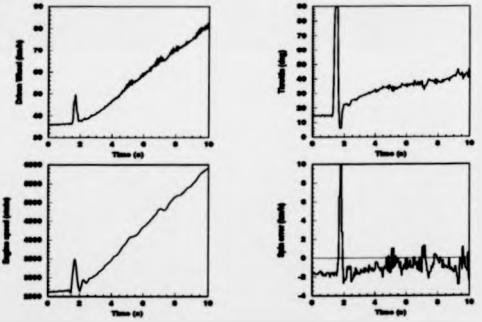

Figure 3.16 response of vehicle and model to the same throttle actuation signal on a similar surface.

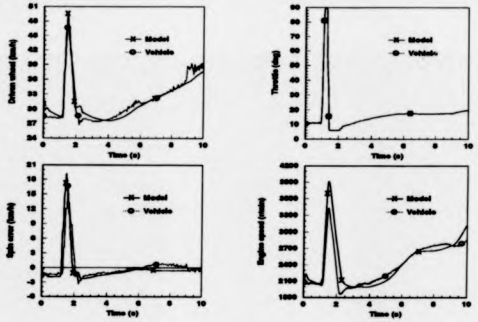

4 Non-linear engine model

4.1 Introduction

The intention of the work in this chapter is to develop a model of the 2.0 litre Zeta engine which is fitted to the FWD vehicle. This engine is an in-line four cylinder four-stroke petrol engine. The engine is required to meet Clean Air Act requirements and as such requires the fitting of Exhaust Gas Recirculation (EGR) apparatus. Whilst the addition of EGR is unlikely to affect the traction control algorithm, the work reported here was required for other studies within the company and hence was included within this model.

The modelling work is generic and if other engines are to be modelled then the physical characteristics such as flywheel inertia and manifold volume, and the regressed equations discussed below, clearly will need to be adjusted.

The dynamic model has been built along the lines developed by Powell et al (74) being based on steady state characteristics of the engine. Validation of the throttle and spark dynamic characteristics has been performed.

The model is a low order representation of the engine. It includes steady-state throttle flow characteristics, manifold dynamics, engine pumping effects, the induction-to-combustion stroke delay, steady-state torque characteristics and EGR dynamics. The output of this model is engine torque, and the flywheel dynamics are represented in the transmission model.

The model does not include Air Fuel Ratio (AFR) dynamics. However, the model has been structured so as to allow its inclusion at a later date. Cylinder-to-cylinder variation is also not included, and whilst the induction-to-combustion stroke delay is represented, the individual firing pulses are not.

4.2 Structure

The model is broken into the following sub-models:

i) Throttle characteristic

ii) Manifold characteristic

iii) Induction-to-combustion-to-exhaust delay.

iv) Torque characteristic

v) EGR characteristics

A schematic overview of the model is shown in Figure 4.1 which shows the communication between the above sub-models.

4.2.1 Throttle Characteristic

The flow through the throttle is assumed to be one dimensional steady compressible flow as developed by Novak (76) & Hamburg & Hyland (77). Mass flow through the throttle is a function of manifold pressure and throttle angle. The flow rate is assumed to be a separable function:-

$$\dot{m}_a = f(\theta)g(p_m) \tag{4.1}$$

The basis for this model is outlined in reference (74). The structure of the Matrix$_x$ implementation is shown in Figure 4.1. When the pressure downstream of the throttle is below approximately half the upstream pressure, the flow through the throttle is sonic. Hence at this condition:-

$$g(p_m) = 1 \tag{4.2}$$

For pressures above half the upstream pressure, flow is dependent upon both manifold pressure and throttle angle. The manifold pressure relationship becomes:-

$$g(p_m) = \frac{2}{p_{atm}}\sqrt{(p_m p_{atm} - p_m^2)} \tag{4.3}$$

The upstream pressure will be slightly below atmospheric pressure due to the pressure drop across the Mass Air Flow (MAF) sensor, connecting tube and air cleaner sub-assembly. Powell et al (78) developed an expression for this upstream flow along similar lines to the manifold analysis i.e.

$$\dot{m}_a = \hat{K}_a \sqrt{P_a P_{amb} - P_a^2} \qquad (4.4)$$

where

$$\hat{K}_a = 2A_a \left(\frac{\gamma}{RT_a}\right)^{\frac{1}{2}} \left(\frac{2}{\gamma+1}\right)^{\frac{\gamma+1}{2(\gamma-1)}} \qquad (4.5)$$

For the 2.0 litre Zeta engine we have:-

$\gamma = 4/3$

$R = 287 J/kg/K$

$T_a = 288K$

$P_{amb} = 10^5 N/m^2$

$P_a = 0.99*10^5 N/m^2$

$A_a = 0.00212 m^2$

Substituting this data into equations 4.4 and 4.5, for mass flow rates of 100 g/s (maximum mass flow rate for the engine at 7500 rpm), the pressure drop is approximately 0.01 bar. It is therefore reasonable to ignore the effects of this restriction in the model.

For the throttle function ($f(\theta)$) a cubic equation regressed to mapped data has been used:-

$$f(\theta) = 2.82 - 0.0523\theta + 0.103\theta^2 - 0.00063\theta^3 \qquad (4.6)$$

This regression equation is based on over 1300 data points of mass air flow obtained at widely varying operating points. This effectively models the relationship between throttle angle and air flow. The quality of fit can be seen in Figure 4.2 which shows the data points and the above equation as well as the residuals. Note the high value of the residuals at high manifold pressures. This is due to the sensitivity in mass air flow at large throttle angles.

An alternative approach is to use a physically based model along the lines developed by Harrington (79) who modelled the throttle as a variable area orifice, with an analytical expression for the area as a function of angle. Such an approach is useful to provide insight into the throttle operation or where throttle plate design/progression is being considered. However, in this case the throttle geometry is fixed and a regression fit is satisfactory.

4.2.2 Manifold characteristic

This model is based on the analysis carried out by Powell (80) and Moskwa and Hedrick (81). The manifold model is complicated by the introduction of EGR. The pressure rate equation (assuming no EGR initially) is usually of the form (15):-

$$\dot{p} = \frac{RT}{V}(\dot{m}_i - \dot{m}_o) \tag{4.7}$$

Assuming uniform mixing of air and EGR, and by applying the principles of conservation of mass and energy, this basic equation with two manifold constituents becomes:-

(i) for air

$$\dot{p}_a = \frac{RT}{V}\left(\left(1+\frac{p_a}{p_m}(\gamma-1)\right)\dot{m}_{ai} + \frac{P_a}{p_m}(\gamma-1)\dot{m}_{ri} - \frac{p_a}{p_m}\gamma\dot{m}_o\right) \tag{4.8}$$

(ii) for EGR

$$\dot{p}_r = \frac{RT}{V}\left(\frac{p_a}{p_m}(\gamma-1)\dot{m}_{ai} + \left(1+\frac{p_a}{p_m}(\gamma-1)\right)\dot{m}_{ri} - \frac{p_a}{p_m}\gamma\dot{m}_o\right) \tag{4.9}$$

The structure of the above two equations is highly convenient, with no cross product terms, and this comes about because Powell assumes that a small amount of heat is transferred to the manifold constituents which allows the cancellation of terms. Beaumont (82) assumed adiabatic flow through the manifold to reach a slightly different equation but with basically the same structure.

The total pressure in the manifold is the sum of partial pressures of air and EGR:-

$$p_m = p_a + p_{egr} \tag{4.10}$$

The proportion of EGR and air mass flow out of the manifold is determined using the ratio of partial pressures:-

(i) for air flow

$$\dot{m}_{ao} = \frac{p_a}{p_m}\dot{m}_o \tag{4.11}$$

(ii) for EGR flow

$$\dot{m}_{eo} = \frac{p_e}{p_m}\dot{m}_o \tag{4.12}$$

The engine pumping is assumed to be a function of manifold pressure and engine speed only:-

$$\dot{m}_o = -0.366 + 0.08979\omega p_m + 0.0337\omega p_m^2 + 0.0001035 p_m \omega^2 \tag{4.13}$$

This representation is based upon a regression of over 1300 data points. It takes into account the volumetric efficiency and swept volume of the engine acting as a pump. The quality of fit of this model to the data is shown in Figure 4.3.

The induction map for the throttle and engine pumping characteristic is given in Figure 4.4.

4.2.3 Induction-to-combustion stroke delay

The delays associated with the discrete nature of the induction, compression and combustion strokes are represented in a Fortran user code block. This is necessary because Matrix$_x$ will only represent single rate discrete blocks and cannot handle

variable delay routines. The routine integrates the engine speed to yield crankshaft position, and each 180° mass charge is calculated. The mass charge is based upon the mass flow rates ($\dot{m}_{air}$ and $\dot{m}_{egr}$) integrated over the same 180° period. Due to the fact that we are considering a four cylinder four-stroke engine, we can assume contiguous (without overlap) combustion, intake, compression and exhaust strokes from each cylinder in turn. For this reason only one cylinder can be assumed to be on its intake, compression or combustion stroke at any time which greatly simplifies the Fortran routine. Specifically, the routine represents each stroke as follows:-

a)Induction

The delay is made up of the integration of the mass air flow and mass EGR flow independently over 180° to give a mass air charge and mass EGR charge.

b)Compression

This is a sample and hold for 180°

c)Combustion

At the end of the compression stroke the mass charge output from the Fortran routine is then used in the torque calculation. This effectively gives a torque pulse delayed by 180°.

4.2.4 Torque characteristic

Torque has been fitted to static mapped data using multiple linear regression of torque as a function of the key predictors:-

$$T = f(AFR, \sigma, m_a, m_e, \omega_e)$$

The equation which gave an adequate fit over the whole range is:-

$$T = -181.3 + 379.36m_a + 21.91AFR - 0.85AFR^2 + \quad (4.14)$$
$$0.26\sigma - 0.0028\sigma^2 + 0.027\omega_e - 0.000107\omega_e^2 +$$
$$0.00048\omega_e\sigma + 2.55\sigma m_a - 0.05\sigma^2 m_a + 2.36\sigma m_e$$

The quality of the regression is good, with a correlation coefficient of 0.9962 and rms error of 2.22Nm. The statistical analysis package RS1 was used to derive this relationship starting with all quadratic terms and using the t-statistic associated with each predictor to eliminate terms (i.e. backward elimination). Including more terms improves the correlation coefficient by negligible amounts only, and it is considered that this equation represents the optimum balance between computational efficiency and prediction accuracy.

This equation is similar in structure to that derived by Powell (15) with the m_a term replaced by the σm_a term. This σm_a relationship is known to occur since the addition of EGR decreases the burn rate (83) and hence an earlier spark is necessary to achieve maximum torque. The positive sign on the σm_a term is due to the fact that we are using mass charge of EGR and mass charge of air. Hence, for constant mass air charge, we see more torque with EGR due to the reduction in throttling losses. The quality of the regression is seen in Table 4.1.

Table 4.1 Torque regression coefficients

Term	Coefficient	Standard Error	t-value	Significance
Const.	-181.304	5.0577	-35.85	0.0001
m_a	379.359	2.8693	132.21	0.0001
AF	21.91	0.6866	31.91	0.0001
σ	0.266	0.0581	4.58	0.0001
ω	0.0266	0.001801	14.78	0.0001
$\omega\sigma$	0.000482	0.000039	12.45	0.0001
σ^2	-0.002821	0.001022	-2.76	0.0058
ω^2	-0.000107	0.000003	-40.91	0.0001
AF^2	-0.85395	0.02396	-35.64	0.0001
σm_a	2.5524	0.233	10.96	0.0001
$\sigma^2 m_a$	-0.0546	0.00459	-11.89	0.0001
σm_a	2.3555	0.1800	13.08	0.0001

Number of data points = 1317.

Correlation Coefficient (R^2) = 0.9962

RMS error = 2.221

Condition No = 619.7

Figure 4.5, Figure 4.6 and Figure 4.7 show the variation of torque with the predictors. These curves exhibit good agreement with expected trends such as:-

i) MBT (Minimum spark advance for Best Torque) spark advance increases with speed (Figure 4.5).

ii) Torque versus air-fuel ratio is the correct shape i.e. a rapid fall off of torque with lean air-fuel ratios and a peak torque rich of stoichiometry (Figure 4.6).

iii) The addition of EGR (keeping mass air charge constant) increases the torque output of the engine through a reduction in pumping losses (Figure 4.7).

Together with the good statistical parameters associated with the regression, these trends indicate a high degree of confidence for this representation of torque within the boundary of the data used.

4.2.5 Exhaust Gas Recirculation (EGR) Characteristic

The systems fitted to all 2.0 litre Zeta engine are all 'delta pfe' systems. A schematic of this system is show in Figure 4.8. Referring to Figure 4.8, operation of the EGR control will now be described. Flow through the EGR system is controlled by the Electronic Vacuum Regulator (EVR). This generates a vacuum control signal (p_{vac}) which opens the EGR valve, thereby providing a flow of exhaust gas from exhaust to intake manifolds. The flow rate depends upon the EGR valve position and the pressure difference between intake and exhaust manifolds. The flow is estimated by measuring the change in pressure across an orifice in the EGR tube using the 'delta pfe' sensor.

Electronic Vacuum Regulator

The EVR produces a variable vacuum from the manifold vacuum source. The dynamics of the EVR are very fast and can be ignored; the dominant dynamics are associated with the EGR valve (75). For this reason, a static characteristic giving vacuum as a function of pulse-width-modulated (PWM) signal and manifold pressure is used. This is based on regressed data:-

$$p_{vac} = 0.9914 - 0.1861 d_c^2 + 0.01055 p_m \qquad (4.15)$$

EGR Valve Flow

Flow through the EGR valve is assumed to be one-dimensional steady compressible flow and follows a similar relationship to that developed for the throttle (equation 4.1) described above viz:-

$$\dot{m}_{egr} = f(x_{egr}) g(p_{exh}, p_m) \qquad (4.16)$$

Note now that in contrast to the throttle system, the upstream pressure can vary.

The dynamics between x_{egr} and p_{vac} are significant. Throop et al (85) showed that the dynamics could be represented as a first order lag cascaded with a pure time delay. This time delay is due to stiction in the EGR valve and this is physically represented in this model and described below. The dynamics here are therefore simply represented as a first-order lag with a time constant of one second (85). Unfortunately, the EGR valve position (x_{egr}) is not measurable and so the dynamics of the EGR valve have been represented at the vacuum regulator viz:-

$$\frac{p'_{vac}}{p_{vac}} = \frac{1}{1 + sT_{egr}} \tag{4.17}$$

The flow through the system can now be described by the following modified equation:-

$$\dot{m}_{egr} = f(p'_{vac}) g(p_{exh}, p_m) \tag{4.18}$$

The system is non-linear with the EGR valve position saturating with control pressure. A certain vacuum is required to open the valve, which then rapidly opens to full position over quite a small vacuum signal change and opens no further for subsequent increases in vacuum. This saturation characteristic coupled with the dynamics give a stiction-like behaviour as EGR is introduced.

In order to parameterise the above equation, the EGR sub-system was separately characterised on a flow-rig in which both signal vacuum and downstream (i.e. intake manifold) pressure were varied. The upstream pressure (exhaust manifold) was fixed at atmospheric pressure. Care was taken to precisely identify the pressure at which the valve opens.

The saturation characteristic is represented with the control vacuum (p'_{vac}) saturating between an upper and lower value. The upper limit of 0.9492 bar represents the opening pressure for the valve. The lower limit of 0.9 bar represents the pressure at which the valve is fully open. Between these pressures, the relationship is based upon a regression analysis similar to that for describing the throttle characteristic:-

$$f(p'_{vac}) = -2005.5 + 4514.5p_{vac} - 2530.2p_{vac}^2 \qquad (4.19)$$

Since the upstream pressure (p_{mh}) can now vary, the transition between sonic and sub-sonic flow is described by the following relationship:-

$$g(p_{mh}, p_m) = 1 \qquad \text{for } \frac{p_m}{p_{mh}} < 0.5 \qquad (4.20)$$

$$g(p_{mh}, p_m) = \frac{2}{p_{mh}}\sqrt{(p_m p_{mh} - p_m^2)} \qquad \text{for } \frac{p_m}{p_{mh}} \geq 0.5 \qquad (4.21)$$

Exhaust back pressure

The exhaust manifold dynamics could be modelled in a similar way to the intake manifold. This is not necessary since the exhaust manifold dynamics are only required for the EGR calculation and are fast in comparison with the most significant dynamics associated with the EGR valve. In order to justify this assumption, the exhaust manifold dynamics can be represented as a non-linear first-order lag. Re-writing the intake manifold equations for the exhaust manifold yields:-

$$\dot{p}_{mh} = K_{mh}(\dot{m}_{ac} - \dot{m}_{mh} - \dot{m}_{egr}) \qquad (4.22)$$

where

$$K_{mh} = \frac{R\gamma T_{mh}}{V_{mh}} * 10^{-5} \qquad (4.23)$$

The exhaust 'manifold' is assumed to be delimited by the engine and the three way catalytic converter (TWC). At the TWC, the pressure drop between exhaust pressure and ambient is assumed to occur.

Figure 4.9 shows the measured relationship between exhaust back pressure and exhaust flow. The relationship is quadratic viz:-

$$\dot{m}_{exh} = K_{fe}\sqrt{p_{exh} - p_{amb}} \tag{4.24}$$

Small signal analysis of this non-linear equation yields:-

$$\Delta\dot{m}_{exh} = \frac{1}{2}K_{fe}\frac{1}{\sqrt{p_{exh} - p_{amb}}}\Delta p_{exh} \tag{4.25}$$

Sustituting into the exhaust manifold equation above yields:-

$$\Delta p_{exh} = K_{exh}\left(\Delta\dot{m}_{out} - \frac{1}{2}\frac{K_{fe}}{\sqrt{p_{exh} - p_{amb}}}\Delta p_{exh}\right) \tag{4.26}$$

The time constant of the first order lag is therefore:-

$$\tau_{exh} = \frac{2\sqrt{p_{exh} - p_{amb}}}{K_{fe}K_{exh}} \tag{4.27}$$

Now, assuming the following data,

$T_{exh} = 900K$

$\gamma = 1.4$

$R = 287J/kg/K$

$V_{exh} = 5ltrs$

$p_{exh} = 1.4$

$p_{amb} = 1.0$

we arrive at,

$$\dot{p}_{exh} = 0.72(\dot{m}_{out} - \dot{m}_{exh} - \dot{m}_{egr}) \tag{4.28}$$

Regressing the data in Figure 4.9 yields:-

$$\dot{m}_{exh} = 168\sqrt{p_{exh} - p_{amb}} \tag{4.29}$$

and hence

$$\Delta\dot{m}_{exh} = 133\Delta p_{exh} \tag{4.30}$$

The exhaust 'manifold' time constant is therefore:

$\tau_{exh} = 10.4ms$

This is the slowest dynamics associated with exhaust manifold filling and is reasonable to ignore. Hence the exhaust back pressure is predicted from the static relationship shown in Figure 4.9:-

$$P_{exh} = \left(\frac{\dot{m}_{out}}{168}\right)^2 \qquad (4.31)$$

Delta Pfe

The pressure drop across can be calculated based on mass-air flow using the characteristic which the EEC uses in an inverse manner.

4.3 Validation

4.3.1 Experimental set-up

The intention of the experimental work here was to obtain the correct response of torque to throttle and spark perturbations. Whereas the steady state characteristics were obtained on a steady-state dynamometer, the validation work here needs to be carried out on a transient dynamometer which is capable of holding engine speed constant during a transient. This is desirable so that the important torque generation dynamics are not complicated by the relatively straightforward flywheel dynamics. The work consisted of applying step perturbations to:-

i) Throttle keeping spark advance, EGR and A/F constant

ii) Spark advance keeping throttle, EGR and A/F constant

The validation work described here was performed on another engine of the same type (2.0 l Zeta) with nominally the same characteristics. Despite being carried out on a different engine with a different dynamometer the engine model predicts well the engine behaviour with the differences being mainly in the steady state values.

Figure 4.10 shows the experimental set up. The experimental facilities required involved standard engine test bed equipment used for steady-state mapping work suitably enhanced for dynamic testing. For the dynamic tests the key features of the set-up are:-

i) The dynamometer used had a high moment of inertia (approx $7 kgm^2$) which when operated in constant speed mode could maintain speed to within 12 rpm for a step change in load of 20Nm. For this reason the magnitude of the spark and throttle steps were adjusted so as to give approximately a 20Nm change in torque.

ii) A fast throttle actuator in order to apply repeatable fast and accurate steps to the throttle. A Brown Boveri (Type ABB DKSG 50) actuator was used which could give the required change in throttle to yield 20 to 30 Nm changes in typically less than

10ms.

iii) High bandwidth Kistler pressure transducers located in the intake manifold.

iv) Fast measurement of exhaust A/F using an NTK UEGO sensor.

v) A high bandwidth torque transducer located on the driveshaft.

vi) A fast data acquisition system - AVL indiskop logged 8 channels at 500Hz per channel.

4.3.2 Throttle validation

Figure 4.11 to Figure 4.20 show the model response and real response data for the same throttle step at speeds of 1000, 3000, 4000, 5000 & 6000 rpm and at 15% and 75 % of full load, where full load is the engine operating under wide open throttle conditions. Features to note are:

a) Focussing initially upon Figure 4.11 the pressure rise in the manifold and the mass flow rate are correct with a slight offset in absolute value. This offset is consistent in that the higher manifold pressures in the model give rise to higher mass flow rates. The difference in steady values could therefore be explained by the model operating at too high an atmospheric pressure. The high frequency (33.33 Hz at 1000 rpm) induction process is not represented in the model.

Figure 4.11 to Figure 4.20 each represent the manifold dynamics extremely accurately with some offsets in steady values. These variations are not consistent and since the experimental work was carried out over a few days this variation could be explained by variation in atmospheric pressure (as explained in (a) above) which unfortunately was not measured.

b) The high firing frequency seen on the real torque signal is not fully captured. This is due to the reciprocating diacrete nature of the engine which is only partly reflected in the simulated torque response as a discrete uniform pulse. The discrete torque simulation is intended to capture the induction-to-combustion stroke delay rather than

model the actual firing pulse.

c) The torque response is oscillatory in Figure 4.16, Figure 4.18 and Figure 4.20. In each of these cases the frequency of the fluctuation is approx 10Hz. This is the natural frequency of the engine on its mounts and it is suggested that at these high loads this engine mount mode is excited.

d) The speed/load dependence of the manifold time constant. The time constant varies from approx 170 ms (Figure 4.11) to less than 5ms (Figure 4.20).

4.3.3 Spark validation

The relatively fast response of the spark in comparison with throttle can be seen in general in Figure 4.21 to Figure 4.29. However the restricted range is also evident since in order to get a sizeable difference in spark advance the engine was operated in regimes where combustion stability is not good causing large fluctuation in torque. The responses also show the 10Hz mode (referred to above in 4.3.2) excited by the sudden change in torque which occurs with a step change in spark advance. This is eventually damped out but not within the time frame of the experiment. If this is ignored then the real torque response should be similar to the simulated response.

The steady torque values are poor at zero spark advance. This highlights the problems of using a single regression equation involving only quadratic terms which is not good at these extreme values of spark advance where combustion quality seriously deteriorates. A more complex equation may help. This was not tried because only a sparse amount of data was obtained under these conditions. Smaller steps in spark advance which were better for steady state did not change torque significantly enough to be seen within the engine mount oscillation.

4.4 Application to Traction Control

The work reported in this chapter has shown that the model used accurately reflects the low-order dynamics of the real engine. The relatively slow manifold dynamics are significant at low load and low speed conditions. Hence on low μ surfaces (where the engine will spin the wheels at low throttle openings), the inclusion of spark intervention will be necessary. Using this simulation with the FWD vehicle dynamics model, spark advance intervention was used in addition to throttle and was shown to have minimal effect due to its restricted authority (72). The same result is shown in Figure 4.30. Figure 4.30 shows two simulation results each with the same PID controller acting on throttle. The simulation result shown by the dotted line includes proportional control on spark advance and clearly shows only a minimal improvement in response of the controller. Clearly, the addition of spark intervention should include the option of cutting the spark and hence cutting torque to zero, thereby increasing the range of authority, during the initial over-spin.

4.5 Figures

Figure 4.1 Matrix, model structure

Figure 4.2 Throttle characteristic

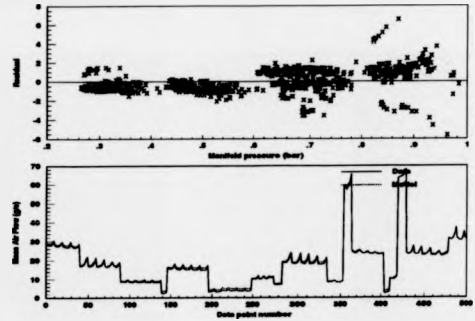

Figure 4.3 Manifold characteristic

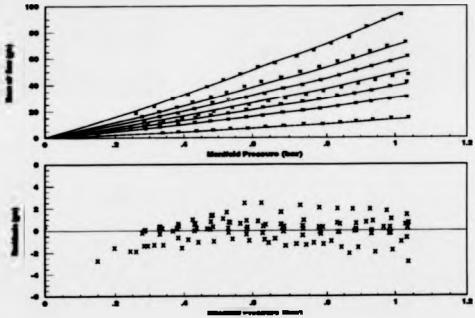

Figure 4.4 Induction Map

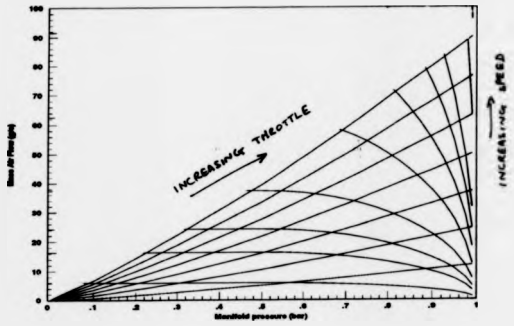

Figure 4.5 The effect of engine speed on engine torque.

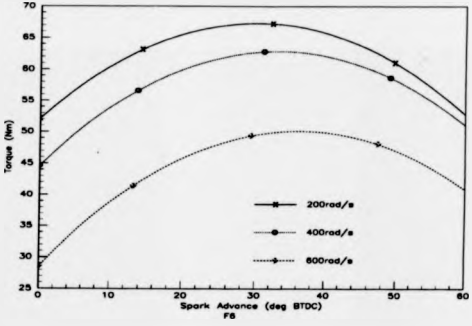

Figure 4.6 The effect of AFR on engine torque

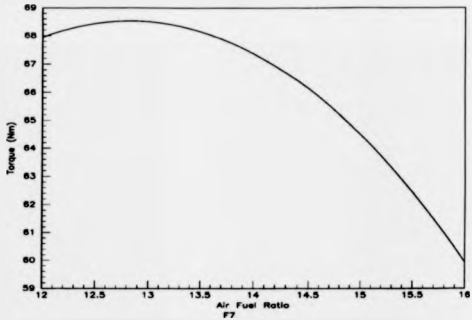

Figure 4.7 The effect of EGR on engine torque

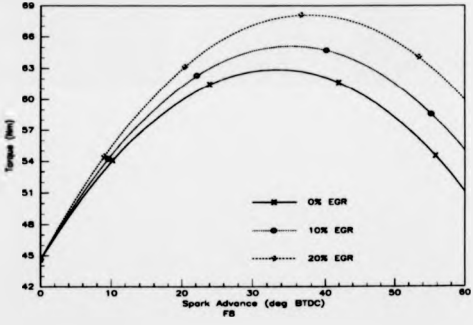

Figure 4.8 Delta pfe Exhaust Gas Recirculation System

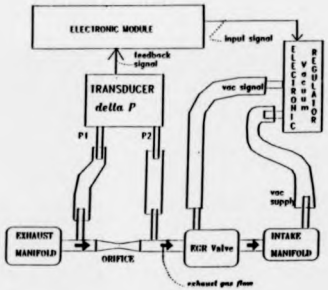

Figure 4.9 Exhaust gas flow versus exhaust back pressure

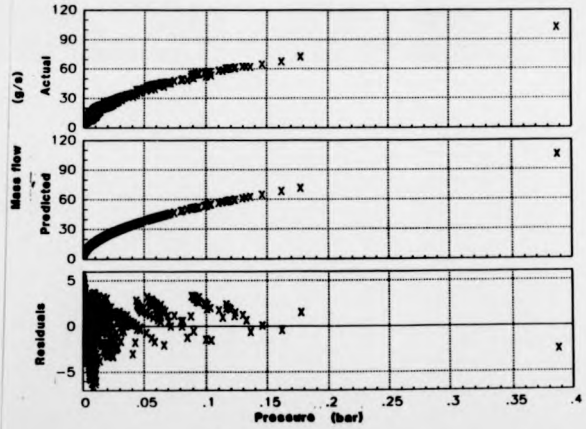

Figure 4.10 Experimental set-up

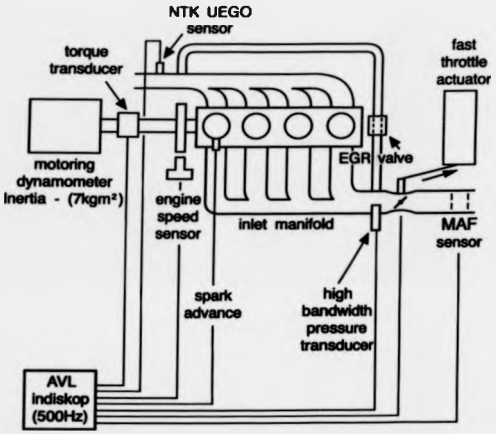

Figure 4.11 Throttle step at constant engine speed of 1000 rpm and at 15% of maximum torque

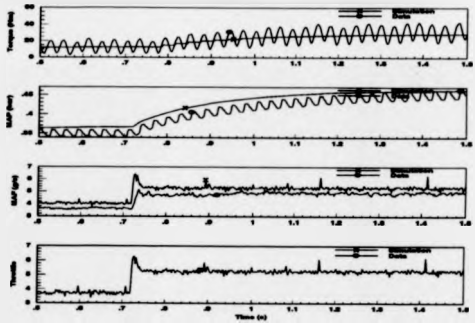

Figure 4.12 Throttle step at constant engine speed of 1000 rpm and at 75% of maximum torque

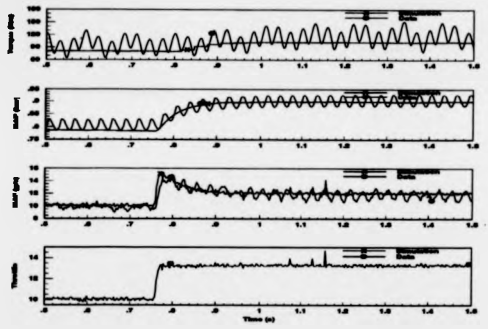

Figure 4.13 Throttle step at constant engine speed of 3000 rpm and at 15% of maximum torque

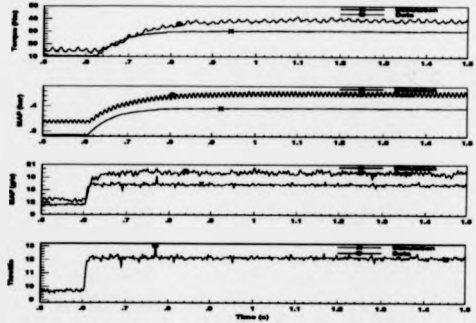

Figure 4.14 Throttle step at constant engine speed of 3000 rpm and at 75% of maximum torque

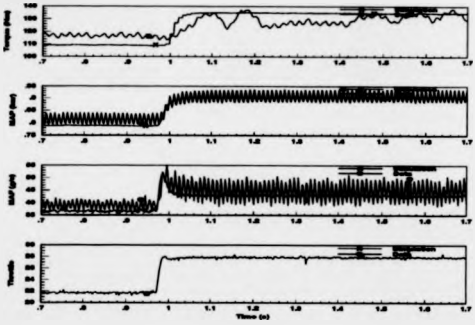

Figure 4.15 Throttle step at constant engine speed of 4000 rpm and at 15% of maximum torque

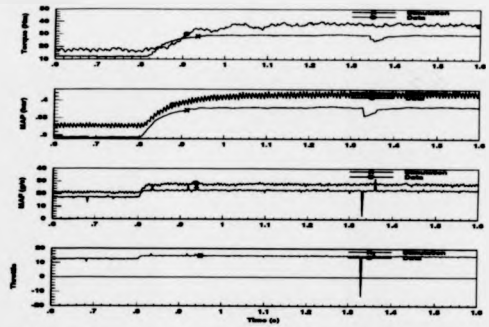

Figure 4.16 Throttle step at constant engine speed of 4000 rpm and at 75% of maximum torque

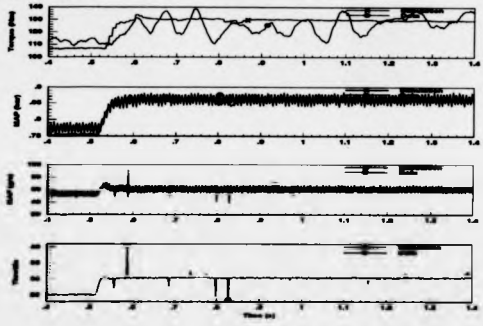

Figure 4.17 Throttle step at constant engine speed of 5000 rpm and at 15% of maximum torque

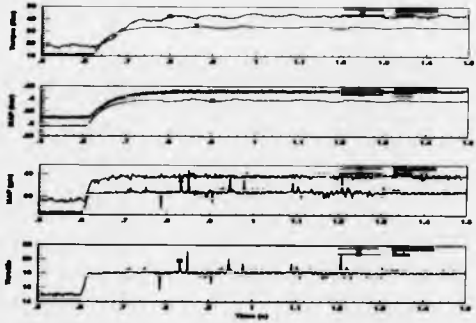

Figure 4.18 Throttle step at constant engine speed of 5000 rpm and at 75% of maximum torque

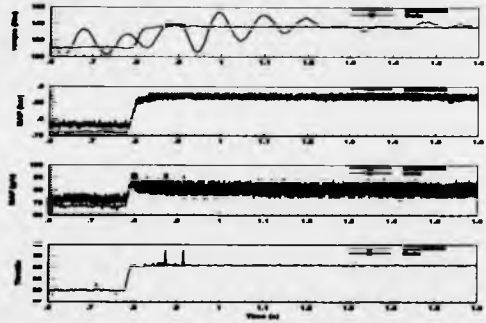

Figure 4.19 Throttle step at constant engine speed of 6000 rpm and at 15% of maximum torque

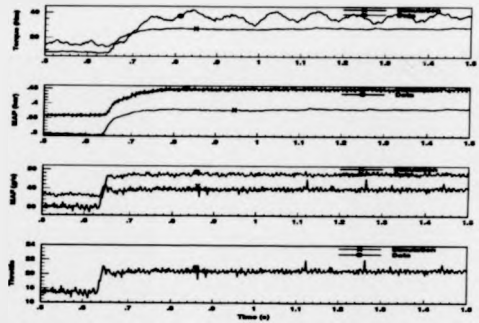

Figure 4.20 Throttle step at constant engine speed of 6000 rpm and at 75% of maximum torque

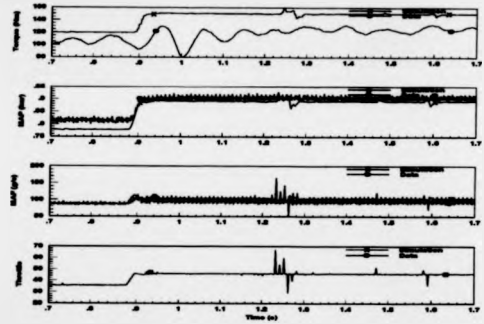

Figure 4.21 Spark step at constant engine speed of 1000 rpm and at 15% of maximum torque

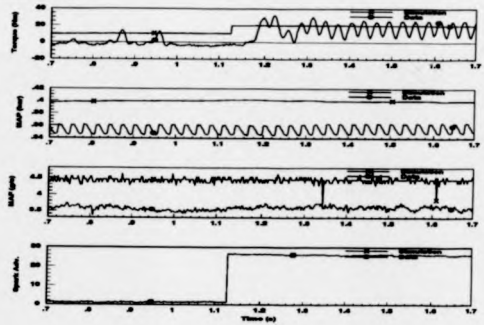

Figure 4.22 Spark step at constant engine speed of 3000 rpm and at 15% of maximum torque

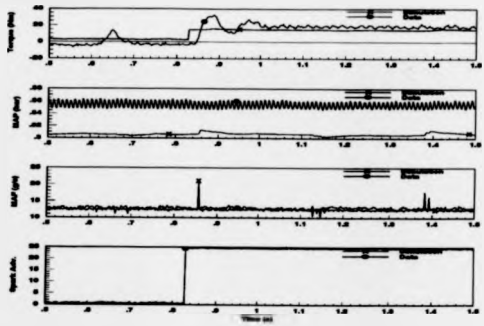

Figure 4.23 Spark step at constant engine speed of 3000 rpm and at 75% of maximum torque

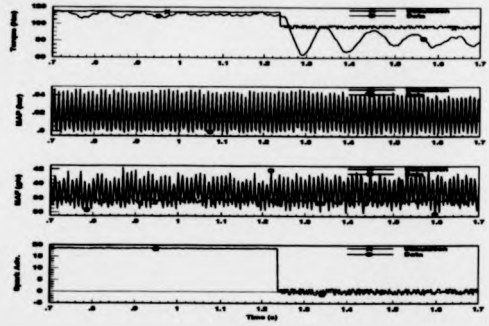

Figure 4.24 Spark step at constant engine speed of 4000 rpm and at 15% of maximum torque

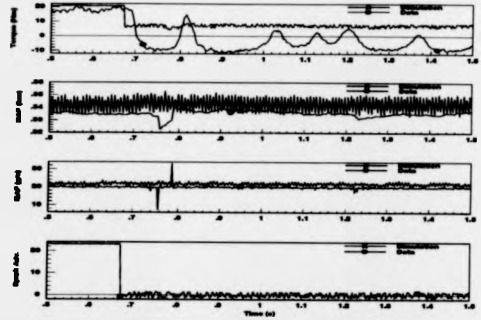

Figure 4.25 Spark step at constant engine speed of 4000 rpm and at 75% of maximum torque

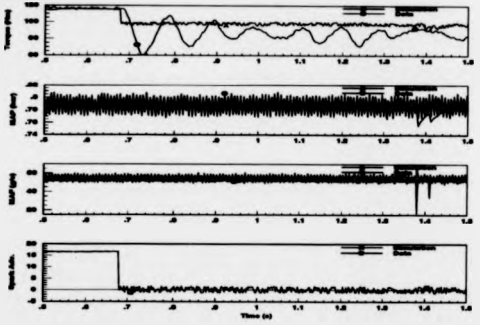

Figure 4.26 Spark step at constant engine speed of 5000 rpm and at 15% of maximum torque

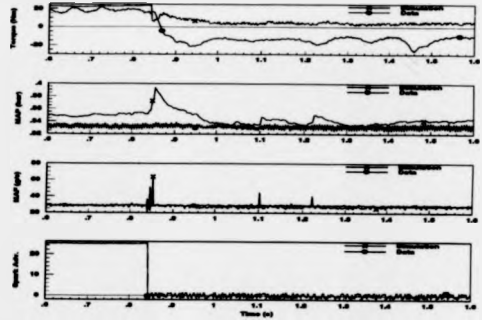

Figure 4.27 Spark step at constant engine speed of 5000 rpm and at 75% of maximum torque

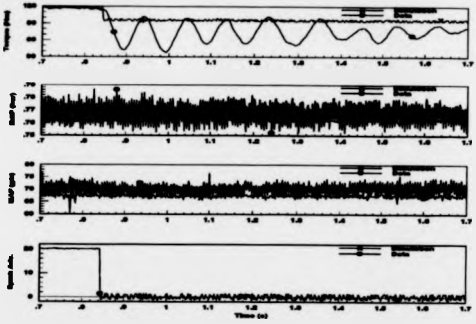

Figure 4.28 Spark step at constant engine speed of 6000 rpm and at 15% of maximum torque

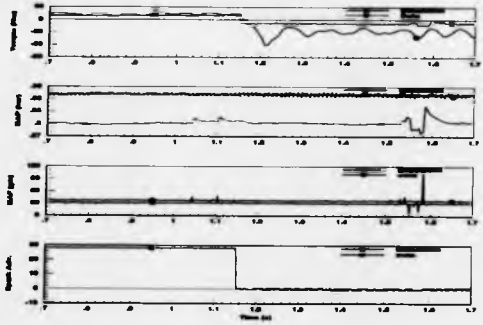

Figure 4.29 Spark step at constant engine speed of 6000 rpm and at 75% of maximum torque

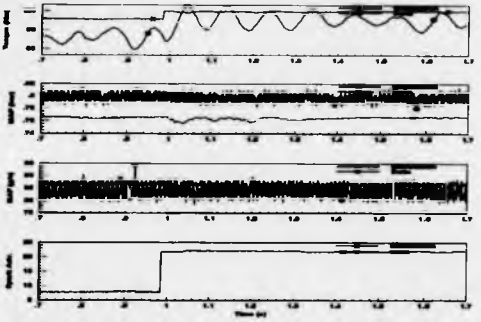

Figure 4.30 Traction control system simulation. Throttle intervention with and without spark intervention.

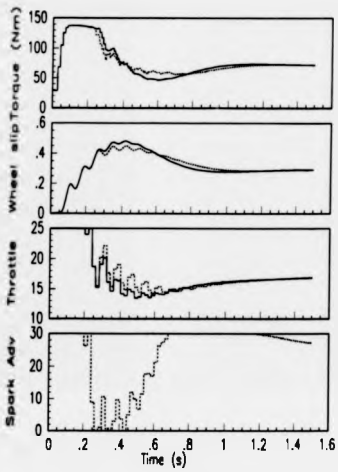

5 Brake Control Analysis

5.1 Background

Following the conclusion of the RWD work reported in chapter 3, it was evident that there was a great deal of scope for improvement in the design and calibration of brake intervention traction control systems. In that work, the objective was to develop an electronic throttle control system to work with the rule based brake system to control wheel slip. This work revealed that whilst the rule based brake intervention offered adequate performance, the system was slow. In addition the control system had many parameters to be calibrated (23) which led to a calibration intensive procedure to tune the control system.

The objective of the work reported in this chapter is to investigate the use of control theory based strategies in brake control. In particular the work has consisted of the design and implementation of a 'diagonally dominant' PID controller to control wheel-spin using brake intervention.

The original intention was to operate this brake controller with the existing PID controller (used by Bendix) on the throttle control loop. However, hardware limitations have resulted in being only able to design and implement the brake only controller. The structure of the controller is such that the closing of the throttle control loop should be fairly straightforward.

It will be recalled that the purpose of the brake traction controller is to maximise the tractive effort to each wheel whilst maintaining lateral stability of the vehicle. This can be achieved by controlling the wheel slip at its optimum value. This requirement can be achieved by (a) engine intervention together with braking both wheels together on uniform low μ surfaces and (b) braking one wheel on split μ surfaces. Assuming that the optimum level of slip is the same for both wheels then this amounts to:-

a) maintaining a certain average slip and

b) maintaining a zero slip difference across the axle.

If the optimum slip is different for each wheel, the target slip can still be specified in terms of average slip error and slip error difference i.e:-

c) maintain a certain average slip and

d) maintain a *non-zero* slip difference across the axle.

Specifying the objective of a brake only traction controller in this way is important for the analysis in section 5.2 below. In addition, it readily allows the incorporation of engine torque control since this then only needs to operate on the average slip control loop. The slip difference control attempts to equalise the wheel speeds and hence is analogous to the operation of a locking differential.

The brakes are controlled using a software generated Pulse Width Modulated (PWM) signal to each brake actuator. Generating a PWM this way meant that the it had to be an integer (n) multiple of 5ms with n different PWM levels.

In this chapter it should be remembered that a different driveline has been modelled. In contrast to the earlier work, this is FWD with a manual transmission. The brake hardware needed to be re-modelled. Following this, control analysis, on the engine and driveline dynamics, based on multi-variable frequency domain techniques has been performed. Finally, in this chapter the results of vehicle trials of the multi-variable controller are reported.

5.2 System Analysis

5.2.1 Simulation Model

Overview

The approach followed in this section has been to work with two models:-

(i) a linear representation of the torsional dynamics of the powertrain (21) (25) with non-linear representations of the tyre-road interface (55) and brake actuation dynamics. The non-linear representation of the brake dynamics, based upon work carried out by Hrovat (47) on the Tevea brake system, is enhanced to reflect the changed hardware configuration of the Bendix brake dynamics. For the majority of the analysis, the engine dynamics are excluded since the engine torque dynamics do not affect the response of a brake-only controller. This model has been coded within Matrix$_x$.

ii) an analytically linearised version of (i) above with a linear representation of a 1.6 litre engine (15). The inclusion of the engine dynamics was merely to yield transfer functions with throttle as an input.

Torsional Dynamics

A schematic overview of the torsional model is given in Figure 5.1. Note now that the torque converter is replaced by a compliance and damper in parallel to represent the fully engaged clutch. The equations of motion for this model are identical to those established in chapter 2. The equation for the torque converter (see Section 2.3.3) are now replaced with:-

$$T_c = b(\omega_e - \omega_t) + k\theta_c \qquad 5.1$$

$$\dot{\theta}_c = \omega_e - \omega_t \qquad 5.2$$

Tyre Dynamics

The tyre characteristic is again based upon the work of (55). The equation for this are given in section 2.3.4.

Brake Hydraulics Dynamics

The system fitted to the FWD vehicle is a diagonally split system. This is shown schematically in Figure 5.2. Under normal braking operation, the commutation valve is open and the pumps are not pressurising the system. Brake pressure generated at the brake master cylinder actuates the brakes in each limb of the diagonal split circuit.

During traction control, the commutation valve closes and the pumps start. A separate pump (driven coaxially by one motor) provides the high pressure source to each wheel. A pressure relief valve operates at 130 bar. The solenoid valves to each front wheel are individually controlled to control brake pressure to each wheel. Each solenoid valve returns hydraulic oil to the low pressure accumulator located at the pump feed. This accumulator is at a pressure of approximately 1 bar (gauge) which is assumed to be 0 bar (gauge) in the analysis. A more detailed diagram of the hydraulics showing the individual valves is shown in Figure 5.3.

A schematic overview of the model of the brake hydraulics for one wheel is given in Figure 5.4. In the model, it is assumed that the pump is running at full speed and delivering full flow of $8.333 cm^3/s$ (i.e. $5 ltr/min$ at a working pressure of 100 bar (46). The modulator is cycled (following the PWM) between the high pressure source and a low pressure accumulator which is connected to the master cylinder which is effectively at zero pressure.

The pipework downstream of the pump and upstream of the modulator has a volume of $20 cm^3$ at zero pressure which expands to $20.2 cm^3$ at a pressure of 100 bar. This has been represented as an accumulator, described by equation 5.5 below.

The modulator valve flow is represented as an orifice whose flow is proportional to the square root of the pressure difference across the valve. Step response tests were performed in order to obtain the 'orifice coefficients'. The equations are as follows:-

$$Q_p = 8.333 cm^3/s \quad 5.3$$

$$\dot{V}_{ml} = Q_p - Q_v - Q_s - Q_{rv} \quad 5.4$$

$$p_{ppw} = f(V_{ml}) \quad 5.5$$

$$Q_v = 0.2dc\sqrt{p_{ppw} - p_b} \quad 5.6$$

$$Q_s = 0.5(1 - dc)\sqrt{p_b - p_{am}} \quad 5.7$$

$$\dot{V}_b = Q_v - Q_s \quad 5.8$$

$$p_b = f(V_b) \quad 5.9$$

$$T_b = f(p_b) = 18p_b \quad 5.10$$

Taking each of the equations in turn, equation 5.3 describes the constant delivery pump flow discussed above. Equations 5.4 and 5.5 together describe the pipework acting as an integrator described above (with equation 5.5 describing the pressure-volume characteristic of the pipework).

Equations 5.6 and 5.7 describe the incompressible flow for oil through an orifice for the pressure build and decay valves respectively. The parameter dc can take on the value of 0 or 1 only, following the PWM signal. This means that the valve can either result in pressure build or decay. The brake orifice coefficients were selected so that the model brake pressure response matched the experimental step response to a number of PWM signals to the valve. This can be seen in Figure 5.16 which shows the response of the actual system in the upper curve. The lower curve shows, to the same scales, the response of the simulation. The high frequency pulsations on the real data are due to the individual piston strokes of the hydraulic pump which is not modelled.

The pressure volume characteristic for the brake actuator (i.e. caliper) is described by equation 5.9. The torque generated at the wheel is based on brake design data for the vehicle.

Vehicle linear acceleration dynamics

These are described by the equations given in section 2.3.5.

Model parameterisation

This was based initially upon vehicle data obtained from drawings and data-sheets for the vehicle. This is given in the Table 5.1 below.

Table 5.1 - FWD Model data

Parameter	Symbol	Value
Engine Flywheel Inertia	J_e	$0.146 kgm^2$
Clutch damping	b	$10 Nms/rad$
Clutch stiffness	k	$974 Nm/rad$
Transmission inertia	J_t	$0.0072 kgm^2$
Overall gear ratio	r_o	see Table 5.2 below
Wheel inertia	J_w	$0.75 kgm^2$
Equivalent axle shaft stiffness	k_w	$1500 Nm/rad$
vehicle mass	m_v	$1014 kg$
rolling radius of tyre	r	$0.281 m$
Road load (constant)	al	$103.2 N$
Road load (velocity term)	bl	$2.236 Ns/m$
Road load (aerodynamic term)	cl	$0.38 Ns^2/m$

Table 5.2 - Gear Ratios for FWD vehicle

Gear	1st	2nd	3rd	4th	5th
Ratio	3.154	1.913	1.281	0.951	0.756
Overall ratio r_o	0.0743	0.123	0.183	0.246	0.310

(N.B. Final Drive Ratio 3.82)

It will be recalled that the dominant compliance in the driveline is due to the axle shafts. Calculating the shaft stiffness from the material properties of the axle shafts the predicted stiffness was 2200 Nm/rad. This resulted in a prediction for the wheel mode of 14.12 Hz in first gear. By reducing the axle stiffness to 1500 Nm/rad the wheel mode was reduced to the experimentally observed 10 Hz. This kind of variation in 'measured vs predicted' is due mainly to the stiffness associated with constant velocity joints and other stiffness in the driveline.

5.3 Control Analysis

The traction control system is multi-variable with interaction. By interaction we mean that each input can affect each output i.e:-

i) both the throttle and brakes influence both wheel speeds and

ii) braking one wheel will tend to accelerate the other on icy surfaces due to the action of the free differential.

The throttle intervention scheme has been previously investigated in chapter 3 with rule-based brake control. The major concern with this scheme was the quality of the brake control. Hence in this chapter, it is intended to investigate non rule-based brake control.

Good control has been achieved using a PID algorithm on the throttle loop described in chapter 3 (22) and a similar controller has been adopted in the suppliers base strategy with good results. For these reasons, the default throttle controller was retained.

This means that the control analysis here should be on the two-input two-output system brake only controller to function with the PID controller on throttle. Furthermore, it was decided that the brake controller should remain stable in case of throttle system failure i.e. it should operate independently. Hence the analysis below concentrates on the brake only control.

The analysis reported in this chapter can be broken down into:-

i) de-coupling the interacting brake control loops to produce a diagonally dominant control structure

ii) developing a stable SISO controller for each de-coupled loop and

iii) implementing the resulting linear controller on a full non-linear simulation model of the vehicle.

The analysis in (i) above was performed on an analytically linearised model of the driveline within. The analysis in (ii) above was performed on a computed linearised model of the full non-linear simulation model within Matrix$_x$. The analytically linearised model is described below.

Linear Model

The intention of the linearised model was to determine a diagonally dominant structure for the brake control algorithm. Based upon the non-linear torsional dynamic equations (see above), a reduced order model for control analysis - using Matlab and in particular the multi-variable frequency domain toolbox (MFD) (59) - has been derived. The model has six states. The dominant torsional and vehicle mass dynamics are included. Clutch dynamics are lumped in with the other torsional dynamics and brake dynamics have been ignored. The tyre characteristic has to be linearised around a fixed vehicle velocity (v_x m/s). This appears in the last three rows of the A matrix below.

A linearised representation of the engine dynamics is included (53). It should be noted that the engine dynamics ignore the induction to combustion stroke delay and that manifold pressure (not torque) is the state variable associated with the engine. Engine torque is a function of both manifold pressure and engine speed.

Adopting the familiar state space description:-

$$\dot{x} = Ax + Bu$$

$$y = Cx + Du$$

we have that:-

$$A = \begin{pmatrix} -\frac{1}{\tau_p} & -K_p K_M & 0 & 0 & 0 & 0 \\ \frac{G_p}{(J_e + J_f)} & -\frac{F_R}{(J_e + J_f)} & \frac{-2rk_{ts}}{(J_e + J_f)} & 0 & 0 & 0 \\ 0 & 2r & 0 & -1 & -1 & 0 \\ 0 & 0 & \frac{k_{ts}}{J_e} & \frac{-k_{ts}r^2}{J_e v_x} & 0 & \frac{k_{ts}}{J_e v_x} \\ 0 & 0 & \frac{k_{ts}}{J_t} & 0 & \frac{-k_{ts}r^2}{J_t v_x} & \frac{k_{ts}}{J_t v_x} \\ 0 & 0 & 0 & \frac{k_{ts}r}{mv_x} & \frac{k_{ts}r}{mv_x} & \frac{-(k_{ts}+k_{ts})}{mv_x} - \frac{(\Phi+2rv_x)}{m} \end{pmatrix} \quad 5.11$$

$$B = \begin{pmatrix} K_p K_a & 0 & 0 \\ 0 & 0 & 0 \\ 0 & 0 & 0 \\ 0 & 1 & 0 \\ 0 & 0 & 1 \\ 0 & 0 & 0 \end{pmatrix} \qquad 5.12$$

$$C = \begin{pmatrix} 0 & 0 & 0 & r_r & 0 & -1 \\ 0 & 0 & 0 & 0 & r_r & -1 \end{pmatrix} \qquad 5.13$$

The states are:-

x_1 Manifold pressure (bar)
x_2 Engine speed (rad/s)
x_3 Aggregate axle twist (rad)
x_4 Left wheel speed (rad/s)
x_5 Right wheel speed (rad/s)
x_6 Vehicle speed (m/s)

The inputs are

u_1 Throttle angle (deg)
u_2 Left wheel brake torque (Nm)
u_3 Right wheel brake torque (Nm)

The outputs are

y_1 Slip to left wheel
y_2 Slip to right wheel

Diagonalisation

A simplistic approach to brake control is to design each wheel-spin control loop independently. This approach is likely to give across axle interaction due to the reasons stated above. However, if the two control loops can be re-structured in order to minimise the interaction effects (achieving diagonal dominance) then SISO controllers can be designed for each loop. Approaches using multi-variable Nyquist-like methods are based on improving system dominance (57) and, once achieved, treating the systems as n (i.e. 2) SISO control design problems.

Expressing the above linear state-space system as a transfer function matrix, the symmetry of the system can be readily appreciated. It will be recalled that the transfer function matrix is defined as $G(s) = C(sI - A)^{-1}B$ in terms of the state variable model. Parameters in Table 5.1 with the vehicle in first gear and with the following conditions have been used:-

$v_b = 5ms^{-1}$

$k_w = k_w = 100Nslip^{-1}$

(i.e. just to the left hand side of the μ slip curve)

The transfer function turns out to be symmetrical as follows:-

$$\begin{pmatrix} slip_1(s) \\ slip_2(s) \end{pmatrix} = \begin{pmatrix} g_1(s) & g_2(s) \\ g_2(s) & g_1(s) \end{pmatrix} \begin{pmatrix} T_1(s) \\ T_2(s) \end{pmatrix} + \begin{pmatrix} g_3(s) \\ g_3(s) \end{pmatrix} Throttle(s) \qquad 5.14$$

where

$slip_{1,2}$ is the normalised slip of the driven wheels

$T_{1,2}$ is the brake torque to the driven wheels

$Throttle(s)$ is the throttle angle in degrees

$$g_1(s) = -0.281 * \frac{(s^3 - 1.59s + 2732)(s + 15.61)(s + 0.769)(s + 0.015)}{(s^2 - 1.815s + 4732.8)(s + 15.6)(s + 0.56)(s + 0.02)(s + 2.11)}$$

$$g_2(s) = 562 * \frac{(s + 15.61)(s + 0.252)(s + 0.044)}{(s^2 - 1.815s + 4732.8)(s + 15.6)(s + 0.56)(s + 0.02)(s + 2.11)}$$

$$g_3(s) = 0.229 * \frac{(s + 2.106)(s + 0.006)}{(s^2 - 1.815s + 4732.8)(s + 15.6)(s + 0.56)(s + 0.02)(s + 2.11)}$$

It is the off-diagonal elements (i.e. $g_2(s)$) which give the interaction between the two wheels. The column dominance of this system (equation 5.14) can be calculated using the fcdom utility of MATLAB (59). This is a plot of $\frac{\Sigma|g_i(jw)|}{|g_j(jw)|}$ which in our particular case is $\frac{|g_2(jw)|}{|g_1(jw)|}$ for the second column of equation 5.14. A plot of the column dominance is shown in Figure 5.6 for the above system with $k_w = k_w = 10^3 N/slip$ which is typical of the tyre characteristic on good road surfaces. In this plot, the peak

interaction frequency can be seen at the shuffle mode frequency of 28.4 rad/s (4.52 Hz) and remains below unity at all frequencies and hence shows that across-axle interaction should not be a problem under these conditions. For vehicles operating on low μ surfaces, this assumption would be very optimistic indeed and Figure 5.8 shows that at the peak of the μ-slip curve, the interaction now exceeds unity indicating that the system is not diagonally dominant and control loop interactions would be a problem unless a pre-compensator is designed. The frequency peak occurs at 68.8 rad/s (10.94 Hz) which is around the natural frequency of the mode due to wheel inertias oscillating in anti-phase with the engine inertia. For μ-split surfaces, interactions are again likely as shown in Figure 5.10 where the peak is at 52.5 rad/s (8.35 Hz).

Based on a similar problem described by Owens (56) the plant can be diagonalised by the following matrix manipulation.

$$\begin{pmatrix} g'_1(s) \\ g'_2(s) \end{pmatrix} = \begin{pmatrix} 1 & 1 \\ 1 & -1 \end{pmatrix} \begin{pmatrix} g_1(s) & g_2(s) \\ g_2(s) & g_1(s) \end{pmatrix} \begin{pmatrix} 0.5 & 0.5 \\ 0.5 & -0.5 \end{pmatrix} \qquad 5.15$$

yielding

$$\begin{pmatrix} g'_1(s) \\ g'_2(s) \end{pmatrix} = \begin{pmatrix} g_1(s)+g_2(s) & 0 \\ 0 & g_1(s)-g_2(s) \end{pmatrix} \qquad 5.16$$

Due to the symmetry, and from equations 5.15 and 5.16, the transfer function matrix can be expressed as:-

$$\begin{pmatrix} g_1(s) & g_2(s) \\ g_2(s) & g_1(s) \end{pmatrix} = \begin{pmatrix} 1 & 1 \\ 1 & -1 \end{pmatrix} \begin{pmatrix} g_1(s)+g_2(s) & 0 \\ 0 & g_1(s)-g_2(s) \end{pmatrix} \begin{pmatrix} 0.5 & 0.5 \\ 0.5 & -0.5 \end{pmatrix} \qquad 5.17$$

This structure is said to be the *dyadic* decomposition of the system matrix . It is analogous to an eigenvalue decomposition of the system transfer function matrix with the frequency independent eigenvectors {1 1} and {1 -1} and the eigenvalues being the eigenvalues of $(g_1(s)+g_2(s))$ & $(g_1(s)-g_2(s))$. A *dyadic* decomposition of a

transfer function matrix is a diagonal transfer function matrix sandwiched between two constant matrices. The interaction between the two 'systems' is handled by the constant matrices.

The diagonalisation has turned a multi-variable control problem into two single-input single-output control problems. Physically, the controller is effectively trying to control the average wheel speed error and the difference in wheel speed error. This makes sense based on the controller objectives given in section 5.1 above.

For equation 5.15 above the B & C matrices for the compensated system are:-

$$B = \begin{pmatrix} 0 & 0 \\ 0 & 0 \\ 0 & 0 \\ 1 & -1 \\ -1 & 1 \\ 0 & 0 \end{pmatrix} \qquad 5.18$$

$$C = \begin{pmatrix} 0 & 0 & 0 & r_t & -r_t & -1 \\ 0 & 0 & 0 & -r_t & r_t & 0 \end{pmatrix} \qquad 5.19$$

With this representation the interaction of the compensated system can be investigated. The reduced interaction can be seen in Figure 5.7, Figure 5.9 and Figure 5.11. These figures should be compared with Figure 5.6, Figure 5.8 & Figure 5.10 respectively. This analysis highlights the benefits of diagonalising the plant to reduce the interactions where in all the cases the interactions are reduced. However it should be noted that split μ surfaces interactions could be a problem. This is to be expected since on split μ surfaces the plant is no longer symmetrical.

The above analysis is sound provided the system remains linear. Non-linear plant parameters (see equation 5.11), such as axle stiffness varying with displacement, should not be a problem since provided we have the same non-linear parameter for each wheel, then the plant will remain symmetrical. However, linearity implies that the principle of superposition holds i.e. the system will respond equally, but in

opposite directions, to positive and negative transients. In our particular case, this would imply that 'negative' braking commands should accelerate the wheel. This is clearly not the case and in order to examine the significance, non-linear simulation needs to be used. Figure 5.12 shows a Matrix$_x$ block diagram of the powertrain dynamics (blocks 2, 3, 4 & 15) and Brake dynamics (block 23) cascaded with the average and difference (blocks 13 & 14) calculations. Perturbations in input 1 should affect only output 1 with no interaction seen in output 2 and vice-versa. Figure 5.14 shows the response of the average system dynamics to a positive step in average brake command (i.e. brake pressure increasing) resulting in average slip reducing and no effect on slip difference thereby indicating dominance has been achieved. Figure 5.15 shows the response to a positive command to the brake difference loop. The difference in speeds drops rapidly. However, there is some decrease in average slip, indicating some interaction occurring but the system is diagonally dominant.

Discrete Root Loci

Not included in the structural considerations above is the actuator dynamics, the response of which can be seen in Figure 5.16. These step responses clearly show the very slow pressure build dynamics (Time constant approx 0.8s) and the relatively fast pressure decay dynamics (Time constant approx 0.02s). The structure of the controller and plant is shown in Figure 5.13. For the design used here, each loop (i.e. average and difference loops) was cascaded with each representation of the brake dynamics and then discretised using the 'matrix exponential' (60) transform. It is important to use this particular transformation since other simpler transformations do not map completely the stable region of the s-plane to the z-plane or vice-versa (58) and this is especially important where we have underdamped poles.

This analysis gave four models requiring analysis for each operating point. These are:-

i) average loop during pressure build

ii) average loop during pressure decay

iii) difference loop during pressure build and

iv) difference loop during pressure decay

Figure 5.17,Figure 5.18,Figure 5.19 & Figure 5.20 show the four discrete root loci for the four models described in the previous paragraph for a PD controller with zeros at z=0.8 and 1.0. The open loop poles in the left quadrants of the z-plane are due to the mode associated with wheel and engine inertias in anti-phase and with the tyres 'slipping' just to the left hand side of the μ slip characteristic. Increasing the loop gains show that this mode becomes unstable for the average loop. However, pole/zero cancellations occur within the difference loop and the mode is not destabilised. Great care needs to be taken of pole zero cancellations since the zero may move, due modelling inaccuracies, resulting in unstable modes. The symmetry of this problem indicates that whilst the zero may move, the closed loop pole would always be within the unit disc and hence in a better position than on the average loop for a given loop gain. It is interesting to note that the fast pressure decay pole pulls the root location towards the origin (Figure 5.18), whereas the slower build dynamics results in a low frequency underdamped mode as can be seen in Figure 5.17.

Integral control was not feasible with the loop times used here and this can be seen in the root loci in Figure 5.21 to Figure 5.24. The instability seen is a low frequency mode and this in fact was observed in practice as will be seen in section 5.5 below. It is also interesting to note that the instability only occurs with the slow pressure build dynamics (see Figure 5.21 and Figure 5.23). This leads to the conclusion that the use of a larger pump and the addition of an accumulator, with a

consequent increase in pressure build bandwidth, would enable the use of integral control. Furthermore, it could be concluded that, if the bandwidth were increased, then the difference loop should include integral control and the average loop should not.

5.4 Simulation Trials

Based on the above control system studies, a discrete representation of the PD controller was tried on the non-linear simulation model described above. Figure 5.25 shows the response of the controller to a step change in μ on both left and right wheels. The time of the step change in μ to each wheel is staggered in order to attempt to provoke across axle interaction in the controller. The across axle mode is provoked, and is eventually damped. The response is better damped in practice. A high frequency (approx 10 Hz) oscillation can be seen on the response. This is the wheel/engine inertia mode. The mode is sustained with almost no damping and this is due to the controller operating at the peak of the μ slip tyre curve and the absence of any damping in the powertrain. This undamped mode is evident in the discrete root loci referred to above. In practice, damping due to brake and driveline drag which has not been represented in the model, damps both this mode and the across axle mode. The slow dynamics of the brakes limits the performance of the controller resulting in high initial overshoot. Figure 5.26 shows the results of a speculative simulation in which the brake pressure build dynamics have been increased to the speed of the pressure decay dynamics (i.e. Time constant changed from 0.8s to 0.02 s). The discrete root locus for the brake pressure build is now the same as for the pressure decay shown in Figure 5.18 and Figure 5.20. Comparing Figure 5.25 and Figure 5.26 it can be seen that the interaction and overshoot have been reduced.

5.5 Vehicle Trials

Vehicle tests have been performed on artificial low μ surfaces. This work was carried out by the author in conjunction with personnel from Bendix, France. The initial

developments were performed on a frozen lake in Sweden. This testing revealed a problem with the brake model in that the observed brake dynamics were much slower than those used in the simulation. The simulation model was re-parameterised based on the data in Figure 5.16 and used to develop new controller gains. Unfortunately, it was then only possible to re-test the hardware on artificial surfaces. The μ slip characteristic for each of these surfaces is shown in Figure 5.27. The surfaces are representative of ice (stainless steel) and packed snow (Bridport stone). The tests have consisted of aggressive take-off from rest manoeuvres in order to assess the stability of control. Figure 5.28 to Figure 5.31 show the response of the actual controller on the FWD vehicle. Of interest in these figure is:-

i) one channel of data alternating at 5ms intervals left and right wheel speeds and

ii) left and right driven wheel brake pressure.

Figure 5.28 shows that on a very low μ surface, the stability of control is excellent with the actual desired slip being attained by both wheels. Any tendency to provoke an inter axle oscillation is rapidly damped. The pressure fluctuations seen in Figure 5.28 are due mainly to the 25Hz PWM period and partly due to the cyclical fluctuations produced by the hydraulic pump providing pressure to the system. Figure 5.29 shows the vehicle response on a μ split surface. Again, control is smooth and progressive. The initial slow response is due to the slow dynamics associated with the pressure build/motor start up. Due to this non-linearity in the brake actuation dynamics, a higher gain on entry into traction control would probably help but was not tried. Also note that the high frequency wheel mode in Figure 5.29 (and referred to in 5.4 above) is more highly damped than the simulation predicted due probably to driveline losses and brake drag. The tests were repeated on Bridport stone and the results are shown in Figure 5.30 & Figure 5.31. For uniform Bridport stone (Figure 5.30) there is evidence of an across axle oscillation which is damped out after approximately 1.5 seconds. On

the μ split surface, the control is extremely good with only the wheel/engine inertia mode evident. It is worth noting that this mode, at approximately 7.6 Hz, is almost impossible to control since the bandwidth of the controller is only 25 Hz. This is limited by the bandwidth of the PWM frequency of 25 Hz and the extremely slow brake dynamics.

Subjectively, this control was judged to be comfortable with only the 25 Hz PWM 'chatter' being felt. A higher PWM frequency is feasible with the Bendix hardware and would eliminate this problem. In addition, the use of more levels within the current 25Hz PWM would improve the control and tend to limit the across axle interaction.

5.6 Conclusion

A diagonally dominant brake control algorithm has been designed and demonstrated. This results in two independent control loops which control the average wheel slip and the wheel slip difference. The addition of engine intervention should be a straightforward addition to the average slip loop. The work has shown that a PID algorithm designed using classical techniques is a valid technique for brake only traction control algorithm design. The basic control algorithm consists of six parameters to be calibrated which represents a huge reduction in the number seen in typical rule-based strategies. This resulted in a rapid on-vehicle calibration.

The driveline and brake model structure used is well known to adequately represent the dynamics of a powertrain. With the limited validation performed for this particular vehicle the model has enabled the rapid on-vehicle calibration since it enabled the structure of the multi-variable control algorithm to be checked first on the model. The discrete analysis performed on the linearised models gave the correct PID relative values and meant that only a single parameter needed to be tuned in practice.

The comfort of the brake only traction controller is good with only the 25Hz PWM pulsations being felt by the driver. A higher PWM frequency with a greater number of pressure levels would solve this problem on the current brake hardware. Finally, the simulation work has shown that faster brakes (possibly with accumulator) and faster processors will greatly enhance the performance of this approach.

A considerable advantage with this approach is that a single strategy is used for both μ split and homogeneous surfaces. This means the elimination of decisions to determine the surface encountered and the subsequent scheduling of different control algorithms.

5.7 Figures

Figure 5.1 Schematic diagram of the powertrain

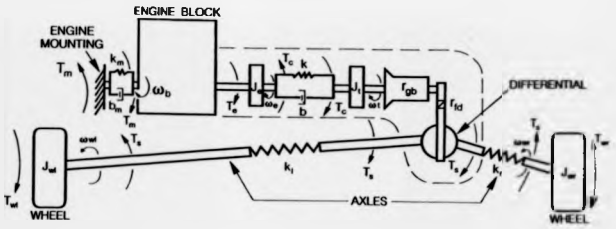

Figure 5.2 Brake hydraulics - diagonal arrangement

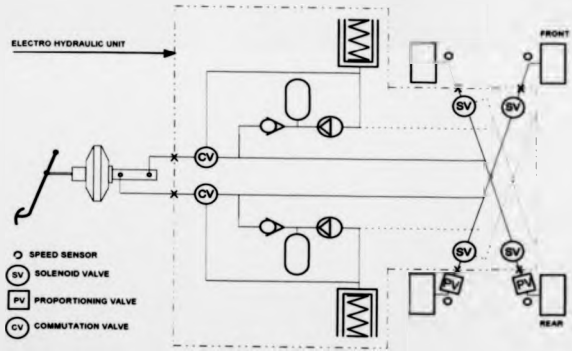

Figure 5.3 Brake hydraulics - valve layout

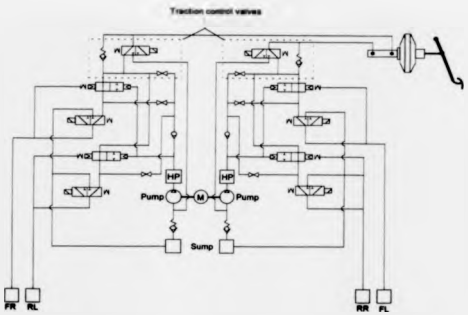

Figure 5.4 Brake hydraulics - representation of a single circuit for model

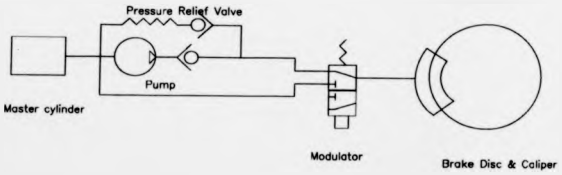

Figure 5.5 Pressure volume characteristic assumed for the Brake cylinder

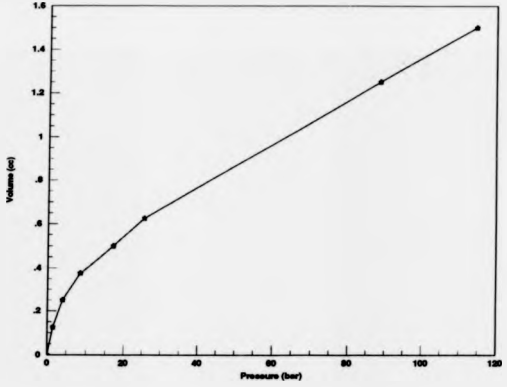

Figure 5.6 Column Dominance of brake system with tyre operating at the left of the peak on the mu/slip characteristic.

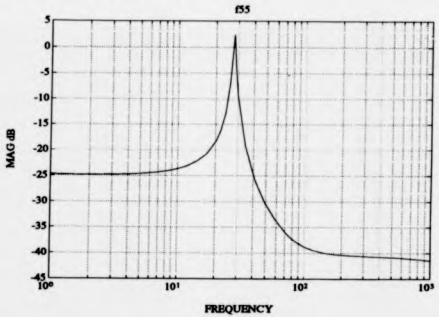

Figure 5.7 Column Dominance of the diagonalised brake system with tyre operating at the left of the peak on the mu/slip characteristic.

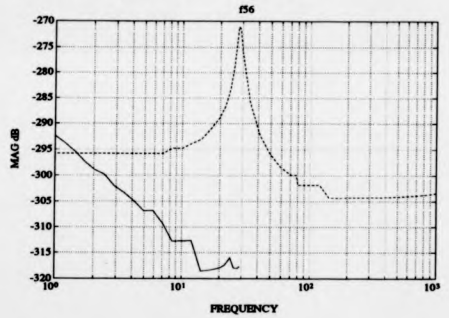

Figure 5.8 Column Dominance of brake system with the tyre at the peak on the mu/slip characteristic.

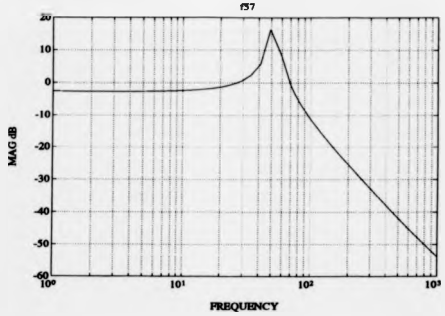

Figure 5.9 Column Dominance of the diagonalised brake system with the tyre at the peak on the mu/slip characteristic.

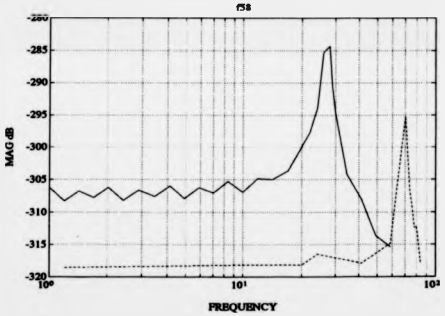

Figure 5.10 Column Dominance of the brake system with one tyre at the peak on the mu/slip characteristic and the other to the left (i.e. split mu)

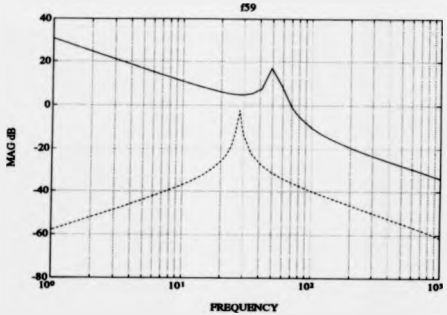

Figure 5.11 Column Dominance of the diagonalised brake system with one tyre at the peak on the mu/slip characteristic and the other to the left (i.e. split mu)

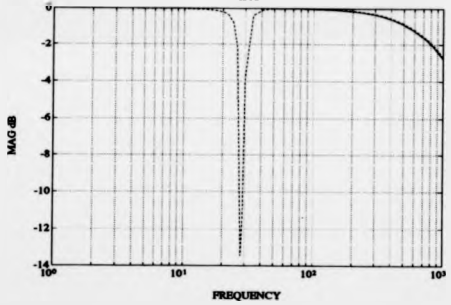

Figure 5.12 Matrix, block diagram of the powertrain dynamics and diagonalisation blocks

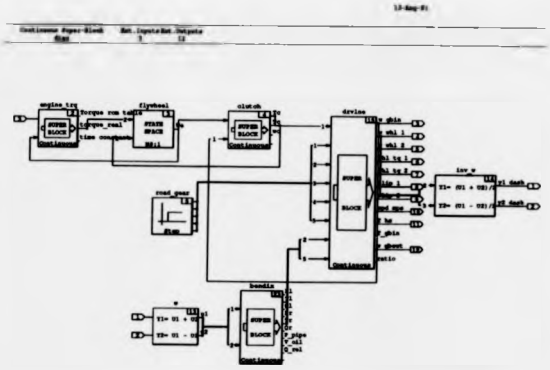

Figure 5.13 Schematic diagram of the compensated powertrain dynamics

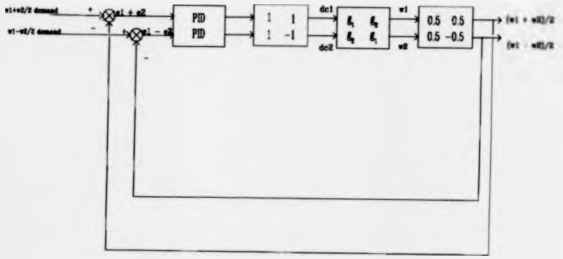

Figure 5.14 Response of compensated powertrain dynamics to a step input on the average loop

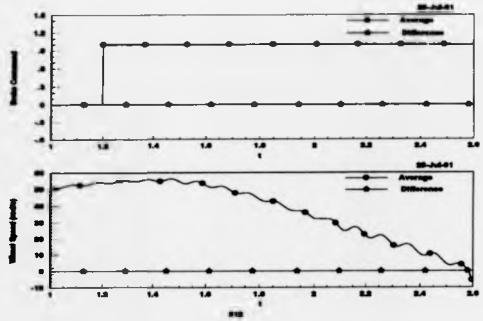

Figure 5.15 Response of compensated powertrain dynamics to a step input on the difference loop

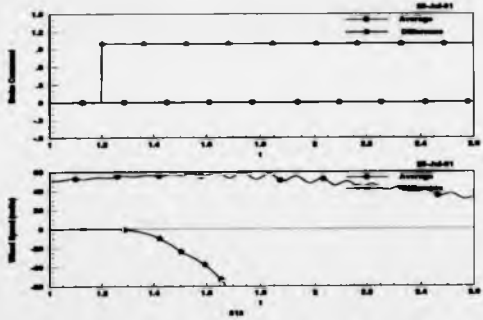

Figure 5.16 Response of the brake system to a step change in pressure demand

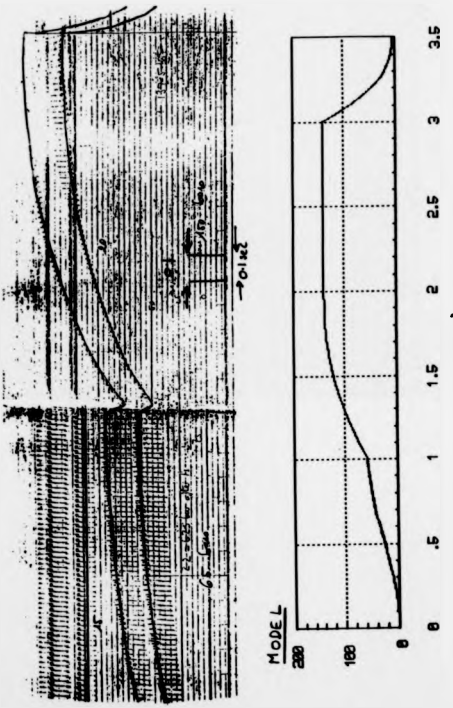

Figure 5.17 Discrete root locus of PD controller operating on the average loop during brake pressure build.

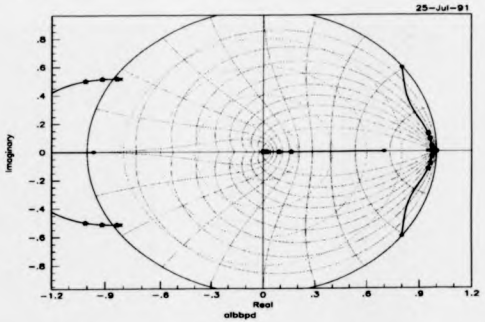

Figure 5.18 Discrete root locus of PD controller operating on the average loop during brake pressure decay.

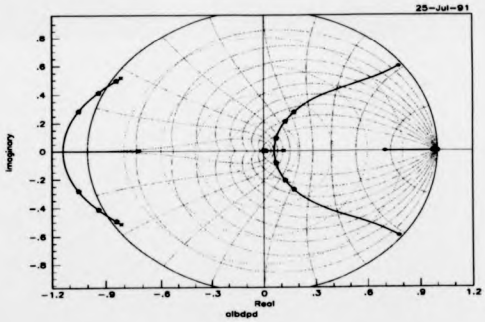

Figure 5.19 Discrete root locus of PD controller operating on the difference loop during brake pressure build.

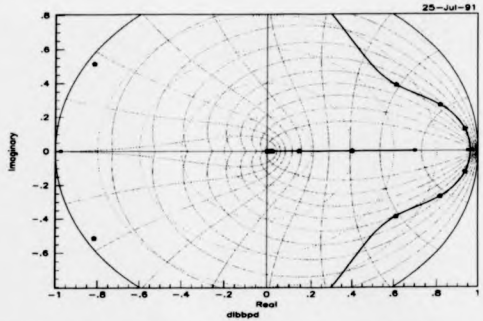

Figure 5.20 Discrete root locus of PD controller operating on the difference loop during brake pressure decay

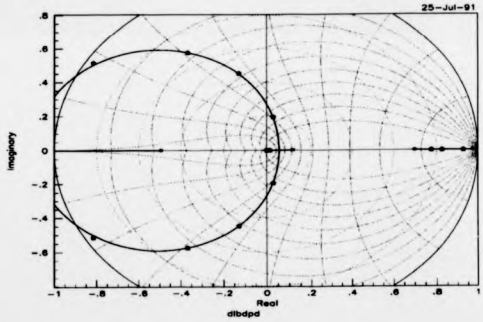

Figure 5.21 Discrete root locus of PID controller operating on the average loop during brake pressure build.

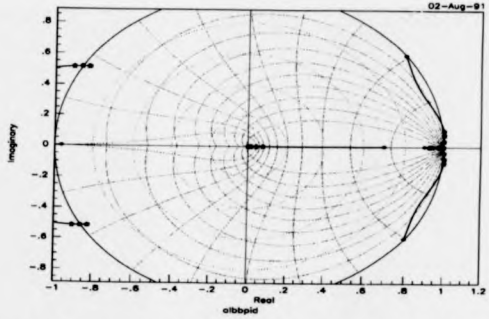

Figure 5.22 Discrete root locus of PID controller operating on the average loop during brake pressure decay.

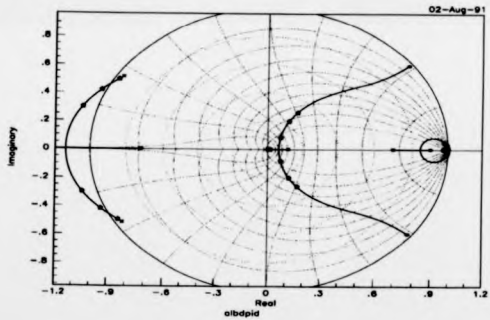

Figure 5.23 Discrete root locus of PID controller operating on the difference loop during brake pressure build.

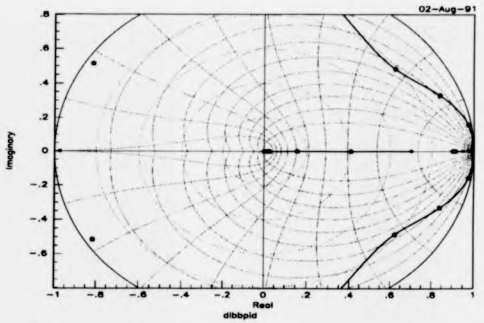

Figure 5.24 Discrete root locus of PID controller operating on the difference loop during brake pressure decay

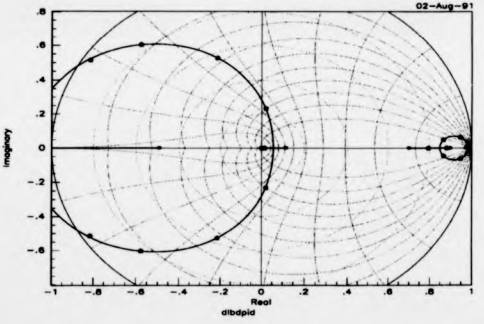

Figure 5.25 Simulation of the response of the PD controller

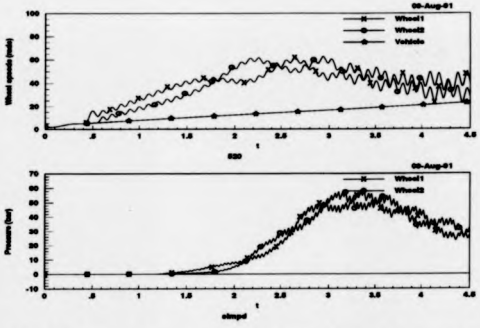

Figure 5.26 Simulation of the response of a PID controller with faster brake pressure build dynamics

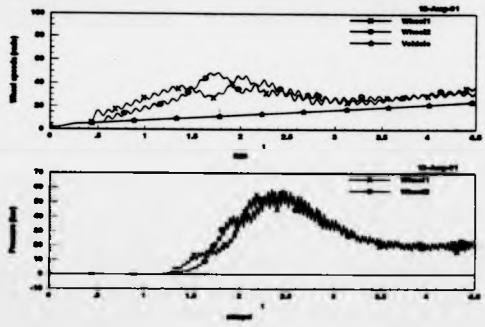

Figure 5.27 μ slip characteristics for Various surfaces

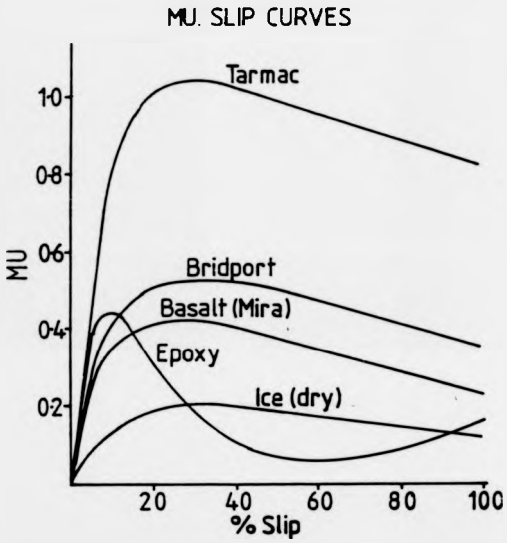

Figure 5.28 Vehicle response to an aggressive take-off from rest on uniform stainless steel.

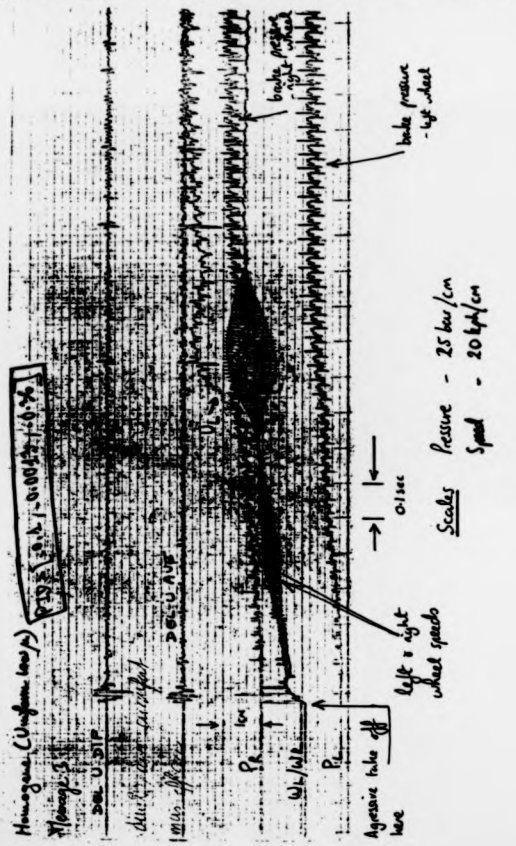

Figure 5.29 Vehicle response to an aggressive take-off from rest on split stainless steel/asphalt.

Figure 5.30 Vehicle response to an aggressive take-off from rest on Bridport stone

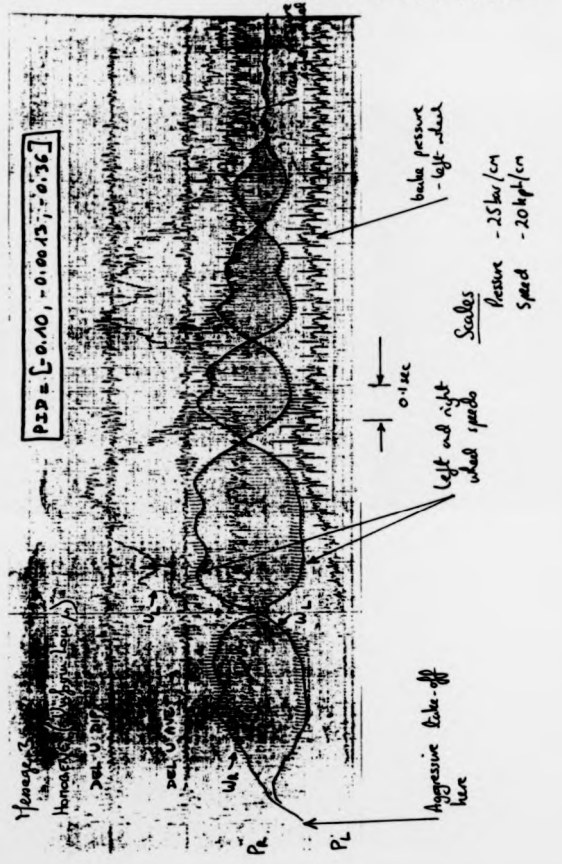

Figure 5.31 Vehicle response to an aggressive take-off from rest on split Bridport stone/asphalt.

6 Review of the Work & Conclusion

The broad intention of this work was to demonstrate the suitability of Computer Aided Control System Design techniques and fundamental control ideas to an automotive system. Such systems are generally multi-rate, multi-variable and non-linear and for these reasons it is a widely held belief within the automotive industry that both classical and modern control theory are merely theoretical concepts with no place in the real automotive world. The majority of control theory is based upon linear systems theory and it is clear that this theory cannot be applied to automotive systems in an automated manner. However, what this thesis shows is that great insight can be obtained through the application of the classical analytical techniques to a non-linear system in order to develop a soundly structured control system. Such systems can then be based upon linear control systems theory.

The specific intention of the work was to define the physical basis of the traction control problem, review the current strategies and propose a new approach. This approach consisted of adapting and developing dynamic models of powertrains and the application of control theory based ideas to these models in order to develop and implement controllers. The approach taken was the standard method of controlling wheel slip on the basis that the maximum tractive effort can be attained by controlling to a specific level of wheel slip. With current sensor technology this is a sound procedure, however there is a clear need for sensors which can measure tractive effort in order to allow optimum traction to be attained. Furthermore, there is even greater scope for improvement through the use of low cost accelerometers, which can be used to measure yaw rate, in which case the vehicle instability can be controlled directly. An alternative approach to measuring tractive effort would be to use an observer to estimate tractive effort based on existing measurements of manifold pressure, throttle

angle, engine speed and wheel speed. Simulation would provide an ideal framework to investigate the development of such an observer and therefore must represent an area where further work is recommended.

Chapter 1 has placed traction control within the wider context of powertrain control. The eventual linking of traction control within a hierarchical vehicle powertrain controller is becoming more attractive for the following reasons; safety and reliability, sharing of sensors and cheaper more powerful microprocessors. For these reasons it is important that individual controllers are analytically based so as to allow the whole system to be analysed from a stability point of view.

Chapter 2 has justified the model complexity adopted. Consideration of other driveline phenomena shows that this level of model is suitable for other studies. Indeed, within Ford Motor Co, models of this level are widely used to address drivetrain design. This has been capitalised on in this study. The key non-linearity - the tyre characteristic - has been physically justified and the effect of this upon the system dynamics has been considered in detail. It was highlighted that the tyre model used was purely a static fit of model parameters to observed data. Whilst this yields a force/slip characteristic typical of most tyre/road interfaces, an improvement would be to enhance the tyre model to a model in which the parameters have physical significance. The basis of such models has been published and therefore this suggestion could be readily carried out. In addition, it is recommended that measurements to parameterise such models are carried out on real low μ surfaces under varying conditions. This is suggested since the behaviour of the real controller actually varies significantly with the condition (probably temperature) of the ice. In particular, the target slip used for the controller was empirically based in order to handle this variation. The reasons for this variation is probably due to a shift in the position of the peak of the μ slip curve. However this needs to be understood.

angle, engine speed and wheel speed. Simulation would provide an ideal framework to investigate the development of such an observer and therefore must represent an area where further work is recommended.

Chapter 1 has placed traction control within the wider context of powertrain control. The eventual linking of traction control within a hierarchical vehicle powertrain controller is becoming more attractive for the following reasons; safety and reliability, sharing of sensors and cheaper more powerful microprocessors. For these reasons it is important that individual controllers are analytically based so as to allow the whole system to be analysed from a stability point of view.

Chapter 2 has justified the model complexity adopted. Consideration of other driveline phenomena shows that this level of model is suitable for other studies. Indeed, within Ford Motor Co, models of this level are widely used to address drivetrain design. This has been capitalised on in this study. The key non-linearity - the tyre characteristic - has been physically justified and the effect of this upon the system dynamics has been considered in detail. It was highlighted that the tyre model used was purely a static fit of model parameters to observed data. Whilst this yields a force/slip characteristic typical of most tyre/road interfaces, an improvement would be to enhance the tyre model to a model in which the parameters have physical significance. The basis of such models has been published and therefore this suggestion could be readily carried out. In addition, it is recommended that measurements to parameterise such models are carried out on real low μ surfaces under varying conditions. This is suggested since the behaviour of the real controller actually varies significantly with the condition (probably temperature) of the ice. In particular, the target slip used for the controller was empirically based in order to handle this variation. The reasons for this variation is probably due to a shift in the position of the peak of the μ slip curve. However this needs to be understood.

Other non-linearities in the system (i.e. torque converter, gear ratio and engine characteristics) have been explored through linearisation of the total system and root locus plots. This work gives a good insight into the dynamics of vehicle powertrains which has more general application than merely for the traction control system development.

Chapter 3 has described the basis behind rule-based traction controllers in terms of the non-linearities associated with the tyre. Since rule based controllers cannot be analysed in a formal control setting, an optimisation routine has been developed in order to tune the PID throttle algorithm. This approach also overcomes the problems associated with linearising a multi-rate system with severe non-linearities. This aspect is typical of many automotive control problems and hence the method has a potentially wide area of application. The routine has been incorporated into a procedure within Matrix$_x$ which should facilitate such an extension. The optimisation algorithm used was a steepest descent algorithm. This is known to be robust but is sub-optimal in finding the optimum. Therefore it is recommended that a more efficient algorithm is tried in order to speed up the process. Stability margins were not examined for the resulting 'optimised' controller and perhaps this area could be addressed using parameter sensitivity studies.

The control scheme discussed here has been implemented on a vehicle and the utility to traction control development has thus been demonstrated. Furthermore, the complete powertrain model including engine has been partially validated.

In Chapter 4, having already validated the approach in Chapter 3, the emphasis of the work shifted to a different configuration which required re-modelling. A significant effort was involved in the engine work. This essentially took the structure developed by others within Ford Motor Company which the author parameterised using multiple linear regression and physical considerations. Following on from this,

the complete engine model was then validated. This work illustrates that low order models can be used to represent the engine over its entire operating range (the term 'low order' is intended to describe both the static and dynamic representation of physical phenomena).

The model was used to investigate the effect of spark retard on speeding up the response of the traction controller. The improvement turned out to be minimal. One solution to improve the response would be to cut the spark completely. This would offer the same speed of response as retarding the spark but would also give better range of authority. It is recommended that this strategy is investigated in further simulation studies. In addition, this model should be used to investigate fuel intervention strategies since fuel intervention offers the same dynamic response as spark intervention but with lower emission difficulties.

An area which has not been investigated but which does need investigating is the extent to which fuel and spark intervention schemes cause emissions to deteriorate. As far as legislated drive cycles are concerned, the impact of fuel and spark traction control schemes is non-existent. This is because emission tests are performed on chassis rolls over specific drive cycles which do not involve driving on low friction surfaces. Hence traction control does not operate during an emission test. However, this factor should not inhibit automotive companies from investigating the emissions issues associated with fuel and spark control schemes. The introduction of the Clean Air Act in the U.S.A., with the requirement for emission conformity within 100,000 miles, should encourage this. This is because vehicles operating extensively in northern regions with significant wintery periods may spend many miles driving with traction control operating. Deterioration in emission quality during traction control may under these conditions lead to premature catalyst failure and hence non-compliance with the 100,000 mile requirement of the Clean Air Act. Provided

emission conformity can be still met, it is the authors view that a properly coordinated fuel and throttle intervention scheme offers the best opportunity for the optimum traction control system.

Chapter 5 has examined the multi-variable structural considerations of the complete axle and brake system. The analysis has focussed on the symmetry of the control problem and has restructured the controller. The restructuring is justified in both mathematical and physical terms. The resulting controller was then examined from a stability viewpoint and directly implemented on a prototype vehicle. Although the work was successfully demonstrated, it is anticipated - and was justified based on simulation - that increasing the bandwidth of the brake hydraulics should improve both the response time and the stability of control. Increasing the bandwidth could be readily accomplished with the addition of an accumulator within the hydraulic circuit. Such a development involves the usual trade off between cost with complexity and quality. Such speculative studies illustrate the importance of developing controllers using both simulation and real hardware.

This vehicle work should be taken further in order to examine its robustness. This could be progressed on the simulation using the improved tyre model recommended above. Additionally, the controller should be assessed on a variety of different surfaces in order to appropriately complement the enhanced modelling work.

In addition to allowing speculative studies, the work has demonstrated the value of control analysis - supported by non-linear simulation - in developing a real control system. However, the value of vehicle development in parallel with the control analysis cannot be overstated. Adopting either approach in isolation suffers from disadvantages. Using hardware alone, the engineer relies on experience, physical

understanding and limited analysis and cannot examine the detailed interactions which occur. Simulation alone, without continual reference to hardware, can result in going off at a tangent if modelling errors or inaccuracies exist.

An additional improvement would arise in increasing the resolution of the PWM control. The improvement would be associated with the NVH associated with the controller. This could be readily demonstrated with only minor hardware changes and it is recommended that this should be pursued.

The majority of the analysis has been carried out using Matrix$_x$. Whilst in general this was found to represent a user friendly interface to simulation, the user is left to manage his own model database. This is time consuming and it is recommended that this is addressed with upgrades of the package.

Finally, since partially validated models for the FWD and RWD vehicle powertrains now exist, it is recommended that more advanced control schemes are investigated on the simulation models initially, followed by vehicle trials if promising ideas emerge.

7 References

(1) Tokuda, T., 1988, 'Cars in the '90s as a humanware', SAE (Society of Automotive Engineers) Paper No. 885049.

(2) Hrovat, D. and Powers, W.F., 1988, 'Computer Control Systems for Automotive Power Trains', IEEE Control Systems , Aug 88.

(3) Sweet, L.M., 1982, 'Automotive Applications of Modern Control Theory', SAE paper No. 820913.

(4) Braess, H.H. and Thompson, B., 1987, 'The motor vehicle - a good example of the wide range of applications of modern control engineering', Proc. of 10th IFAC World Congress, Munich.

(5) Kiencke, U., 1987, 'The role of automatic control in automotive systems', Proc. of 10th IFAC World Congress, Munich.

(6) Heesse, G. and van Zanten, A., 1988, 'System Approach to vehicle dynamic control', SAE Paper No. 885107.

(7) Schweitzer, P.H. and Collins, T.W., 1978, 'Electronic Spark Timing Control for Motor Vehicles', SAE Paper No. 780655.

(8) Bowler, L.L., 1980, 'Electronic Fuel Management - Fundamentals', SAE Paper No. 800539.

(9) Amann, C.A., 1986, 'The powertrain, fuel economy and the environment', Int J. of Vehicle Design, vol 7, no 1/2, pp 1-34.

(10) Cassidy, J.F., 1978, 'A Computerized On-Line Approach to Calculating Optimum Engine Calibrations', SAE Paper No. 770078.

(11) Dohner, A.R., 1978, 'Transient System Optimization of an Experimental Engine Control System Over the Federal Emissions Driving Schedule', SAE Paper No. 780286

(12) Wakeman, A.C., Ironside, J.M., Holmes, M., Edwards, S.I. and Nutton, D., 1987, 'Adaptive Engine Controls for fuel consumption and Emissions Reduction', SAE Paper No. 870083.

(13) Gibbons, E., 1991, 'Discussion Ford U.S.A.'

(14) Morris, R.L. and Powell, B.K., 1983, 'Modern Control Applications in Idle Speed Control', Proc. ACC (American Control Conference) pgs 79-85

(15) Powell, B.K., Cook, J.A. and Grizzle, J.W., 1987, 'Modeling and analysis of an inherently multi-rate sampling fuel injected engine idle speed control loop', Proc. ACC.

(16) Abate, M. and Dosio, N., 1990, 'Use of fuzzy logic for engine idle speed control', SAE Paper No. 900594.

(17) Hedrick, J.K. and Green, J.H., 1990, 'Non-linear speed control for automotive engines', Proc. ACC.

(18) Main, J.J., 1986, 'Ford ELTEC Integrated Powertrain Control', SAE Paper No. 860652.

(19) Stuntz, R., Roller, L. and Swick C., 1989, 'Final report of ELD phase III project ', Ford Internal Report - Traction Control EAO Technology Review Jan 23 1989.

(20) Klein, H.C., 1986, 'Anti-lock brake systems for passenger cars, state of the art', SAE Paper No 865139

(21) Crossley, P.R., 1988, 'Anti-spin Control', SAE paper No. 885106.

(22) Crossley, P.R., 1989, 'Traction Control System Development', Proceedings of IMechE Autotech (Anti-lock braking system engineering and traction control seminar), C399/28.

(23) Crossley, P.R. and Hrovat, D., 1988, 'Report on the Teves Traction Control System Appraisal', Ford Internal Memorandum, 12 May 1988

(24) Farr, G.P.R., 1989, 'Combined anti-lock and traction control' Proceedings of IMechE Autotech (Anti-lock braking system engineering and traction control seminar), C399/28.

(25) Hrovat, D., Tobler, W.E. and Tsangarides, M.C., 1985, 'Bond Graph modeling of dominant dynamics of automotive power trains', Proc. ASME Winter Annual Meeting, Publication DSC Vol 1. Pgs 293-301

(26) Schulze, B.G. and Lissel, E., 1988, 'Anti-slip regulator with high performance and comfort', Proceedings of IMechE conference on Traction Control and Anti wheel-spin systems, C367/88

(27) Tan, H., 1989, 'A Discrete-Time Robust Vehicle Traction Controller Design', Proc. ACC pgs 1053-1058

(28) Inoue, Y., Minegishi, H. and Miyazaki, H., 1988, 'A traction control system for use in rear wheel drive vehicles with automatic transmissions', Proceedings of IMechE conference on Traction Control and Anti wheel-spin systems, C366/88

(29) Maisch, W., Jonner, W.D. and Sigl, A., 1987, 'ASR - Traction control - A logical extension of ABS', SAE Paper No. 870337.

(30) Leiber, H., Czinczel, A. and Anlauf, J., 1982, 'Anti-skid systems (ABS) for passenger cars', Bosch Technische Berichte Feb 1982

(31) Bleckmann, H.W. and Weise, L., 1986, "The new four-wheel anti-lock generation: a compact anti-lock and booster aggregate and an advanced electronic safety concept' Proceedings IMechE Vol. 200 No. D4.

(32) Brandstetter, W. and Lany, E., 1986, 'The Volkswagen Vanagon Synchro - A novel 4WD concept with the new 2.1l water-cooled engine', SAE paper No. 861350.

(33) Shiraishi, S. and Satoh, M., 1983, 'Performance of Antilock Brakes with simplified control technique', SAE Paper No. 830484.

(34) Anon, 1989, 'Delco-Moraine to start ABS output', Wards Automotive Report Oct 9 1989 p322.

(35) Watanebe, M. and Noburu, N., 1990, 'A new algorithm for ABS to compensate for road disturbances', SAE Paper No. 900205

(36) Miyasaki, N., Fukumoto, M., Sogo, Y, and Tsukinoki, H., 1990, 'Anti-lock brake system based on the Friction Coefficient between the wheel and the road surface', SAE Paper No. 900207.

(37) Kraft, H.J. and Leffler, H., 1990, 'An integrated brake and stability control system of the new BMW 850i', SAE Paper No. 900209.

(38) Schopf, H.J., and Paul, J., 1988, 'Acceleration skid control advances' Automotive Engineering August 1988 pp 70 - 76

(39) Schulze, B.G. and Lissel, E. ,1988, 'Anti-slip regulator with high performance and comfort', Proceedings of IMechE conference on Traction Control and Anti wheel-spin systems, C367/88

(40) Kiyotaka, I., Fujita, K., Inoue, Y. and Matutomi, S., 1990, 'The "Lexus" traction control (TRAC) system', SAE Paper No. 900212.

(41) Wallenowitz, H., Egger, G., Herb, E. and Krusche, H., 1988, 'Stability and traction control for four-wheel drive passenger vehicles', Proceedings of IMechE conference on Traction Control and Anti wheel-spin systems, C365/88.

(42) Buschmann, G., Ocvirk, N. and Volz, P., 1988, 'Integrated Traction control function - the consequent extension of highly sophisticated anti-lock systems', Proceedings of IMechE conference on Traction Control and Anti wheel-spin systems, C372/88.

(43) Demel, H. and Czinczel, A., 1988, 'ASR - task, design and function' Proceedings of IMechE conference on Traction Control and Anti wheel-spin systems, C370/88.

(44) Costa, A.N. and Jones R.P., 1990, 'Modelling of an automotive vehicle chassis system for motion control studies', University of Warwick Control Systems Centre Report No 11 November 1990.

(45) Costa, A.N. and Jones, R.P., 1991, 'Motion management for automotive vehicles', Proceedings IEE International Conference 'Control 91'.

(46) Clapeau, V., 1990, 'Conversation with Bendix personnel'.

(47) Hrovat, D., 1988, 'Teves brake dynamics model notes' Ford Internal Memorandum Mar 88.

(48) Hrovat, D , Tobler, W.E. and Tsangarides, M.C., 1985, 'Bond Graph Modelling of Dominant Dynamics of Automotive Powertrains', Proceedings of ASME Winter Annual Meeting.

(49) Hrovat, D., 1988, 'Non-linear engine model notes' Ford Internal Memorandum Mar 88

(50) Hrovat, D., 1988, 'Matrixx, tyre model notes'

(51) Hrovat, D., 1989, 'Influence of Drivetrain/Chassis Dynamics on DE-1 tip-in/backout Driveability', Ford Research Staff Report No SR-89-55 May 5, 1989.

(52) Powell, B.K., Cook, J.A. and Grizzle, J.W., 1987, 'Modelling and analysis of an inherently multi-rate sampling fuel injected engine idle speed control loop' ASME Journal of Dynamic Systems.

(53) Cook, J.A. and Powell, B.K., 1987, 'Discrete simplified linearisation and analytical comparison of IC engine families', Proceedings of the American Control Conference June 8-10, 1987.

(54) Howard, T. and Prasad, R., 1988, 'CDW 27 Anti-lock Brake & Traction Control Supplier Survey', Ford Internal Memorandum.

(55) Dugoff, H., Fancher, P. and Segel, L., 1969, 'Tire Performance affecting vehicle response to steering and braking control inputs', Highway Safety Research Institute (HSRI), University of Michigan Report , Aug 1969

(56) Owens, D.H., 1978, 'Feedback and Multivariable systems' Peter Peregrinus Ltd

(57) Maciejowski, J.M., 1989, 'Multivariable feedback design', Addison Wesley.

(58) Franklin, G.F., Powell, J.D. and Workman, M.L., 1990, 'Digital Control of Dynamic Systems', Addison Wesley.

(59) Ford, M.P., Maciejowski, J.M. and Boyle, J.M., 1988, 'Matlab Multi-variable frequency domain toolbox user guide', Cambridge Control Ltd.

(60) Matrix, user manual, 1990, Integrated Systems Inc, Santa Clara, California.

(61) Pacejka, H.B., 1986, 'Modelling of the pneumatic tyre and its impact on vehicle dynamic behaviour', Course notes, CCG, Munich

(62) Eykhoff P., "System Identification"

(63) Lucas G.G., 1986, 'Road Vehicle Performance', Gordon & Breach, ISBN 0-677-21400-6.

(64) Kotwicki, A.J., 1982, 'Dynamic models for torque converter equipped vehicles', SAE Paper No. 820393.

(65) Crossley, P.R., Jones, R.P. and Howarth, S.I., 1985, 'Modelling and simulation of a HGV powertrain for traction control studies', ISATA Paper No. 85047

(66) Newland, D.E., 1989, 'Mechanical Vibration analysis and computation', Longman ISBN 0-582-02744-6.

(67) Porsche Press Release, January 23 1989

(68) Yoshimori, K., Morimura, H., Yoshimura, Y. and Tsuchiya, M., 1984, 'Dynamic Shock Absorber Effect of Engine Mounting System on the Power Train vibration', SAE Paper No. 840255.

(69) Watanabe, A., Kuroyangi, J. and Hatton, T., 1984, 'Microcomputer Mechanical Clutch and Transmission Control' SAE Paper No. 840055.
(70) Blumberg, P.N., 1976, 'Powertrain Simulation: A tool for the design and evaluation of engine control strategies in vehicles', SAE Paper No. 760158.
(71) Zomotor, A., Leiber, H., Neundorf, S., Richter, K.H. and Buechie, K.H., 1986, 'Mercedes Benz 4Matic, an electronically controlled 4 wheel drive system for improved active safety', SAE Paper No. 861371.
(72) Crossley, P.R. and Cook, J.A., 1991, 'A nonlinear engine model for drivetrain system development', Proceedings IEE International Conference 'Control 91', pp 921 - 925.
(73) Reik, W., 1990, 'Torsional vibrations in the drive train of motor vehicles - Principle considerations' 4th International Symposium Luk, Baden-baden April 20 1990.
(74) Powell, B.K. and Cook, J.A., 1987, 'Non-linear low frequency phenomenological engine modelling and analysis', Proceedings ACC 1987.
(75) Wanat, R.L., (Ford U.S.A.), 1989, 'Technical discussion'
(76) Novak, J.M., 1977, 'Simulation of the breathing processes and air-fuel ratio distribution characteristics of three valve, stratified charge engines', SAE Paper No. 770881.
(77) Hamburg, D.R. and Hyland, J.E., 1976, 'A vaporised fuel metering system for internal combustion engines', SAE Paper No 760288.
(78) Powell, B.K. and Olbrot, A.W., 1990, 'Robustness and Analysis of an Automotive Idle Speed Control System', Ford SRL Report No SR-90-09.
(79) Harrington, D.L., 1968, 'Analysis and digital simulation for Carburettor Metering', PhD Thesis University of Michigan 1968.
(80) Powell, B.K., 1987, 'Notes exchanged with Jeff Cook'

(81) Moskwa, J.J. and Hedrick, J.K., 1987, 'Automotive Engine Modeling for Real Time Control Application', Proceedings of the ACC, Minneapolis.

(82) Beaumont, A., 1991, 'Presentation to Ford by Ricardo.

(83) Heywood, J.B., 'Internal Combustion Engine Fundamentals', McGraw Hill ISBN-0-07-028637-X.

(84) Prabhakar, R., 1975, 'Optimal and Suboptimal Control of Automotive Engine Efficiency and Emissions', PhD Thesis, Purdue University, West Lafayette, IN, U.S.A.

(85) Throop, M.J. and Hamburg, D.R., 1985, 'Dynamic Control of Engine NOx Emissions: Characterisation and Improvement of the Transient Response of an Exhaust Gas Recirculation System', Proceedings of the ACC, Boston, MA.

(86) Hrovat, D. and Tobler, W.E., 'Bond Graph Modelling and Computer Simulation of Automotive Torque Converters' The Journal of the Franklin Institute

(87) Clark, S.K., Ed, 1981, 'Mechanics of pneumatic tires ' Monograph 122, National Bureau of standards, Washington D.C.

(88) General Motors, 1 Aug 1972, U.S. Patent 3,680,655.

(89) Renault, 2 Mar 1976, U.S. Patent 3,941,203.

(90) Volvo, 21 Feb 1984, U.S. Patent 4,432,430.